Universidade de Aveiro Departamento de Física

2016

Mengjie Wang

Aspectos quânticos e clássicos de campos escalares e vectoriais em redor de buracos negros

Quantum and classical aspects of scalar and vector fields around black holes

Universidade de Aveiro Departamento de Física

2016

Mengjie Wang

Aspectos quânticos e clássicos de campos escalares e vectoriais em redor de buracos negros

Quantum and classical aspects of scalar and vector fields around black holes

Dissertação apresentada à Universidade de Aveiro no âmbito do Programa Doutoral MAP-fis para cumprimento dos requisitos necessários à obtenção do grau de Doutor em Física, realizada sob a orientação científica do Doutor Carlos Herdeiro, Professor Auxiliar com Agregação, e co-orientação do Doutor Marco O. P. Sampaio, do Departamento de Física da Universidade de Aveiro.

Apoio financeiro da FCT e do FSE no âmbito do III Quadro Comunitário de Apoio

This thesis is dedicated to my parents
for all their love and support

o júri

presidente

Prof. Doutor António Manuel Rosa Pereira Caetano

professor catedrático da Universidade de Aveiro

Prof. Doutor José Sande Lemos

professor catedrático do Instituto Superior Técnico

Prof. Doutor Sam Dolan

professor auxiliar da Universidade de Sheffield

Prof. Doutor Filipe Artur Pacheco Neves Carteado Mena

professor associado do Universidade do Minho

Prof. Doutor Eugen Radu

investigador principal da Universidade de Aveiro

Prof. Doutor Carlos Alberto Ruivo Herdeiro

investigador principal da Universidade de Aveiro

Acknowledgements

Confucius said, “lost time is never around the clock”. Along my way, studying physics during these years, I have received enormous encouragement and assistance from my family, my friends and my colleagues. I think it is the time to express my gratitude to all of them.

First of all, I am very thankful to my supervisor, Prof. Carlos Herdeiro, for his support and inspiration, for teaching me how to work on physics and for giving me freedom to explore my own interests.

Special thanks are reserved for Marco Sampaio, for our enjoyable collaboration on various projects. As my co-supervisor, he has taught me a lot of physics and numerical techniques, while as a friend, his positiveness always remind me to be optimistic when I face problems. I would also like to thank the other colleagues from the gravitation and high energy physics group at University of Aveiro, for all the great discussions about physics and others, they are Flávio Coelho, Juan Carlos Degollado, Jai Grover, Antonio Morais, João Rosa, Eugen Radu, and Helgi Rúnarsson. In particular, I am grateful to Juan Carlos Degollado and João Rosa for their interesting courses, and various discussions on the topic of superradiance.

I would like to acknowledge the financial support from Fundação para a Ciência e a Tecnologia, with the grant SFRH/BD/51648/2011 during the completion of this thesis.

I owe my deepest gratitude to all my previous colleagues in China, especially Prof. Dezhi Huang, for encouraging me to work in a different field, and Prof. Jiliang Jing, for introducing me the black hole physics and supporting me to study aboard. I would also like to thank all my friends in China, in particular Tao Sun, Pengsong Wei, Xianquan Lei and Shiqi Huang, for their constant encouragement.

Finally, I would like to thank my parents, who taught me to be a virtuous man, my sister,

my aunts, my uncles and all my relatives, thank you for all your endless love and support, regardless of the distance. I love you all!

Keywords: Black holes, Proca fields, Hawking radiation, TeV gravity, scalar fields, Maxwell fields, asymptotically anti-de Sitter spacetimes, quasinormal modes, superradiance.

Abstract: This thesis presents recent studies on test scalar and vector fields around black holes in the classical theory of General Relativity. It is separated in two parts according to the asymptotic properties of the spacetime under study.

In the first part, we investigate scalar and Proca fields on an asymptotically flat background. For the Proca field, we obtain a complete set of equations of motion in higher dimensional spherically symmetric backgrounds. These equations are solved numerically, both to compute Hawking radiation spectra and quasi-bound states. In the former case, for the first time, we carry out a precise study of the longitudinal degrees of freedom induced by the mass of the field. This can be used to improve the modeling of evaporation of black holes coupled to massive vector fields, and black hole event generators currently used at the Large Hadron Collider to probe TeV gravity models with extra dimensions. Regarding quasi-bound states, we find arbitrarily long lived modes for a charged Proca field in a Reissner-Nordström black hole. As a comparison, we also find such long lived modes for a charged scalar field.

The second part of this thesis presents research on superradiant instabilities of scalar and Maxwell fields on an asymptotically anti-de Sitter background. For the scalar case, we introduce a charge coupling between the field and the background, and show that superradiant instabilities do exist for all values of the total angular momentum, ℓ, in higher dimensions. This result corrects a statement in the literature that such instabilities only appear in even dimensions. For the Maxwell case, we first propose a general prescription to impose boundary conditions on the Kerr-anti-de Sitter spacetime, and obtain two Robin boundary conditions which give two different quasinormal modes even in a simpler Schwarzschild-anti-de Sitter black hole. Then these

two boundary conditions are implemented to study superradiant unstable modes and vector clouds. In particular, we find that the new branch of quasinormal modes may be unstable in a larger parameter space. Furthermore, the existence of vector clouds indicates that one may find a vector hairy black hole solution for the Einstein-Maxwell-anti-de Sitter system at the nonlinear level, which implies, in such system, that the Kerr-Newman-anti-de Sitter black hole is not a unique solution.

Palavras-chave: Buracos negros, Campos de Proca, Radiação de Hawking, gravidade à escala do TeV, campos escalares, campos de Maxwell, asimtóticamente anti-de Sitter, modos quasi-normais, super-radiância.

Resumo: Nesta tese apresentamos estudos recentes sobre campos escalares e vetoriais de teste, em torno de buracos negros na teoria clássica da relatividade geral. A tese encontra-se dividida em duas partes, de acordo com as propriedades asimtóticas do espaço-tempo em estudo.

Na primeira parte, investigamos os campos escalar e de Proca num espaço asimtóticamente plano. Para o campo de Proca, obtemos um conjunto completo de equações do movimento em espaços esfericamente simétricos em dimensões elevadas. Estas equações são resolvidas numericamente, tanto para o cálculo de radiação de Hawking como para o cálculo de estados quasi-ligados. No primeiro cálculo, pela primeira vez, efetuamos um estudo preciso dos graus de liberdade longitudinais que são induzidos pelo termo de massa do campo. Este estudo pode ser usado para melhorar o modelo da evaporação de buracos negros acoplados a campos vetoriais massivos e geradores de eventos de buraco negro usados presentemente no Grande Colisor de Hádrons para testar modelos de gravidade com dimensões extra à escala do TeV. Relativamente aos estados quasi-ligados, encontramos estados com tempos de vida arbitrariamente longos para o campo de Proca carregado, no buraco negro de Reissner-Nordström. Como comparação, obtemos estados com tempos de vida arbitrariamente longos também para o campo escalar.

Na segunda parte da tese, apresentamos investigação sobre instabilidades super-radiantes para os campos escalar e de Maxwell em espaço asimtóticamente anti-de Sitter. No caso escalar introduzimos um acoplamento de carga entre o campo e o background e mostramos que instabilidades super-radiantes existem para todos os valores do momento angular total, ℓ, em dimensões mais elevadas. Este resultado

corrige a afirmação na literatura de que estas instabilidades aparecem apenas em dimensões ímpares. Para o caso do campo de Maxwell, propomos primeiro uma prescrição para impor condições fronteira no espaço tempo de Kerr-anti-de Sitter obtendo duas condições fronteira do tipo de Robin que originam dois tipos diferentes de modos quasi-normais, mesmo no caso mais simples do buraco negro de Schwarzschild-anti-de Sitter. Estas duas condições fronteira são implementadas no estudo de modos super-radiantes instáveis e nuvens vetoriais. Em particular, encontramos um novo ramo de modos quasi-normais que podem conter instabilidades mais fortes. Mostramos ainda que a existência de nuvens vetoriais indica a possível existência de soluções de buraco negro com cabelo vetorial para o sistema Einstein-Maxwell-anti-de Sitter a nível não linear, o que implica, nesse sistema, que o buraco negro de Kerr-Newman-anti-de Sitter poderá não ser único.

Contents

List of Tables

List of Figures

Chapter 1

Introduction

1.1 Background and motivation

General Relativity (GR), as one of the pillars of modern physics, was established one hundred years ago by Albert Einstein in 1915. It unifies space and time, and in particular gravity is described by the curvature of spacetime. Mathematically, the theory is formulated by the elegant Einstein field equations [1], where the geometry is related to the distribution of matter and radiation. These equations were interpreted by John Wheeler in his famous statement that *matter tells spacetime how to curve, and spacetime tells matter how to move*. GR has been tested with high accuracy in the regime of weak gravity [2], while in the strong gravity regime the first direct observation on gravitational waves has been reported recently [3]. From an analysis of the waves, black holes are identified as the source for such an event [3].

The concept of black hole (BH) can be dated back to the end of the eighteenth century. At that time, John Michell [4] and Pierre-Simon Laplace [5] put forward an idea that the largest bodies in the universe may be invisible since they are so massive that even light could not escape, which were dubbed as *dark stars*. This idea was revived by Robert Oppenheimer and his collaborators, more than one century later, in their studies of gravitational collapse, where they concluded that neutron stars above the Tolman-Oppenheimer-Volkoff limit (approximately 1.5 to 3 solar masses) would collapse [6]. Such collapsed objects were called *frozen stars*. In 1967, the term *black hole* was introduced by John Wheeler [7], and since then it was quickly accepted for general use.

From a modern viewpoint, BHs are the simplest macroscopic objects in nature, in the sense that they can be uniquely characterized by their mass, spin and charge. This is the well known *no hair conjecture* [8]. This conjecture has been circumvented in different contexts, for example in the Einstein-Yang-Mills theory [9–12], in the Horndeski theory [13–15] and recently in the Einstein-Klein-Gordon system where a Kerr BH with scalar hair was found [16]. Among them, scalar hairy BH solutions are supported by the phenomenon of superradiance [17], which provides a mechanism to generate hairy BH solutions in general [16, 18]. Another interesting phenomenon in BH physics is the Hawking radiation [19]. Hawking radiation has been attracting a lot of attention, not only because it relates gravity to quantum theory which may provide a connection to a *quantum theory* of gravity, but also because it might be visible in high energy processes.

In this thesis, we are going to study BHs interacting with scalar and vector fields at the linear level, in the context of *Hawking radiation* and *superradiance*. The motivation for these studies is as follows.

TeV gravity scenarios

The study of gravitational theories in higher dimensions has been discussed for a century, at least since the works by Nordström [20], Kaluza [21] and Klein [22]. During the last four decades, moreover, the naturalness of extra dimensions within supergravity and string theory made it a topic of intense research within high energy theoretical physics. At the end of the last century, this research led to models that, aiming at solving the hierarchy problem*, predicted that the extra dimensions could be very large (or even infinite) in size, as compared to the traditional Planck scale.

Within such scenario, the true fundamental Planck scale could be as low as the TeV scale [23–26] so that the formation and evaporation of microscopic BHs could be visible in realistic man-made particle accelerators†, such as the Large Hadron Collider (LHC). This motivates our study on Hawking radiation. In particular, the second run of the LHC is ongoing, with a center of mass energy of 13 TeV, where such scenarios will be properly tested. Therefore, any improvements on the phenomenology of these models are quite timely.

*The hierarchy problem refers to the relative weakness of gravity, around sixteen orders of magnitude, by comparing to the other fundamental interactions.

†See, for example, the latest reports from CMS [27] and ATLAS [28] in the search for microscopic BHs.

Asymptotically anti-de Sitter spacetimes

Anti-de Sitter (AdS) spacetime is the unique maximally symmetric solution of the vacuum Einstein equations with a negative cosmological constant. Asymptotically AdS spacetimes, referring to spacetimes which share the conformal boundary with AdS but may be different in the bulk, have attracted a lot of attention in theoretical physics. One reason is the AdS/CFT correspondence [29] which conjectures a duality between gravity in the d-dimensional AdS bulk and a quantum conformal field theory living in the $(d-1)$-dimensional conformal boundary. Another reason is the timelike property of the AdS boundary, which leads to interesting novel features, as compared to asymptotically flat spacetimes, such as the weak turbulent instability [30] and the superradiant instability for massless fields [31–33].

With these motivations in mind, in the following we will briefly describe the physical phenomena of Hawking radiation and superradiance.

1.2 Hawking radiation

Hawking radiation [19] describes black body radiation that is predicted to be released by BHs, due to quantum effects close to the event horizon. It is one of the most important features arising from quantum field theory in curved spacetime, discovered by Hawking in 1974. This effect was derived in a semiclassical framework, in the sense that the background geometry is classical (governed by classical gravitational theories) while the propagating fields are quantized. Since Hawking radiation connects classical gravity with quantum theory, it has inspired many works to re-derive Hawking radiation through alternative methods, see for example [34–38], with an expectation to get a deeper understanding of gravity itself.

Physically, Hawking radiation can be understood through an intuitive picture by considering virtual particles generated from the vacuum*. As it is well known since Dirac, the quantum vacuum is not completely empty but it contains fluctuations which produce particle-antiparticle pairs. Close to the event horizon of a BH, strong gravity effects may separate particle-antiparticle pairs, and if the antiparticle is attracted into the interior of the hole then the particle can escape to infinity thus generating Hawking radiation.

*Note that this interpretation may lead to a flawed intuition on where does Hawking radiation originate [39].

The phenomenon of Hawking radiation found recently an interesting application in TeV gravity models. In such models, scattering processes with center of mass energy well above the fundamental Planck scale, should be dominated by classical gravitational interactions [40]. Then, for sufficiently small impact parameter, miniature BHs should form in particle collisions, and in particular, Hawking radiation would be the main observable signature [41, 42]. This motivation led to an intensive study of Hawking radiation from higher-dimensional BHs– see [43] for a recent review and reference therein.

If a microscopic BH is produced, it is expected that the decay process can be modeled by the following four phases [44], namely

- *Balding phase*: all original "hair" inherited from incoming particles (except mass and angular momentum) is lost through gravitational and Hawking radiation and, at the end of this stage, the BH is axisymmetric and rotating.
- *Spin-down phase*: then the BH emits Hawking radiation, losing mass and angular momentum evolving towards the end, into a spherically symmetric BH.
- *Schwarzschild phase*: the spherically symmetric BH continues to radiate losing its mass, until it reaches the Planck scale.
- *Planck phase*: the semiclassical approximation of Hawking radiation becomes invalid at this stage, and quantum gravity starts to play a significant role in the BH emission process.

It is believed that the spin-down and Schwarzschild phases will dominate the lifetime of the BH, therefore they are the most promising stages to generate observational signatures of Hawking radiation. Indeed these phases have been modeled in BH event generators, such as CHARYBDIS2 [45,46] and BLACKMAX [47] currently in use at the LHC. These event generators, however, can still be improved.

One of the Hawking radiation channels that has not been properly addressed in the literature is that of massive vector bosons, both electrically neutral and electrically charged, to describe the emission of Z and $W^{\pm}$ particles of the Standard Model. As our first goal in this thesis, we are going to study Hawing radiation for both a neutral and a charged Proca field in higher dimensions, to bridge this gap.

1.3 Superradiance

Superradiance is a phenomenon which refers to a radiation enhancement process in several physical contexts. This term was coined by Dicke, to describe an effect in quantum optics that radiation of a group of emitters could be amplified in a coherent fashion [48]. In 1971, Zel'dovich [49, 50] pointed out that scalar and electromagnetic radiation, impinging on a rotating cylinder with absorbing surfaces can be amplified if the condition

$$\omega < m\Omega \,, \tag{1.3.1}$$

holds. Here ω and m are the waves' frequency and the azimuthal number, and Ω is the angular velocity of the cylinder.

Since the event horizon of a BH provides a natural absorbing surface at the classical level, Zel'dovich anticipated that a rotating BH with horizon angular velocity Ω_H should display superradiant amplification within the regime given by Eq. (1.3.1). This was indeed observed by Misner in unpublished calculations, who found that certain modes of scalar fields are amplified by Kerr BHs, as a wave analogue of the Penrose process [51]. This work was then generalized and verified by Teukolsky and Press [52] who found that the amplification process also occurs for electromagnetic and gravitational waves on the same background. According to these observations, Bekenstein [53] realized that in order to satisfy Hawking's area theorem [54], superradiant amplification is classically required when condition (1.3.1) holds. From the same reasoning he also derived that superradiance of charged bosonic waves by a charged BH exists when [53]

$$\omega < q\Phi_H \,, \tag{1.3.2}$$

is satisfied, where q is the field charge and Φ_H is the electrostatic potential at the horizon.

This story changes dramatically for fermion fields. As first shown by Unruh [55], superradiance is absent for neutral massless Dirac fields on the Kerr background. This conclusion was then generalized to massive Dirac fields [56] (by correcting a previous work [57]) and on the Kerr-Newman background [58]. Absence of superradiance for fermions originates from the fact that the net number current flowing down the horizon is positive definite, which implies that it is impossible for fermion fields to extract energy and angular momentum from the hole [55]. Moreover, the argument [53] based on the area theorem does not apply to a fermion field since

its energy-momentum tensor does not obey the weak energy condition [34]. At the quantum level, it can also be understood as a consequence of the exclusion principle which does not allow for more than one particle in each outgoing wave and therefore the scattered wave can not be stronger than the incident wave [34].

By placing a reflecting mirror around a rotating BH, the system composed with bosonic fields may become unstable. This was first addressed by Press and Teukolsky [59], and was dubbed as *black hole bomb*. The role of the mirror is to feed back to the BH the amplified scattered wave, as to recurrently extract rotational energy. Then, the wave bounces back and forth between the mirror and the BH until radiation pressure destroys the mirror. In fact, the reflecting mirror is not necessarily artificial, and it has several realizations in nature. One realization is the field's mass. For a massive bosonic field with mass μ satisfying the bound state condition $\omega < \mu$, the mass term can provide a confining mechanism similar to a mirror [60–69]. Another realization is AdS asymptotics, which may also bind superradiant modes [31, 70–75]. Recently a considerable interest has been devoted to study superradiant scattering and instabilities using numerical methods at the non-linear level [66, 76–83].

Since superradiance also exists for charged BHs under the condition in Eq. (1.3.2), it is natural to ask if charged superradiant modes can be confined by the field's mass and the AdS asymptotics as in the rotating case, and generate instabilities by extracting Coulomb energy and BH charge. As proved by Hod [84–86] for the scalar case, the field's mass *cannot* bound the superradiant modes since the superradiance condition and the bound state condition for a charged massive scalar field in an asymptotically flat charged BH cannot be satisfied simultaneously. This statement has been generalized to charged Proca fields recently, showing that Reissner-Nordström BHs are also stable against those massive vector fields [87]. There is still a possibility, however, to circumvent Hod's results by considering a non-minimal coupling between the field and the background since Hod's results only hold for minimally coupled scalar fields [85, 86]. At this moment it might be safe to state that a charged BH bomb may be only achieved with AdS asymptotics [75, 88, 89]*.

The phenomenon of superradiance is interesting for various reasons†. Among others, we

*Alternatively, a charged BH bomb in an asymptotically flat spacetime can be also built artificially by imposing mirror-like boundary conditions [82, 90–92].

†To find more applications of superradiance, we refer to a recent review on this topic [17].

would like to mention that superradiance provides a systematic mechanism to construct (quasi-) stationary BH-field systems at the linear level, and generates hairy BH solutions at the nonlinear level [16, 18]. As we mentioned before, in an asymptotically flat BH, the superradiant instability is absent for a charged massive bosonic field. But as shown in [87,93], one can still find quasi-stationary states for such a BH-field system, when gravity is balanced with the electric field. Adding a mirror, as recently shown in [81], a charged hairy BH solution was found. An even more interesting result was obtained on a rotating BH. As we explained above, the field mass can be used as a mirror and therefore the superradiant instability is present for a massive scalar field on a Kerr BH. At the linear level, stationary states can be found in such a system [94–96], which are dubbed as *clouds*. Considering the back reaction of a complex scalar field, scalar hairy Kerr solutions have been found in [16, 97, 98].

Because the AdS asymptotics is another realization of the mirror, one may expect similar effects in an asymptotically AdS spacetime. Indeed the superradiant instability for scalar and gravitational fields has been studied on a Kerr-anti-de Sitter (Kerr-AdS) BH [31, 32]. In this thesis, we will complete this study by exploring the superradiant instability for the Maxwell field. Furthermore, since such an instability exists in AdS, one expects to find clouds for various fields on Kerr-AdS BHs. The only studied case before this thesis on a Kerr-AdS BH was the gravitational field [31]. To fill this gap, we will present studies of scalar and vector clouds on the same background.

1.4 Structure

The structure of this thesis is as follows. In Chapter 2, we review two important perturbative methods, the Kodama-Ishibashi formalism and the Newman-Penrose formalism, which set the foundations for the other chapters. In Chapter 3, we employ the Kodama-Ishibashi formalism to derive equations of motion for a Proca field (either neutral or charged), on a D-dimensional spherically symmetric background. Then these equations are used to study a quantum semi-classical effect on BHs, i.e. Hawking radiation, for a neutral Proca field on a D-dimensional Schwarzschild BH in Chapter 4. Following this line, in Chapter 5 we explore Hawking radiation for a charged Proca field in a brane charged BH. We turn to classical properties in Chapter 6, to study quasi-bound states for a charged Proca field in a Reissner-

Nordström BH. In Chapter 7, we study superradiant instabilities for a charged scalar field in a D-dimensional Reissner-Nordström-AdS BH. This is then generalized to the Maxwell field on a Kerr-AdS BH, leading to the study of superradiant instabilities and vector clouds, in Chapter 8. Conclusions and outlook are drawn in Chapter 9.

Chapter 2

Preliminaries

We start in this chapter by introducing the mathematical tools to deal with perturbations of test fields around BHs, as the foundation to perform the study for Proca and Maxwell fields. Two types of perturbation methods, the Kodama-Ishibashi formalism and the Newman-Penrose formalism, will be illustrated, respectively, in the following.

Throughout this thesis we will use the signature $(-,+,...,+)$ and natural units $G = c = \hbar = 1$, unless explicitly stated otherwise.

2.1 Kodama-Ishibashi formalism

The Kodama-Ishibashi (KI) formalism [99–102] (for a review see [103, 104]), is the generalization of the Regge-Wheeler-Zerilli formalism [105, 106] to higher dimensions. This method is applicable to any higher dimensional spacetime with maximal symmetry whose manifold structure can be locally written as a warped product between a Lorentzian manifold and an Einstein space. The basic idea of this method is to classify the perturbations into different types (scalar, vector and tensor types), based on their tensorial behavior in the Einstein space.

To be specific, let us consider the following gravitational background with the manifold structure $\mathcal{M} = \mathcal{N} \times \mathcal{K}$ in the form [99, 103, 104]

$$g_{MN}dx^M dx^N = h_{ab}(y)dy^a dy^b + r(y)^2 d\sigma_n^2 \,, \tag{2.1.1}$$

where $x^M = (y^a, z^j)$. Note that the Lorentzian manifold is denoted by $\mathcal{N}$ with metric h_{ab},

and the Einstein space is denoted by $\mathcal{K}$ with constant curvature $K(K = 0, \pm 1)$ and metric σ_{ij},

$$d\sigma_n^2 = \sigma_{ij}(z)dz^i dz^j \ . \tag{2.1.2}$$

Then the Riemann tensor and Ricci tensor on an Einstein space are given by

$$\hat{R}_{ijkl} = K(\sigma_{ik}\sigma_{jl} - \sigma_{il}\sigma_{jk}) \ , \qquad \hat{R}_{ij} = (n-1)K\sigma_{ij} \ . \tag{2.1.3}$$

We use indices $\{a, b, c, \ldots\}$ for the first set of coordinates, $\{y^a\}$, spanning on the m-dimensional space with metric $h_{ab}(y)$; and indices $\{i, j, k, \ldots\}$ for the second set of coordinates, $\{z^i\}$, spanning on the n-dimensional Einstein space. Then the spacetime dimension is $d = m+n$. We denote the covariant derivatives, the Christoffel connection coefficients and the Riemann tensors on the manifolds $\{\mathcal{M}, \mathcal{N}, \mathcal{K}\}$, by $\{\nabla_M, D_a, \hat{D}_i\}$, $\{\Gamma^M_{NL}, \bar{\Gamma}^a_{bc}, \hat{\Gamma}^i_{jk}\}$, and $\{R_{MNLS}, \bar{R}_{abcd}, \hat{R}_{ijkl}\}$, respectively. We also define the Laplace operator on the Einstein space as $\hat{\Delta} = \hat{D}_i\hat{D}^i$. The metric form in Eq. (2.1.1) covers several interesting cases such as $2+n$-dimensional spherically symmetric BHs or a singly rotating BH in $4+n$-dimensions.

The expressions of Γ^M_{NL} and $R^M{}_{NLS}$ can be written in terms of the corresponding quantities on the manifold $\mathcal{N}$ with metric $h_{ab}(y)$ and on the Einstein space with metric σ_{ij} [99], i.e.

$$\Gamma^a_{bc} = \bar{\Gamma}^a_{bc} \ , \quad \Gamma^a_{ij} = -rD^a r\sigma_{ij} \ , \quad \Gamma^i_{aj} = \frac{D_a r}{r}\delta^i_j \ , \quad \Gamma^i_{jk} = \hat{\Gamma}^i_{jk} \ , \tag{2.1.4}$$

where the other components of Γ^M_{NL} vanish, and

$$\begin{aligned} &R^a{}_{bcd} = \bar{R}^a{}_{bcd} \ , \quad R^i{}_{ajb} = -\frac{D_a D_b r}{r}\delta^i_j \ , \quad R^a{}_{ibj} = -\frac{D^a D_b r}{r}g_{ij} \ , \\ &R^i{}_{jkl} = (K - D_a r D^a r)(\delta^i_k\sigma_{jl} - \delta^i_l\sigma_{jk}) \ . \end{aligned} \tag{2.1.5}$$

Then the Ricci tensors and Einstein tensors can be derived directly [99]

$$R_{ab} = \bar{R}_{ab} - \frac{n}{r}D_a D_b r \ , \quad R_{ai} = 0 \ , \quad R_{ij} = \left(-\frac{\Box r}{r} + (n-1)\frac{K - D_a r D^a r}{r^2}\right)g_{ij} \ , \tag{2.1.6}$$

where we have defined $\Box \equiv D^a D_a$, and

$$G_{ab} = \bar{G}_{ab} - \frac{n}{r}D_a D_b r - \left(\frac{n(n-1)}{2r^2}(K - D_a r D^a r) - \frac{n}{r}\Box r\right)g_{ab} \ , \tag{2.1.7}$$

$$G_{ij} = \left(-\frac{\bar{R}}{2} - \frac{(n-1)(n-2)}{2r^2}(K - D_a r D^a r) + \frac{n-1}{r}\Box r\right)g_{ij} \ , \tag{2.1.8}$$

$$G_{ai} = 0 \ , \tag{2.1.9}$$

with the definition $G_{MN} = R_{MN} - \frac{1}{2}g_{MN}R$.

To write down the equations of motion, we shall decompose the perturbations in terms of their tensorial harmonics on $\mathcal{K}$ [103, 104].

For a vector field v_i, it can be uniquely decomposed into a scalar field $v^{(s)}$ and a transverse vector field $v_i^{(t)}$ as

$$v_i = \hat{D}_i v^{(s)} + v_i^{(t)} , \qquad \hat{D}_i v^{(t)i} = 0 , \tag{2.1.10}$$

where $v^{(s)}$ and $v_i^{(t)}$ satisfy the corresponding scalar and vector eigenvalue equations

$$(\hat{\Delta} + \kappa_s^2) v^{(s)} = 0 , \tag{2.1.11}$$

$$(\hat{\Delta} + \kappa_v^2) v_i^{(t)} = 0 , \tag{2.1.12}$$

on an Einstein space with spherical topology, with $\kappa_s^2 = \ell(\ell+n-1)$ and $\kappa_v^2 = \ell(\ell+n-1)-1$. Note that the angular momentum quantum number, ℓ, starts from zero in the scalar eigenvalue κ_s and one in the vector eigenvalue κ_v, respectively. Then taking a derivative $\hat{D}_i$ on Eq. (2.1.10), we have the relation

$$\hat{\Delta} v^{(s)} = \hat{D}_i v^i , \tag{2.1.13}$$

which determines $v^{(s)}$ from Eq. (2.1.11), and $v_i^{(t)}$ from Eq. (2.1.10) after $v^{(s)}$ is obtained.

The scalar and vector harmonic functions on n-spheres, used in Eqs. (2.1.11) and (2.1.12), are defined as follows [104]. Let us denote the homogeneous cartesian coordinates on n-spheres by $\Omega^A (A = 1, \cdots, n+1)$, and define the function $Y_{\mathbf{a}}$ by

$$Y_{\mathbf{a}}(\Omega) = a_{A_1 \cdots A_\ell} \Omega^{A_1} \cdots \Omega^{A_\ell} , \tag{2.1.14}$$

in terms of a constant tensor $\mathbf{a} = (a_{A_1 \cdots A_\ell})$ $(A_1, \cdots, A_\ell = 1, \cdots, n+1)$. Then $Y_{\mathbf{a}}$ is a scalar harmonic function with the eigenvalue κ_s^2 if and only if $\mathbf{a}$ satisfies the conditions

$$a_{A_1 \cdots A_\ell} = a_{(A_1 \cdots A_\ell)} , \quad a_{A_1 \cdots A_{\ell-2}}{}^B{}_B = 0 \quad (\ell \geq 2) . \tag{2.1.15}$$

Similarly, we can define the vector field $V_{\mathbf{b}}^i$ by

$$V_{\mathbf{b}}^i = b_{A_1 \cdots A_\ell ; B} \Omega^{A_1} \cdots \Omega^{A_\ell} \hat{D}^i \Omega^B , \tag{2.1.16}$$

in terms of a constant tensor $\mathbf{b} = (a_{A_1 \cdots A_\ell ; B})(A_1, \cdots, A_\ell, B = 1, \cdots, n+1)$. Then, $V_{\mathbf{b}}^i$ is a vector harmonic function on n-spheres with eigenvalue κ_v^2, if and only if the constant tensor

b satisfies the conditions

$$b_{A_1\cdots A_\ell;B} = b_{(A_1\cdots A_\ell);B} \ , \quad b_{A_1\cdots A_{\ell-2}i}{}^{i}{}_{;B} = 0 \ , \quad b_{(A_1\cdots A_\ell;A_{\ell+1})} = 0 \ . \tag{2.1.17}$$

For more details on these harmonic functions on n-spheres and the corresponding properties, we refer readers to [104].

2.2 Newman-Penrose formalism

The Newman-Penrose formalism [107], as the name indicates, was developed by Newman and Penrose in 1962, as an alternative way to formulate field equations, such as the Einstein equations and the Maxwell equations. This formalism is extremely useful in various contexts in GR, for example to construct exact solutions of the Einstein equations [108], to study perturbations of massless test fields on various BH backgrounds [109, 110], and to extract gravitational radiation in numerical relativity [111]. For the problems we are interested in this thesis, we focus on the application of this formalism in the context of perturbation theory.

As first exhibited in the celebrated work of Teukolsky [112], linear perturbations of gravitational and electromagnetic fields on the Kerr background both separate and decouple, in terms of the Newman-Penrose variables. This was subsequently generalized to rotating BHs with a cosmological constant [113–116]. In this section, we review the Newman-Penrose formalism with application to the Maxwell field on Kerr-AdS BHs, and further present some new ingredients which have not been derived in the literature, in the presence of a cosmological constant, with details, including

- the derivation of Teukolsky-Starbinski identities, which was given in [114] without proof,
- the derivation for a complete set of solutions for the Maxwell field, in particular for Φ_1, which is relevant for proving Appendix D.

2.2.1 Basics

In order to introduce the Newman-Penrose formalism, we first define a complex null tetrad $\{l^\mu, n^\mu, m^\mu, \bar{m}^\mu\}$, where the normalization conditions

$$l_\mu n^\mu = -1 \ , \qquad m_\mu \bar{m}^\mu = 1 \ , \tag{2.2.1}$$

are satisfied, and all the other scalar products vanish. Note that here $\bar{m}^\mu$ is the complex conjugate of m^μ. The tetrad is related with the metric*

$$g_{\mu\nu} = -l_\mu n_\nu - l_\nu n_\mu + m_\mu \bar{m}_\nu + m_\nu \bar{m}_\mu \ . \tag{2.2.2}$$

Then spin coefficients are defined in terms of the tetrad

$$\begin{aligned}
-\kappa &= l_{\mu;\nu} m^\mu l^\nu \ , \quad -\rho = l_{\mu;\nu} m^\mu \bar{m}^\nu \ , \quad -\sigma = l_{\mu;\nu} m^\mu m^\nu \ , \quad -\tau = l_{\mu;\nu} m^\mu n^\nu \ , \\
\mu &= n_{\mu;\nu} \bar{m}^\mu m^\nu \ , \quad \nu = n_{\mu;\nu} \bar{m}^\mu n^\nu \ , \qquad \lambda = n_{\mu;\nu} \bar{m}^\mu \bar{n}^\nu \ , \qquad \pi = n_{\mu;\nu} \bar{m}^\mu l^\mu \ , \\
-\epsilon &= \frac{1}{2}(l_{\mu;\nu} n^\mu l^\nu - m_{\mu;\nu} \bar{m}^\mu l^\nu) \ , \qquad -\beta = \frac{1}{2}(l_{\mu;\nu} n^\mu m^\nu - m_{\mu;\nu} \bar{m}^\mu m^\nu) \ , \\
-\gamma &= \frac{1}{2}(l_{\mu;\nu} n^\mu n^\nu - m_{\mu;\nu} \bar{m}^\mu n^\nu) \ , \qquad -\alpha = \frac{1}{2}(l_{\mu;\nu} n^\mu \bar{m}^\nu - m_{\mu;\nu} \bar{m}^\mu \bar{m}^\nu) \ .
\end{aligned} \tag{2.2.3}$$

Next we introduce the projection of the covariant derivatives in the null tetrad vectors, with the following notations

$$D = l^\mu \partial_\mu \ , \quad \Delta = n^\mu \partial_\mu \ , \quad \delta = m^\mu \partial_\mu \ , \quad \bar{\delta} = \bar{m}^\mu \partial_\mu \ . \tag{2.2.4}$$

With the above spin coefficients in Eq. (2.2.3) and the directional derivatives in Eq. (2.2.4) at hand, one may rewrite the Maxwell field equations. For the reader who is interested in the equations of motion for other spin fields in this formalism, such as the gravitational field and the Dirac field, a detailed account can be found in [109, 110].

In the Newman-Penrose formalism, the Maxwell tensor is decomposed into three complex scalars

$$\phi_0 = F_{\mu\nu} l^\mu m^\nu \ , \qquad \phi_1 = \frac{1}{2} F_{\mu\nu}(l^\mu n^\nu + \bar{m}^\mu m^\nu) \ , \qquad \phi_2 = F_{\mu\nu} \bar{m}^\mu n^\nu \ . \tag{2.2.5}$$

Then the Maxwell equations become

$$\begin{aligned}
D\phi_1 - \bar{\delta}\phi_0 &= (\pi - 2\alpha)\phi_0 + 2\rho\phi_1 - \kappa\phi_2 \ , \\
D\phi_2 - \bar{\delta}\phi_1 &= -\lambda\phi_0 + 2\pi\phi_1 + (\rho - 2\epsilon)\phi_2 \ , \\
\delta\phi_1 - \Delta\phi_0 &= (\mu - 2\gamma)\phi_0 + 2\tau\phi_1 - \sigma\phi_2 \ , \\
\delta\phi_2 - \Delta\phi_1 &= -\nu\phi_0 + 2\mu\phi_1 + (\tau - 2\beta)\phi_2 \ ,
\end{aligned} \tag{2.2.6}$$

*Note that this relation depends on the conventions.

where the differential operators appearing on the left hand side are defined in Eq. (2.2.4) and the spin coefficients on the right hand side are given by Eq.(2.2.3).

To obtain the explicit form of the Maxwell equations, we shall specify a background geometry. For that purpose and for later application in the problems we are interested in, we first review the Kerr-AdS spacetimes in the next subsection.

2.2.2 Kerr-AdS black holes

In an asymptotically AdS background, the most general stationary and axisymmetric BH solution of the four dimensional Einstein-AdS system, is the Kerr-AdS BH. It was found by Carter [117] firstly, a few years after the finding of the Kerr solution.

The line element for a Kerr-AdS BH, in Boyer-Lindquist coordinates, can be written as

$$ds^2 = -\frac{\Delta_r}{\rho^2\Xi^2}\Big(dt - a\sin^2\theta d\varphi\Big)^2 + \rho^2\left(\frac{dr^2}{\Delta_r} + \frac{d\theta^2}{\Delta_\theta}\right) + \frac{\Delta_\theta \sin^2\theta}{\rho^2\Xi^2}\Big(a\,dt - (r^2+a^2)d\varphi\Big)^2 \ , \quad (2.2.7)$$

with metric functions

$$\begin{aligned} &\rho^2 \equiv \bar{\rho}\bar{\rho}^* = r^2 + a^2\cos^2\theta \ , \quad \Delta_r = \Big(r^2+a^2\Big)\left(1+\frac{r^2}{L^2}\right) - 2Mr \ , \\ &\Delta_\theta = 1 - \frac{a^2\cos^2\theta}{L^2} \ , \quad \Xi = 1 - \frac{a^2}{L^2} \ , \end{aligned} \quad (2.2.8)$$

where $\bar{\rho}^*$ is the complex conjugate of $\bar{\rho}$, and $\bar{\rho} = r + ia\cos\theta$. The other parameters shown in Eq. (2.2.8) include, L, which is the AdS radius; M and a, which are the mass and spin parameters and relate to the BH energy and angular momentum.

In this frame, the angular velocity of the event horizon and the Hawking temperature are given by

$$\Omega_H = \frac{a}{r_+^2 + a^2} \ , \quad (2.2.9)$$

$$T_H = \frac{1}{\Xi}\left[\frac{r_+}{2\pi}\left(1+\frac{r_+^2}{L^2}\right)\frac{1}{r_+^2+a^2} - \frac{1}{4\pi r_+}\left(1-\frac{r_+^2}{L^2}\right)\right] \ , \quad (2.2.10)$$

where the event horizon r_+ is determined as the largest root of $\Delta_r(r_+) = 0$. For a given r_+, the mass parameter M can be expressed as

$$M = \frac{(r_+^2+a^2)(L^2+r_+^2)}{2r_+L^2} \ .$$

To require the existence of BHs and to avoid singularities, one may impose the following constraints on the rotation parameter a

$$\begin{aligned} &\frac{a}{L} \leq \frac{r_+}{L}\sqrt{\frac{3r_+^2+L^2}{L^2-r_+^2}}\,, && \text{for} \quad \frac{r_+}{L} < \frac{1}{\sqrt{3}}\,, \\ &\frac{a}{L} < 1\,, && \text{for} \quad \frac{r_+}{L} \geq \frac{1}{\sqrt{3}}\,, \end{aligned} \tag{2.2.11}$$

where the equality sign in the first line corresponds to an extremal BH.

The Boyer-Lindquist coordinates are convenient to solve the perturbation equations for test fields. These coordinates, however, obscure the structure of the geometry at infinity. In fact, the metric in Eq. (2.2.7) describes the Kerr-AdS spacetime in a rotating frame, which can be seen by calculating the angular velocity at infinity [118]

$$\Omega_\infty = \frac{a}{a^2+L^2}\,, \tag{2.2.12}$$

which is apparently non-zero. In order to obtain a non-rotating frame, which is relevant to BH thermodynamics [119], we can make the following coordinate transformation [120, 121]

$$\hat{t} = \frac{t}{\Xi}\,, \quad \hat{\varphi} = \varphi + \frac{a}{L^2}\frac{t}{\Xi}\,, \quad \hat{r}^2 = \frac{r^2\Delta_\theta + a^2\sin^2\theta}{\Xi}\,, \quad \hat{r}\cos\hat{\theta} = r\cos\theta\,, \tag{2.2.13}$$

so that in these new frame the Kerr-AdS geometry (2.2.7) is simply AdS space in the usual spherical coordinates

$$ds^2 = -\left(1+\frac{\hat{r}^2}{L^2}\right)d\hat{t}^2 + \left(1+\frac{\hat{r}^2}{L^2}\right)^{-1}d\hat{r}^2 + \hat{r}^2(d\hat{\theta}^2 + \sin^2\hat{\theta}d\hat{\varphi}^2)\,, \tag{2.2.14}$$

when $r \to \infty (\hat{r} \to \infty)$. The angular velocity of the event horizon in these coordinates then becomes

$$\hat{\Omega}_H = \Omega_H\Xi + \frac{a}{L^2}\,, \tag{2.2.15}$$

where Ω_H, defined in Eq. (2.2.9), is measured relative to a rotating observer at infinity. Since the metric in coordinates $(\hat{t}, \hat{r}, \hat{\theta}, \hat{\varphi})$ is complicated, and also because we have the coordinate transformations in Eq. (2.2.13), in practice we always work in Boyer-Lindquist coordinates. Our goal is to solve the Maxwell equations in the frequency domain, therefore it is useful to relate the frequencies in these two different coordinates. This is given by

$$e^{-i\omega t}e^{im\varphi} = e^{-i\hat{\omega}\hat{t}}e^{im\hat{\varphi}}\,, \qquad \Rightarrow \qquad \hat{\omega} = \omega\Xi + m\frac{a}{L^2}\,. \tag{2.2.16}$$

2.2.3 Maxwell equations on Kerr-AdS

By specializing the general Maxwell equations (2.2.6) to the Kerr-AdS background (2.2.7), and using a generalization of the Kinnersley tetrad [113], i.e.

$$
\begin{aligned}
l^\mu &= \left(\frac{(r^2+a^2)\Xi}{\Delta_r}, 1, 0, \frac{a\Xi}{\Delta_r}\right) , \qquad n^\mu = \frac{1}{2\rho^2}\Big((r^2+a^2)\Xi, -\Delta_r, 0, a\Xi\Big) , \\
m^\mu &= \frac{1}{\sqrt{2\Delta_\theta}\bar{\rho}}\left(ia\Xi\sin\theta, 0, \Delta_\theta, \frac{i\Xi}{\sin\theta}\right) , \qquad \bar{m}^\mu = (m^\mu)^* ,
\end{aligned} \tag{2.2.17}
$$

where $\bar{\rho} = r + ia\cos\theta$, one obtains

$$
\left(\mathscr{D}_0 + \frac{1}{\bar{\rho}^*}\right)\Phi_1 = \sqrt{\Delta_\theta}\left(\mathscr{L}_1 - \frac{ia\sin\theta}{\bar{\rho}^*}\right)\Phi_0 , \tag{2.2.18}
$$

$$
\left(\mathscr{D}_0 - \frac{1}{\bar{\rho}^*}\right)\Phi_2 = \sqrt{\Delta_\theta}\left(\mathscr{L}_0 + \frac{ia\sin\theta}{\bar{\rho}^*}\right)\Phi_1 , \tag{2.2.19}
$$

$$
-\Delta_r\left(\mathscr{D}_1^\dagger - \frac{1}{\bar{\rho}^*}\right)\Phi_0 = \sqrt{\Delta_\theta}\left(\mathscr{L}_0^\dagger + \frac{ia\sin\theta}{\bar{\rho}^*}\right)\Phi_1 , \tag{2.2.20}
$$

$$
-\Delta_r\left(\mathscr{D}_0^\dagger + \frac{1}{\bar{\rho}^*}\right)\Phi_1 = \sqrt{\Delta_\theta}\left(\mathscr{L}_1^\dagger - \frac{ia\sin\theta}{\bar{\rho}^*}\right)\Phi_2 , \tag{2.2.21}
$$

where

$$
\begin{aligned}
\mathscr{D}_n &= \frac{\partial}{\partial r} - \frac{i\Xi K}{\Delta_r} + \frac{n}{\Delta_r}\frac{d\Delta_r}{dr} , \\
\mathscr{D}_n^\dagger &= \frac{\partial}{\partial r} + \frac{i\Xi K}{\Delta_r} + \frac{n}{\Delta_r}\frac{d\Delta_r}{dr} , \\
\mathscr{L}_n &= \frac{\partial}{\partial\theta} - \frac{\Xi H}{\Delta_\theta} + \frac{n}{\sqrt{\Delta_\theta}\sin\theta}\frac{d}{d\theta}\left(\sqrt{\Delta_\theta}\sin\theta\right) , \\
\mathscr{L}_n^\dagger &= \frac{\partial}{\partial\theta} + \frac{\Xi H}{\Delta_\theta} + \frac{n}{\sqrt{\Delta_\theta}\sin\theta}\frac{d}{d\theta}\left(\sqrt{\Delta_\theta}\sin\theta\right) ,
\end{aligned} \tag{2.2.22}
$$

with

$$
K = \omega(r^2+a^2) - am , \quad H = a\omega\sin\theta - \frac{m}{\sin\theta} , \tag{2.2.23}
$$

and where the following transformations have been made

$$
\phi_0 = \Phi_0 , \quad \phi_1 = \frac{1}{\sqrt{2}\bar{\rho}^*}\Phi_1 , \quad \phi_2 = \frac{1}{2(\bar{\rho}^*)^2}\Phi_2 . \tag{2.2.24}
$$

Note that the time and azimuthal dependence, $e^{-i\omega t + im\varphi}$, has been factored out. By acting with the operator $\sqrt{\Delta_\theta}(\mathscr{L}_0^\dagger + \frac{ia\sin\theta}{\bar{\rho}^*})$ on Eq. (2.2.18), and with the operator $(\mathscr{D}_0 + \frac{1}{\bar{\rho}^*})$ on Eq. (2.2.20), one obtains a decoupled equation for Φ_0 by eliminating Φ_1, i.e.

$$
[\sqrt{\Delta_\theta}\mathscr{L}_0^\dagger\sqrt{\Delta_\theta}\mathscr{L}_1 + \Delta_r\mathscr{D}_1\mathscr{D}_1^\dagger + 2i\omega\Xi\bar{\rho}]\Phi_0 = 0 , \tag{2.2.25}
$$

with aid of the identities

$$\begin{cases} \left(\mathscr{D}_0 + \dfrac{1}{\bar{\rho}^*}\right)\Delta_r\left(\mathscr{D}_1^\dagger - \dfrac{1}{\bar{\rho}^*}\right) = \Delta_r\mathscr{D}_1\mathscr{D}_1^\dagger + \dfrac{2i\Xi K}{\bar{\rho}^*} \ , \\ \sqrt{\Delta_\theta}\left(\mathscr{L}_0^\dagger + \dfrac{ia\sin\theta}{\bar{\rho}^*}\right)\sqrt{\Delta_\theta}\left(\mathscr{L}_1 - \dfrac{ia\sin\theta}{\bar{\rho}^*}\right) = \sqrt{\Delta_\theta}\mathscr{L}_0^\dagger\sqrt{\Delta_\theta}\mathscr{L}_1 - \dfrac{2ia\sin\theta}{\bar{\rho}^*}\Xi H \ . \end{cases}$$

Following the same procedure, by acting with the operator $\sqrt{\Delta_\theta}(\mathscr{L}_0 + \frac{ia\sin\theta}{\bar{\rho}^*})$ on Eq. (2.2.21) and with the operator $\Delta_r(\mathscr{D}_0^\dagger + \frac{1}{\bar{\rho}^*})$ on Eq. (2.2.19), Φ_1 is again eliminated so that we obtain a decoupled equation for Φ_2

$$[\sqrt{\Delta_\theta}\mathscr{L}_0\sqrt{\Delta_\theta}\mathscr{L}_1^\dagger + \Delta_r\mathscr{D}_0^\dagger\mathscr{D}_0 - 2i\omega\Xi\bar{\rho}]\Phi_2 = 0 \ , \tag{2.2.26}$$

with aid of the identities

$$\begin{cases} \Delta_r\left(\mathscr{D}_0^\dagger + \dfrac{1}{\bar{\rho}^*}\right)\left(\mathscr{D}_0 - \dfrac{1}{\bar{\rho}^*}\right) = \Delta_r\mathscr{D}_0^\dagger\mathscr{D}_0 - \dfrac{2i\Xi K}{\bar{\rho}^*} \ , \\ \sqrt{\Delta_\theta}\left(\mathscr{L}_0 + \dfrac{ia\sin\theta}{\bar{\rho}^*}\right)\sqrt{\Delta_\theta}\left(\mathscr{L}_1^\dagger - \dfrac{ia\sin\theta}{\bar{\rho}^*}\right) = \sqrt{\Delta_\theta}\mathscr{L}_0\sqrt{\Delta_\theta}\mathscr{L}_1^\dagger + \dfrac{2ia\sin\theta}{\bar{\rho}^*}\Xi H \ . \end{cases}$$

Now taking

$$\Phi_0 = R_{+1}(r)S_{+1}(\theta) \quad \text{and} \quad \Phi_2 = R_{-1}(r)S_{-1}(\theta) \ , \tag{2.2.27}$$

we finally obtain the Maxwell equations with separated variables

$$\left(\Delta_r\mathscr{D}_1\mathscr{D}_1^\dagger + 2i\omega\Xi r\right)R_{+1} = \lambda R_{+1} \ , \tag{2.2.28}$$

$$\left(\sqrt{\Delta_\theta}\mathscr{L}_0^\dagger\sqrt{\Delta_\theta}\mathscr{L}_1 - 2a\omega\Xi\cos\theta\right)S_{+1} = -\lambda S_{+1} \ , \tag{2.2.29}$$

and

$$\left(\Delta_r\mathscr{D}_0^\dagger\mathscr{D}_0 - 2i\omega\Xi r\right)R_{-1} = \lambda R_{-1} \ , \tag{2.2.30}$$

$$\left(\sqrt{\Delta_\theta}\mathscr{L}_0\sqrt{\Delta_\theta}\mathscr{L}_1^\dagger + 2a\omega\Xi\cos\theta\right)S_{-1} = -\lambda S_{-1} \ , \tag{2.2.31}$$

from Eqs. (2.2.25) and (2.2.26). Note that λ refers to the separation constant from now on, and should not be confused with the spin coefficient. Using the commutative property $\Delta_r\mathscr{D}_{n+1} = \mathscr{D}_n\Delta_r$, Eq. (2.2.28) can be rewritten as

$$\left(\Delta_r\mathscr{D}_0\mathscr{D}_0^\dagger + 2i\omega\Xi r\right)(\Delta_r R_{+1}) = \lambda\left(\Delta_r R_{+1}\right) \ , \tag{2.2.32}$$

which shows that $\Delta_r R_{+1}$ and R_{-1} satisfy complex conjugate equations, by comparing with Eq. (2.2.30).

The decoupled equations (2.2.18)- (2.2.21) provide solutions for Φ_0, Φ_1 and Φ_2. In particular, Φ_0 and Φ_2 can be separated into radial parts which satisfy Eqs. (2.2.28) and (2.2.30), and angular parts which satisfy Eqs. (2.2.29) and (2.2.31). The solution of Φ_1 is ignored for now and we will be back to this problem later. There is an additional issue to discuss, which is related to the solutions of Φ_0 and Φ_2.

As we have already shown in Eqs (2.2.30) and (2.2.32), Φ_0 and Φ_2 satisfy equations which are complex conjugate of each other, but the relative normalization between these two solutions still remains to be determined. The answer to this problem is given by the famous Starobinsky-Teukolsky identities. In the following we will address this issue by proving the Starobinsky-Teukolsky identities for the Maxwell field on the Kerr-AdS background.

Starobinsky-Teukolsky identities

Theorem 1. *$\bar{\mathscr{L}}_0\bar{\mathscr{L}}_1 S_{+1}$ is a constant multiple of S_{-1}, i.e. $\bar{\mathscr{L}}_0\bar{\mathscr{L}}_1 S_{+1} = BS_{-1}$,*
${\bar{\mathscr{L}}_0}^\dagger{\bar{\mathscr{L}}_1}^\dagger S_{-1}$ is a constant multiple of S_{+1}, i.e. ${\bar{\mathscr{L}}_0}^\dagger{\bar{\mathscr{L}}_1}^\dagger S_{-1} = BS_{+1}$.

Note that the new angular operators are defined as

$$\bar{\mathscr{L}}_n = \sqrt{\Delta_\theta}\mathscr{L}_n\ , \qquad {\bar{\mathscr{L}}_n}^\dagger = \sqrt{\Delta_\theta}\mathscr{L}_n^\dagger\ , \tag{2.2.33}$$

so that this theorem can be written in the same form as its counterpart for the Kerr background [109]. Also note that the two proportionality constants in this theorem have been set to the same (denoted by B), which is guaranteed if we normalize both S_{+1} and S_{-1} to unity, i.e.

$$\int_0^\pi S_{+1}^2 \sin\theta d\theta = \int_0^\pi S_{-1}^2 \sin\theta d\theta = 1\ . \tag{2.2.34}$$

Theorem 1 is proved in Appendix C with details, by taking $\bar{\mathscr{L}}_0\bar{\mathscr{L}}_1 S_{+1} = BS_{-1}$, as an example.

To evaluate B, we start by applying the operator ${\bar{\mathscr{L}}_0}^\dagger{\bar{\mathscr{L}}_1}^\dagger$ to the first expression in Theorem 1 and with aid of the second expression in this theorem, then we have

$$\begin{aligned}
B^2 S_{+1} &= {\bar{\mathscr{L}}_0}^\dagger{\bar{\mathscr{L}}_1}^\dagger\bar{\mathscr{L}}_0\bar{\mathscr{L}}_1 S_{+1} = {\bar{\mathscr{L}}_0}^\dagger(\bar{\mathscr{L}}_1 + 2\mathcal{Q}\sqrt{\Delta_\theta})({\bar{\mathscr{L}}_0}^\dagger - 2\mathcal{Q}\sqrt{\Delta_\theta})\bar{\mathscr{L}}_1 S_{+1} \\
&= {\bar{\mathscr{L}}_0}^\dagger\left(\bar{\mathscr{L}}_1{\bar{\mathscr{L}}_0}^\dagger - \frac{2}{\sin\theta}\frac{d}{d\theta}(\sin\theta H)\right)\bar{\mathscr{L}}_1 S_{+1} \\
&= {\bar{\mathscr{L}}_0}^\dagger\bar{\mathscr{L}}_1(2a\omega\Xi\cos\theta - \lambda)S_{+1} - 4a\omega\Xi{\bar{\mathscr{L}}_0}^\dagger\cos\theta\bar{\mathscr{L}}_1 S_{+1} \\
&= 2a\omega\Xi{\bar{\mathscr{L}}_0}^\dagger(\cos\theta\bar{\mathscr{L}}_1 - \sin\theta\sqrt{\Delta_\theta})S_{+1} - \lambda{\bar{\mathscr{L}}_0}^\dagger\bar{\mathscr{L}}_1 S_{+1} - 4a\omega\Xi{\bar{\mathscr{L}}_0}^\dagger\cos\theta\bar{\mathscr{L}}_1 S_{+1}
\end{aligned}$$

$$
\begin{aligned}
&= -2a\omega\Xi(\cos\theta\bar{\mathscr{L}}_0^{\dagger} - \sin\theta\sqrt{\Delta_\theta})\bar{\mathscr{L}}_1 S_{+1} - 2a\omega\Xi\sin\theta\sqrt{\Delta_\theta}\bar{\mathscr{L}}_1^{\dagger} S_{+1} - \lambda\bar{\mathscr{L}}_0^{\dagger}\bar{\mathscr{L}}_1 S_{+1} \\
&= -(2a\omega\Xi\cos\theta + \lambda)\bar{\mathscr{L}}_0^{\dagger}\bar{\mathscr{L}}_1 S_{+1} + 2a\omega\Xi\sin\theta\sqrt{\Delta_\theta}(\bar{\mathscr{L}}_1 - \bar{\mathscr{L}}_1^{\dagger}) S_{+1} \\
&= -(2a\omega\Xi\cos\theta + \lambda)(2a\omega\Xi\cos\theta - \lambda) S_{+1} - 4a\omega\sin\theta\Xi^2 H S_{+1} \\
&= \left(\lambda^2 - 4\omega^2\Xi^2(a^2 - \frac{am}{\omega})\right) S_{+1} \ , \qquad (2.2.35)
\end{aligned}
$$

where the angular equation (2.2.29) was used in the above derivations, and $\mathcal{Q}$ is defined as

$$\mathcal{Q} = \frac{\Xi H}{\Delta_\theta} \ . \qquad (2.2.36)$$

Eq. (2.2.35) finally gives the value of B, i.e.

$$B^2 = \lambda^2 - 4\omega\Xi^2(\omega a^2 - ma) \ . \qquad (2.2.37)$$

The sign of B can be fixed by comparing with the spherical case ($a = 0$) when the angular functions reduce to the spin-weighted spherical harmonics [122]. This comparison requires us to choose the positive square root in Eq. (2.2.37).

Theorem 2. *$\Delta_r\mathscr{D}_0\mathscr{D}_0 R_{-1}$ is a constant multiple of $\Delta_r R_{+1}$, i.e. $\Delta_r\mathscr{D}_0\mathscr{D}_0 R_{-1} = B\Delta_r R_{+1}$, $\Delta_r\mathscr{D}_0^{\dagger}\mathscr{D}_0^{\dagger}\Delta_r R_{+1}$ is a constant multiple of R_{-1}, i.e. $\Delta_r\mathscr{D}_0^{\dagger}\mathscr{D}_0^{\dagger}\Delta_r R_{+1} = BR_{-1}$.*

The proportionality stated in this theorem can be proved as follows, by taking the first expression as an example. By applying the operator $\mathscr{D}_0\mathscr{D}_0$ to Eq. (2.2.30), we have

$$
\begin{aligned}
\lambda\mathscr{D}_0\mathscr{D}_0 R_{-1} &= \mathscr{D}_0\mathscr{D}_0(\Delta_r\mathscr{D}_0^{\dagger}\mathscr{D}_0 - 2i\omega\Xi r) R_{-1} \\
&= \mathscr{D}_0\mathscr{D}_0\Delta_r\mathscr{D}_0\mathscr{D}_0 R_{-1} + 2i\Xi\mathscr{D}_0\mathscr{D}_0 K\mathscr{D}_0 R_{-1} - 2i\omega\Xi\mathscr{D}_0\mathscr{D}_0(rR_{-1}) \\
&= \mathscr{D}_0\Delta_r\mathscr{D}_1\mathscr{D}_0\mathscr{D}_0 R_{-1} + 2i\Xi\mathscr{D}_0(K\mathscr{D}_0 + 2\omega r)\mathscr{D}_0 R_{-1} - 2i\omega\Xi\mathscr{D}_0\mathscr{D}_0(rR_{-1}) \\
&= \mathscr{D}_0(\Delta_r\mathscr{D}_1 + 2i\Xi K)\mathscr{D}_0\mathscr{D}_0 R_{-1} + 2i\omega\Xi(2\mathscr{D}_0 r\mathscr{D}_0 R_{-1} - r\mathscr{D}_0\mathscr{D}_0 R_{-1} + 2\mathscr{D}_0 R_{-1}) \\
&= \mathscr{D}_0\Delta_r\mathscr{D}_1^{\dagger}\mathscr{D}_0\mathscr{D}_0 R_{-1} + 2i\omega\Xi r\mathscr{D}_0\mathscr{D}_0 R_{-1} \\
&= (\Delta_r\mathscr{D}_1\mathscr{D}_1^{\dagger} + 2i\omega\Xi r)(\mathscr{D}_0\mathscr{D}_0 R_{-1}) \ . \qquad (2.2.38)
\end{aligned}
$$

Therefore, $\mathscr{D}_0\mathscr{D}_0 R_{-1}$ satisfies the same equation as R_{+1}, by comparing with Eq. (2.2.28). The second part in this theorem can be proved following the same logic. Notice that the constants of proportionality in this theorem have been fixed to B, the same constant used in Theorem 1. This fact, indeed, is a consequence of Theorem 1, and can be understood as follows. The Maxwell scalars Φ_0 and Φ_2 are governed by their equations (2.2.25) and (2.2.26),

but their relative normalization is still undetermined. To obtain this relative normalization constant, by applying the operator $\sqrt{\Delta_\theta}(\mathscr{L}_0 + ia\sin\theta/\bar{\rho}^*)$ to Eq. (2.2.18) and $(\mathscr{D}_0 + 1/\bar{\rho}^*)$ to Eq. (2.2.19), and eliminating Φ_1, we obtain

$$\left(\mathscr{D}_0 + \frac{1}{\bar{\rho}^*}\right)\left(\mathscr{D}_0 - \frac{1}{\bar{\rho}^*}\right)\Phi_2 = \sqrt{\Delta_\theta}\left(\mathscr{L}_0 + \frac{ia\sin\theta}{\bar{\rho}^*}\right)\sqrt{\Delta_\theta}\left(\mathscr{L}_1 - \frac{ia\sin\theta}{\bar{\rho}^*}\right)\Phi_0 \tag{2.2.39}$$

which can be further simplified

$$\mathscr{D}_0\mathscr{D}_0\Phi_2 = \bar{\mathscr{L}}_0\bar{\mathscr{L}}_1\Phi_1 \ , \tag{2.2.40}$$

with aid of the commutative property of the angular operator

$$\sqrt{\Delta_\theta}\sin\theta\mathscr{L}_{n+1} = \mathscr{L}_n\sqrt{\Delta_\theta}\sin\theta \ . \tag{2.2.41}$$

With the field decompositions (2.2.27) and the identity $\bar{\mathscr{L}}_0\bar{\mathscr{L}}_1 S_{+1} = BS_{-1}$ in Theorem 1, Eq. (2.2.40) becomes

$$\mathscr{D}_0\mathscr{D}_0 R_{-1} = BR_{+1} \ . \tag{2.2.42}$$

This gives the first identity in Theorem 2, by multiplying Δ_r on both sides.

The solution for Φ_1

To complete the solutions, now we step back to look for the solution for Φ_1. We start from Eq. (2.2.18), by multiplying $\bar{\rho}^*$ on both sides, then we have

$$\Big(\bar{\rho}^*\mathscr{D}_0 + 1\Big)\Phi_1 = \Big(\bar{\rho}^*\bar{\mathscr{L}}_1 - ia\sin\theta\sqrt{\Delta_\theta}\Big)\Phi_0 \ , \tag{2.2.43}$$

which, from the definition of $\mathscr{D}_0$, may be rewritten as

$$\mathscr{D}_0\Big(\bar{\rho}^*\Phi_1\Big) = \Big(\bar{\rho}^*\bar{\mathscr{L}}_1 - ia\sin\theta\sqrt{\Delta_\theta}\Big)\Phi_0 \ . \tag{2.2.44}$$

Then multiplying by Δ_r and expanding Φ_0 as in Eq. (2.2.27), Eq. (2.2.44) becomes

$$\begin{aligned}
\Delta_r\mathscr{D}_0\Big(\bar{\rho}^*\Phi_1\Big) &= \Big(\bar{\rho}^*\bar{\mathscr{L}}_1 - ia\sin\theta\sqrt{\Delta_\theta}\Big)\Big(\Delta_r\Phi_0\Big) \\
&= r\Big(\Delta_r R_{+1}\Big)\bar{\mathscr{L}}_1 S_{+1} - ia\Big(\Delta_r R_{+1}\Big)\Big(\cos\theta\bar{\mathscr{L}}_1 S_{+1} + \sin\theta\sqrt{\Delta_\theta}S_{+1}\Big) \\
&= \Delta_r\Big(\mathscr{D}_0 g_{+1}\bar{\mathscr{L}}_1 S_{+1} - iaf_{-1}\mathscr{D}_0\mathscr{D}_0 P_{-1}\Big) \ ,
\end{aligned} \tag{2.2.45}$$

which gives

$$\mathscr{D}_0\Big(\bar{\rho}^*\Phi_1\Big) = \mathscr{D}_0\Big(g_{+1}\bar{\mathscr{L}}_1 S_{+1} - iaf_{-1}\mathscr{D}_0 P_{-1}\Big) \ , \tag{2.2.46}$$

where we defined

$$g_{+1} = \frac{1}{B}\Big(r\mathscr{D}_0 P_{-1} - P_{-1}\Big) \,, \tag{2.2.47}$$

$$f_{-1} = \frac{1}{B}\left(\cos\theta\bar{\mathscr{L}}_1 S_{+1} + \sin\theta\sqrt{\Delta_\theta}S_{+1}\right) \,, \tag{2.2.48}$$

and

$$\Delta_r\Phi_0 \equiv P_{+1}S_{+1} \,, \quad \Phi_2 \equiv P_{-1}S_{-1} \,, \tag{2.2.49}$$

and where the Starobinski-Teukolsky identity in Theorem 2, i.e.

$$\Delta_r\mathscr{D}_0\mathscr{D}_0 P_{-1} = BP_{+1} \,, \tag{2.2.50}$$

has been used.

Applying a similar procedure to Eq. (2.2.19), we obtain

$$\bar{\mathscr{L}}_0\Big(\bar{\rho}^*\Phi_1\Big) = \bar{\mathscr{L}}_0\Big(g_{+1}\bar{\mathscr{L}}_1 S_{+1} - iaf_{-1}\mathscr{D}_0 P_{-1}\Big) \,. \tag{2.2.51}$$

By comparing Eqs. (2.2.46) and (2.2.51), and considering that $\mathscr{D}_0$ is the differential operator only for the radial part while $\bar{\mathscr{L}}_0$ is the differential operator only for the angular part, we conclude that*

$$\bar{\rho}^*\Phi_1 = g_{+1}\bar{\mathscr{L}}_1 S_{+1} - iaf_{-1}\mathscr{D}_0 P_{-1} \,, \tag{2.2.52}$$

which determines Φ_1 uniquely. This equation is relevant to derive the angular momentum flux for the Maxwell field on Kerr-AdS background, see Appendix D for details.

Although the scalar Φ_1 is obtained in Eq. (2.2.52), $\bar{\mathscr{L}}_1 S_{+1}$ is still yet unknown. Indeed $\bar{\mathscr{L}}_1 S_{+1}$ can be expressed in terms of S_{+1} and S_{-1}, by

$$\begin{cases} \bar{\mathscr{L}}_1 S_{+1} = \dfrac{(2a\omega\Xi\cos\theta - \lambda)S_{+1} - BS_{-1}}{2\sqrt{\Delta_\theta}\mathcal{Q}} \,, & (2.2.53) \\ {\bar{\mathscr{L}}_1}^\dagger S_{-1} = \dfrac{(2a\omega\Xi\cos\theta + \lambda)S_{-1} + BS_{+1}}{2\sqrt{\Delta_\theta}\mathcal{Q}} \,, & (2.2.54) \end{cases}$$

where B and $\mathcal{Q}$ are given in Eqs. (2.2.37) and (2.2.36).

To prove Eq. (2.2.53), we start from Eq. (2.2.29),

$$\Big({\bar{\mathscr{L}}_0}^\dagger\bar{\mathscr{L}}_1 - 2a\omega\Xi\cos\theta + \lambda\Big)S_{+1} = 0 \Rightarrow \Big(\bar{\mathscr{L}}_0 + 2\mathcal{Q}\sqrt{\Delta_\theta}\Big)\bar{\mathscr{L}}_1 S_{+1} + (\lambda - 2a\omega\Xi\cos\theta)\,S_{+1} = 0 \,, \tag{2.2.55}$$

*Strictly, we could add an extra function, say F, satisfying homogenous equations $\mathscr{D}_0(F) = \bar{\mathscr{L}}_0(F) = 0$, to the solution of Φ_1 in Eq. (2.2.52). The solution of F, however, is singular at $\theta = 0$ and $\theta = \pi/2$, similar to the Kerr case [109]. Therefore, we have not included F in the solution for Φ_1.

and considering $\bar{\mathscr{L}}_0\bar{\mathscr{L}}_1 S_{+1} = BS_{-1}$ in Theorem 2, we obtain

$$BS_{-1} + 2\mathcal{Q}\sqrt{\Delta_\theta}\bar{\mathscr{L}}_1 S_{+1} + (\lambda - 2a\omega\Xi\cos\theta)\, S_{+1} = 0\,, \tag{2.2.56}$$

which finally gives Eq. (2.2.53). Following a similar procedure, Eq. (2.2.54) can be proved.

Part I

Scalar and Proca fields on asymptotically flat spacetimes

Chapter 3

Proca field equations

In the first part of this thesis, we are going to study Hawking radiation, for neutral and charged Proca fields; and quasi-bound states, for charged scalar and Proca fields. To explore these problems on a particular background, the first step is to obtain the wave equations for those fields. Two key properties that will allow the study of these wave equations are: separation of variables and decoupling of degrees of freedom. For scalar fields, which are governed by the Klein-Gordon equation, there is only one degree of freedom, and variables in general can be separated on Kerr-like spacetimes [123]. This is in part the reason why scalar fields have been explored so intensively in the literature*. The situation becomes complicated for massive bosonic fields, with spin.

In the standard model of particle physics (SM), massive spin-1 (Proca) fields describe the Z and W particles, where the former is neutral and the latter is charged. Perturbations of a neutral Proca field were first studied in [126, 127] on spherically symmetric backgrounds. In these studies only the $\ell = 0$ mode was considered since the corresponding wave equation is directly decoupled and separated. Later on by using the Kodama-Ishibashi formalism, see Section 2.1 for details, we were able to obtain a set of equations on D-dimensional spherically symmetric backgrounds, to cover all the possible modes for both neutral and charged Proca fields. This was done in the context of Hawking radiation and quasi-bound states [87,128,129]. Similar equations for neutral Proca fields on Schwarzschild BHs were shortly after obtained

*It is now known that at least one fundamental scalar field exists in Nature with the discovery of the Higgs boson [124, 125].

using different perturbation variables, and these equations were applied to study quasinormal modes and quasi-bound states [130]. In the Kerr background, separation of variables for Proca fields can be only achieved in the slow rotation limit, and the corresponding coupled wave equations were obtained in [131, 132], to study superradiant instabilities. A fully numerical study of the BH-Proca system was recently implemented [133], in nonrotating spacetimes.

In this chapter, we present a complete set of Proca equations on spherically symmetric backgrounds, by using the Kodama-Ishibashi formalism introduced in Section 2.1.

We start by describing scalar and Proca fields, which may be complex and charged under a $U(1)$ electromagnetic field, with the Lagrangian

$$\mathcal{L} = -(\mathcal{D}_\mu \Psi)^* \mathcal{D}^\mu \Psi - \mu_s^2 \Psi^* \Psi - \frac{1}{2} W^\dagger_{\mu\nu} W^{\mu\nu} - \mu_p^2 W^\dagger_\mu W^\mu - iq W^\dagger_\mu W_\nu F^{\mu\nu} \,, \tag{3.0.1}$$

where $W_{\mu\nu} = \mathcal{D}_\mu W_\nu - \mathcal{D}_\nu W_\mu$, $\mathcal{D}_\mu \equiv \partial_\mu - iqA_\mu$ and the field charge is q^*. Scalar and Proca fields are denoted by Ψ and W_μ, with mass μ_s and μ_p, respectively. As one observes from the above Lagrangian, both scalar and Proca fields are coupled to the electromagnetic potential A_μ through the gauge covariant derivative, while the latter one also couples to the electromagnetic field strength tensor $F_{\mu\nu} = \partial_\mu A_\nu - \partial_\nu A_\mu$, as determined by gauge invariance in the SM.

The equations of motion for Proca fields, when all the background fields are fixed, are

$$\frac{1}{\sqrt{-g}} \mathcal{D}_\nu \left(\sqrt{-g} W^{\mu\nu} \right) + \mu_p^2 W^\mu + iq W_\nu F^{\mu\nu} = 0 \,. \tag{3.0.2}$$

For the gravitational background with an Einstein symmetric space shown in Eq. (2.1.1), the Kodama-Ishibashi formalism [99] can be applied. For a Proca field $W_\mu = \{W_a, W_i\}$, W_a are m-scalars, with respect to the Einstein space σ_n, so they must obey the scalar eigenvalue equations (2.1.11). W_i is a covector field, so it can be decomposed into a scalar Φ obeying the scalar eigenvalue equation (2.1.11), and a transverse covector W_i^T obeying the vector eigenvalue equation (2.1.12).

This decomposition allows for an expansion of the various degrees of freedom $\{W_a, \Phi, W_i^T\}$ in a basis of harmonics of the Einstein space. Furthermore, this decomposition allows for a decoupling of the field equations into an independent vector mode W_i^T and $m+1$ coupled scalar

*In general, scalar and Proca fields may have different charge. Since they will be studied separately, for simplicity here we denote both charges by the same symbol q.

fields for each set of quantum numbers labeling the basis of harmonic functions. Observe, however, that not all these modes correspond to physically independent degrees of freedom, as we will show.

In the following we shall consider, separately, two cases according to the scalar eigenvalue, i.e. κ_s.

3.1 Modes with $\kappa_s \neq 0$

Expanding the field equations (3.0.2), with the decomposition (2.1.10) for W_i, and using conditions (2.1.11) for $\{W_a, \Phi\}$ and (2.1.12) for W_i^T, we obtain

$$\frac{\kappa_s^2}{r^2}B_a + \frac{h_{af}}{r^n}\mathcal{D}_b\left[h^{db}h^{cf}r^n\left(\mathcal{D}_cB_d - \mathcal{D}_dB_c\right)\right] - \mu_p^2 B_a - \mathcal{D}_a\left[\frac{1}{r^{n-2}}\mathcal{D}_b\left(r^{n-2}h^{bc}B_c\right)\right] + iqB_bF_a{}^b$$
$$= 0 \ , \tag{3.1.1}$$

$$\frac{1}{r^{n-2}}\mathcal{D}_a\left(r^{n-2}h^{ab}B_b\right) - \mu_p^2\Phi = 0 \ , \tag{3.1.2}$$

$$\left[\frac{1}{r^2}\left(\kappa_v^2 + \frac{\hat{R}}{n}\right) + \mu_p^2 + \frac{1}{r^{n-2}}\mathcal{D}_a\left(r^{n-2}h^{ab}\mathcal{D}_b\right)\right]\hat{W}^{Tj} = 0 \ , \tag{3.1.3}$$

with definition* $B_a \equiv W_a - \mathcal{D}_a\Phi$, and $\hat{W}^{Ti} = r(y)^2 W^{Ti}$.

We consider the spherically symmetric case, by specifying the metric in Eq. (2.1.1) with $\{y^a\} = \{t, r\}$, $|h| = 1$, h_{ab} is diagonal, $h_{tt} = -1/h_{rr} \equiv -V$. Since Φ is given by the second equation in terms of the other fields, it is a non-dynamical degree of freedom. In four dimensions, this agrees with the fact that a spin-1 massive field has three possible physical polarizations which in this case will be the two dynamical scalars and the transverse vector. In higher dimensions we will see that the transverse vector on the n-sphere contains more (degenerate) polarizations.

We can factor out the spherical harmonics through the decomposition

$$B_a = \beta_a^\Lambda(y)\mathcal{Y}_\Lambda(x) \ ,$$
$$\hat{W}^{Ti} = q^\Lambda(y)\mathcal{Y}_\Lambda^i(x) \ , \tag{3.1.4}$$

*Here we use the variables B_a, since Φ can be determined by B_a and becomes a non-dynamical degree of freedom, as shown in Eq. (3.1.2).

where $\mathcal{Y}_\Lambda$ is the scalar harmonic function with the definition (2.1.14), $\mathcal{Y}^i_\Lambda$ is the vector harmonic function with the definition (2.1.16), and Λ denotes the mode eigenvalues for the corresponding harmonic functions. Furthermore, making the ansatz

$$\beta_t^\Lambda = e^{-i\omega t}\psi(r)\ , \qquad \beta_r^\Lambda = e^{-i\omega t}\frac{\chi(r)}{V}\ , \qquad q^\Lambda = e^{-i\omega t}\Upsilon(r)\ ,$$

and using Eqs. (3.1.1) and (3.1.3), we obtain*

$$\left[V^2\frac{d}{dr}\left(\frac{1}{r^{n-2}}\frac{d}{dr}r^{n-2}\right)+(\omega+qA_t)^2-\left(\frac{\kappa_s^2}{r^2}+\mu_p^2\right)V\right]\chi - i\left((\omega+qA_t)V'+2qA_t\frac{V}{r}\right)\psi = 0\ , \tag{3.1.5}$$

$$\left[\frac{V^2}{r^n}\frac{d}{dr}\left(r^n\frac{d}{dr}\right)+(\omega+qA_t)^2-\left(\frac{\kappa_s^2}{r^2}+\mu_p^2\right)V\right]\psi + i\left(\frac{2\omega V}{r}-(\omega+qA_t)V'\right)\chi = 0\ , \tag{3.1.6}$$

$$\left[\frac{V}{r^{n-2}}\frac{d}{dr}\left(r^{n-2}V\frac{d}{dr}\right)+(\omega+qA_t)^2-\left(\frac{\kappa_v^2+\frac{\hat{R}}{n}}{r^2}+\mu_p^2\right)V\right]\Upsilon = 0\ , \tag{3.1.7}$$

where A_t is the only nonvanishing component of electromagnetic potential due to the spherically symmetric background. Thus we obtain two second order coupled radial equations for $\{\psi,\chi\}$ and a decoupled equation for Υ. Note that $\kappa_s^2=\ell(\ell+n-1)$ and $\kappa_v^2=\ell(\ell+n-1)-1$ with ℓ starting at zero and one respectively. The third combination is $\kappa_v^2+\frac{\hat{R}}{n}=\ell(\ell+n-1)+n-2$.

The manipulations leading to the two coupled equations above are only valid for non-zero μ_p. In the exactly massless theory, a similar calculation leads to a single decoupled equation for one of the scalar modes which is

$$\left[V\frac{d}{dr}\left(\frac{V}{r^{n-2}}\frac{d}{dr}r^{n-2}\right)-\frac{2qd_rA_tV^2}{(\omega+qA_t)r^{n-2}}\frac{d}{dr}r^{n-2}+\Big(\omega+qA_t\Big)^2-\frac{\kappa_s^2}{r^2}V\right]\chi=0\ , \tag{3.1.8}$$

whereas the other mode $\psi = iVd_r(r^{n-2}\chi)/((\omega+qA_t)r^{n-2})$ becomes non-dynamical†. Here $d_r\equiv d/dr$. The transverse mode – described by equation (3.1.7) – remains the same for any μ_p; in particular, for $\mu_p=0$, and (only) $n=2$ it becomes equivalent to (3.1.8). This will be manifest in the numerical results.

*Note that there is a symmetry for the coupled system, i.e. for real ω, if (ψ,χ) is a solution to the equations, $(-\psi^*,\chi^*)$ is also a solution. For complex ω, this statement still can be made as: if $(\psi,\chi)e^{-i\omega t}$ is a solution to the equations, then $(-\psi^*,\chi^*)e^{-i\omega^* t}$ is also a solution.

†Note that the coupled equations have only one dynamical degree of freedom in the massless limit. One can use either ψ or χ to describe the dynamical mode, then the other one becomes non-dynamical and is determined in terms of the dynamical mode.

3.2 Modes with $\kappa_s = 0$

For the exceptional modes with $\kappa_s = 0$, Φ does not enter the wave equation so it is a free non-dynamical field. The corresponding equation for $W_a^{(0)}$ is (the superscript denotes it is the exceptional mode)

$$\frac{h_{af}}{r^n\sqrt{|h|}}\mathcal{D}_b\left[h^{db}h^{cf}r^n\sqrt{|h|}\left(\mathcal{D}_cW_d^{(0)}-\mathcal{D}_dW_c^{(0)}\right)\right]+\mu_p^2W_a^{(0)}+iqW_b^{(0)}F_a{}^b=0\,. \tag{3.2.1}$$

When $\mu_p^2 \neq 0$ one uses an ansatz similar to the previous section to obtain a radial equation for a dynamical degree of freedom

$$\left[\frac{\mu_p^2}{r^n}\frac{d}{dr}\left(\frac{r^nV}{(\omega+qA_t)^2-\mu_p^2V}\frac{d}{dr}\right)+\frac{\mu_p^2}{V}+\frac{\mu_p^2qd_rA_t}{((\omega+qA_t)^2-\mu_p^2V)^2}\Big(2qVd_rA_t-(\omega+qA_t)V'\Big)\right.$$
$$\left.-\frac{\omega+qA_t}{r^n((\omega+qA_t)^2-\mu_p^2V)}\frac{d}{dr}\Big(qr^nd_rA_t\Big)\right]\psi^{(0)}=0\,, \tag{3.2.2}$$

and a non-dynamical one,

$$\chi^{(0)}=\frac{iV}{(\omega+qA_t)^2-\mu_p^2V}\Big((\omega+qA_t)d_r\psi^{(0)}-q\psi^{(0)}d_rA_t\Big)\,,$$

where $d_r \equiv d/dr$. Otherwise, for $\mu_p^2 = 0$, we recover the well known result that all the exceptional modes are non-dynamical (see e.g. [127]).

Now that we have covered all possibilities, several comments are in order. First there is a discrete difference between the small mass limit and the exactly massless theory since we have different sets of equations for each case. This should not be surprising since there is an extra longitudinal mode for massive vector bosons. Second, the equations for the Maxwell theory case are all decoupled, in agreement with previous work [134].

With all of the Proca equations at hand, we are going to apply them to study Hawking radiation in Chapter 4 for a neutral Proca field, and in Chapter 5 for a charged Proca field. In Chapter 6, we will then apply them to the computation of quasi–bound states in the Reissner-Nordström BH.

Chapter 4

Hawking radiation for a Proca field: neutral case

4.1 Introduction

Hawking radiation, as we described in Section 1.2, is an interesting quantum phenomenon. It has been widely studied on different backgrounds, for various types of emitting particles, and in diverse gravitational theories. In particular, the study of Hawking radiation from higher-dimensional BHs has gained a lot attention recently, motivated by the possibility of producing microscopic BHs at the LHC. This is a prediction of TeV gravity scenarios in which the fundamental Planck scale could be as low as the TeV scale. This motivation led to an intensive study of Hawking radiation from higher-dimensional BHs [128, 129, 135–147].

One of the Hawking radiation channels that has not been properly addressed in the literature is that of massive vector bosons, both neutral and charged, to describe the emission of Z and $W^{\pm}$ particles of the SM. The basic difficulty is that the Proca equations do not decouple even in a spherically symmetric BH background*. To bridge this gap, in this chapter, we study Hawking radiation for a neutral Proca field, by solving the Proca equations derived in Chapter 3, in the background of a D-dimensional spherically symmetric Schwarzschild BH [148].

*In a rotating background, it appears that the Proca field can neither be decoupled nor separated.

In order to perform such a study, we have designed a numerical strategy to solve the coupled equations* without decoupling and showed that the coupled system may be treated by an **S**-matrix type formalism which allows decoupling in the asymptotic regions. This **S**-matrix is used to define a transmission matrix which gives the transmission factors as its eigenvalues. We have computed transmission factors for various modes, masses and spacetime dimensions. The mass term lifts the degeneracy between transverse modes, in $D = 4$, and excites the longitudinal modes, in particular the s-wave. Moreover, it increases the contribution of waves with larger ℓ, which can be dominant at intermediate energies. The transmission factors are then used to obtain the Hawking fluxes in this channel.

This chapter is organized as follows. In Section 4.2 we study the near horizon and far region asymptotic behaviors of the coupled Proca equations, which can be used to extract relevant information to study Hawking radiation. In Section 4.3 we discuss how the scattering matrix is used to compute the transmission factor and the Hawking spectrum. In Section 4.4 we discuss the numerical method and results, and we summarize our results in Section 4.5. Some technical relations are left to Appendix A.

4.2 Boundary conditions and radial system

In this section, we study the wave equation for a neutral Proca field by setting the field charge $q = 0$ in all the field equations derived in Chapter 3, i.e. Eqs. (3.1.5), (3.1.6), (3.1.8) and (3.2.2), in the Schwarzschild-Tangherlini background with the metric function $V = 1 - \frac{M}{r^{n-1}}$. In the numerics, we choose units such that the horizon radius is $r_H = 1$, so then $M = r_H^{n-1}$. Since decoupled radial equations have been extensively studied in the literature we will not present the details of our analysis of such modes and refer to the method in [146,147]. Thus in the following we will focus on the solutions of the coupled system for the massive theory, which will be used in conjunction with the decoupled modes to obtain the full Hawking spectrum in Section 4.4.

We start by finding a series expansion of the solution near the horizon for the coupled system $\{\psi, \chi\}$. This will be used to initialize the corresponding fields for the radial integration at

*The decoupled equations have been solved simultaneously.

$r = 1.001$. If we define $y = r - 1$, Eqs. (3.1.5) and (3.1.6) become

$$\left[M(r)\frac{d^2}{dy^2} + N(r)\frac{d}{dy} + P(r)\right]\psi + Q(r)\chi = 0 \ , \tag{4.2.1}$$

$$\left[\tilde{M}(r)\frac{d^2}{dy^2} + \tilde{N}(r)\frac{d}{dy} + \tilde{P}(r)\right]\chi + \tilde{Q}(r)\psi = 0 \ , \tag{4.2.2}$$

where the polynomials are defined in Appendix A. Making use of Frobenius' method to expand ψ and χ as

$$\psi = y^\rho \sum_{j=0}^{\infty} \mu_j y^j \ , \qquad \chi = y^\rho \sum_{j=0}^{\infty} \nu_j y^j \ , \tag{4.2.3}$$

and inserting the above two equations into Eqs. (4.2.1) and (4.2.2), we obtain

$$\rho = \pm\frac{i\omega}{n-1} \ \text{ or } \ \rho = 1 \pm \frac{i\omega}{n-1} \ . \tag{4.2.4}$$

We want to impose an ingoing boundary condition at the horizon, so we must choose the minus sign. Furthermore, after this sign choice, the right hand side solution produces a series expansion which is a special case of the left hand side (where the first coefficient is set to zero), so without loss of generality we choose $\rho = -i\omega/(n-1)$. One then writes down the recurrence relations and concludes that a general solution, close to the horizon, can be parameterized by the two coefficients ν_0 and ν_1. The other coefficients are generated by the recurrence relations (A.0.1).

To understand the asymptotic behavior of the waves at infinity we now study a large r asymptotic expansion in the form

$$\psi = e^{\beta r} r^p \sum_{j=0} \frac{a_j}{r^j} \ , \qquad \chi = e^{\beta r} r^p \sum_{j=0} \frac{b_j}{r^j} \ . \tag{4.2.5}$$

Inserting this into Eqs. (3.1.5) and (3.1.6) we obtain, at leading order,

$$\beta = \pm ik \ , \qquad k = \sqrt{\omega^2 - \mu_p^2} \ , \qquad p = 1 - \frac{n}{2} \pm i\varphi \ \text{ or } \ p = -\frac{n}{2} \pm i\varphi \ , \tag{4.2.6}$$

where $\varphi = \delta_{n,2}(\omega^2 + k^2)/(2k)$. Thus one can show that asymptotically*

$$\psi \to \frac{1}{r^{\frac{n}{2}-1}}\left[\left(a_0^+ + \frac{a_1^+}{r} + \dots\right)e^{i\Phi} + \left(a_0^- + \frac{a_1^-}{r} + \dots\right)e^{-i\Phi}\right] \ ,$$

$$\chi \to \frac{1}{r^{\frac{n}{2}-1}}\left[\left(\left(-\frac{k}{\omega} + \frac{c^+}{r}\right)a_0^+ + \dots\right)e^{i\Phi} + \left(\left(\frac{k}{\omega} + \frac{c^-}{r}\right)a_0^- + \dots\right)e^{-i\Phi}\right] \ , \tag{4.2.7}$$

*We have used, without loss of generality, the leading power behavior for p and discarded the second option which produces the same solution, similarly to the near horizon expansion.

where $\Phi \equiv kr + \varphi \log r$ and $c^{\pm}$ is defined in the Appendix, Eq. (A.0.2). So as expected, each field is a combination of ingoing and outgoing waves at infinity. This asymptotic expansion also shows that, for a generic wave at infinity, we can choose four independent constants $\left\{a_0^{\pm}, a_1^{\pm}\right\}$ to characterize the solution. This is expected, since we have two coupled scalar fields and for each scalar degree of freedom we must have an associated ingoing wave and outgoing wave. Thus we can define four new fields $\{\chi^{\pm}, \psi^{\pm}\}$ (which will asymptote respectively to $\left\{a_0^{\pm}, a_1^{\pm}\right\}$), by truncating the expansion for the fields and for their first derivatives at infinity. Such a transformation can be written in matrix form by defining the 4-vector $\mathbf{\Psi}^T = (\psi_+, \psi_-, \chi_+, \chi_-)$ for the new fields, and another 4-vector $\mathbf{V}^T = (\psi, d_r\psi, \chi, d_r\chi)$ for the original fields and derivatives. Then the transformation is given in terms of an r-dependent matrix $\mathbf{T}$ defined through

$$\mathbf{V} = \mathbf{T}\mathbf{\Psi} \ , \tag{4.2.8}$$

which we provide in the Appendix, Eq. (A.0.3). In order to obtain a first order system of ordinary differential equations (ODEs) for the new fields, we first define a matrix $\mathbf{X}$ through

$$\frac{d\mathbf{V}}{dr} = \mathbf{X}\mathbf{V} \ , \tag{4.2.9}$$

which is read out from the original system in Eqs. (3.1.5) and (3.1.6). Its explicit form is given in the Appendix, Eq. (A.0.4). Then we obtain

$$\frac{d\mathbf{\Psi}}{dr} = \mathbf{T}^{-1}\left(\mathbf{X}\mathbf{T} - \frac{d\mathbf{T}}{dr}\right)\mathbf{\Psi} \ . \tag{4.2.10}$$

We can write other equivalent systems using different $\mathbf{T}$ matrices. In particular, we have also integrated a first order system using the fields $\psi_s = k\psi - isd_r\psi$ and $\chi_s = k\chi - isd_r\chi$ with $s = \pm$, which produced numerically equivalent results. The only difference is that for such fields we need to extract $\mathcal{O}(r^{-1})$ coefficients to obtain a_1^s.

4.3 The Hawking spectrum

The boundary conditions we have chosen in Section 4.2 are suitable for the computation of the Hawking spectrum of radiated quanta from the BH. The Hawking spectrum is generically given by a sum over a complete set of modes with labels ζ, of the transmission factor $\mathbb{T}_\zeta$ times a thermal average number of quanta produced at the horizon $\langle n_\zeta \rangle$. This is defined for a basis

of decoupled modes. In our problem, we have a sub-set of modes, the transverse vector mode, and the $\ell = 0$ ($\kappa_s = 0$) mode, which are decoupled. But we also have a tower of modes which are coupled two by two for each $\ell > 0$, the two scalars ψ and χ. It is not obvious how to decouple them for all r through an explicit transformation. Instead, let us try to understand how to extract the relevant information in the asymptotic regions.

Let us denote the two coupled fields by a 2-vector $\mathbf{U^T} = (\psi, \chi)$ and represent the coupled system of radial equations through a (linear) second order matrix differential operator $\mathcal{D}^{(2)}$ acting on $\mathbf{U}$, i.e. $\mathcal{D}^{(2)}\mathbf{U} = 0$. The system is coupled because of the off diagonal elements of the $\mathcal{D}^{(2)}$ operator. To decouple the system we would have to find a transformation of the fields $\mathbf{U} = \mathcal{A}\bar{\mathbf{U}}$, such that the new differential operator $\bar{\mathcal{D}}^{(2)} = \mathcal{D}^{(2)} \circ \mathcal{A}$ is diagonal, i.e.

$$\bar{\mathcal{D}}^{(2)} = \begin{pmatrix} \bar{\mathcal{D}}_1^{(2)} & 0 \\ 0 & \bar{\mathcal{D}}_2^{(2)} \end{pmatrix} . \tag{4.3.1}$$

Even without finding such a transformation explicitly, one can draw some conclusions by assuming its existence*. In particular we may establish a map between our general solution of the coupled system and the actual decoupled solution, for each of the asymptotic regions (horizon and far field). To find such a map let us first summarize the information we have on the general solution of the coupled system.

In Section 4.2 we have found that a general solution is parameterized by four independent coefficients in one of the asymptotic regions; either at the horizon or at infinity. Once we have chosen one set of coefficients, say at the horizon, due to the linearity of the equations, the four independent wave components at infinity are a linear combination of the four coefficients at the horizon. Let us formally denote the ingoing and outgoing wave coefficients at the horizon (+/− respectively) by

$$\vec{\mathbf{h}} = (\mathbf{h}^+, \mathbf{h}^-) = (h_i^+, h_i^-) ,$$

where $i = 1, 2$ since we have two fields. Similarly, the coefficients at infinity are defined as the large r limit of the $\mathbf{\Psi}$ field components (up to linear transformation which we will define next), i.e.

$$\vec{\mathbf{y}} = (\mathbf{y}^+, \mathbf{y}^-) = (y_i^+, y_i^-) ,$$

*In fact, for example, if we consider $\mathcal{A}$ to be a general r-dependent matrix, we can write down two conditions for the four arbitrary functions of such a matrix. Thus, in principle, there is enough freedom.

with $i = 1, 2$ for ψ and χ respectively. Due to linearity, we can define a scattering matrix

$$\begin{aligned} \vec{\mathbf{y}} = \mathbf{S}\vec{\mathbf{h}} \qquad &\Leftrightarrow \quad \left(\begin{array}{c} \mathbf{y}^+ \\ \mathbf{y}^- \end{array}\right) = \left(\begin{array}{c|c} \mathbf{S}^{++} & \mathbf{S}^{+-} \\ \hline \mathbf{S}^{-+} & \mathbf{S}^{--} \end{array}\right) \left(\begin{array}{c} \mathbf{h}^+ \\ \mathbf{h}^- \end{array}\right) , \\ &\Leftrightarrow \quad \left(\begin{array}{c} y_i^+ \\ y_i^- \end{array}\right) = \sum_j \left(\begin{array}{c|c} S_{ij}^{++} & S_{ij}^{+-} \\ \hline S_{ij}^{-+} & S_{ij}^{--} \end{array}\right) \left(\begin{array}{c} h_j^+ \\ h_j^- \end{array}\right) , \end{aligned} \tag{4.3.2}$$

which is a set of numbers (depending on energy, angular momentum, etc...) containing all the information on the scattering process. It can be fully determined by considering specific modes at the horizon and integrating them outwards. In our problem, we have imposed an ingoing boundary condition at the horizon which is simply $\mathbf{h}^+ = 0$. Then

$$\mathbf{y}^s = \mathbf{S}^{s-}\mathbf{h}^- . \tag{4.3.3}$$

Taking the $s = -$ component, and denoting the inverse matrix of $\mathbf{S}^{--}$ by $(\mathbf{S}^{--})^{-1}$, we invert (4.3.3) to obtain the wave at the horizon given the ingoing wave at infinity

$$\mathbf{h}^- = \left(\mathbf{S}^{--}\right)^{-1} \mathbf{y}^- . \tag{4.3.4}$$

Inserting this relation back in the $s = +$ component of (4.3.3), we obtain the outgoing wave in terms of the ingoing wave, at infinity

$$\mathbf{y}^+ = \mathbf{S}^{+-}(\mathbf{S}^{--})^{-1}\mathbf{y}^- \equiv \mathbf{R}\,\mathbf{y}^- , \tag{4.3.5}$$

where in the last line we have defined the reflection matrix $\mathbf{R}$. Before proceeding, we note that there is still some freedom in the definition of the asymptotic coefficients since any (non-singular) linear combination is equally good from the point of view of satisfying the boundary condition. This freedom can be written in terms of 3 matrices $\mathbf{M}^s$, $\mathbf{M}_H^-$ relating some new fields (hatted) to the old fields

$$\mathbf{y}^s = \mathbf{M}^s\hat{\mathbf{y}}^s , \qquad \mathbf{h}^- = \mathbf{M}_H^-\hat{\mathbf{h}}^- . \tag{4.3.6}$$

Since this represents the most general parametrization of the solution in the asymptotic regions, there must be a choice which decouples the fields in those regions. To find the correct transformation we need a physical prescription.

To obtain the transmission factor for the decoupled components, it is instructive to remind ourselves of the calculation of the transmission factor for a single decoupled field. It is defined

as the fraction of the incident wave which is transmitted to the horizon. If we look at a wave with energy ω (for an observer at infinity), with ingoing/outgoing amplitudes $Y_{\mp}^{(\infty)}$, then [149]

$$\mathbb{T} = \frac{|Y_-^{(\infty)}|^2 - |Y_+^{(\infty)}|^2}{|Y_-^{(\infty)}|^2} = \frac{\omega\left(|Y_-^{(\infty)}|^2 - |Y_+^{(\infty)}|^2\right)}{\omega|Y_-^{(\infty)}|^2} = \frac{\mathcal{F}_H^{in}}{\mathcal{F}_\infty^{in}} \,, \tag{4.3.7}$$

where in the last step we note that $\mathbb{T}$ can be re-expressed as a ratio between the total incident energy flux $\mathcal{F}_H^{in}$ (which is the difference between the energy carried by the ingoing wave and the energy of the outgoing wave) and the incident energy flux associated with the ingoing wave at infinity ($\mathcal{F}_\infty^{in}$). The former is the flux of energy transmitted down to the horizon.

We now compute the energy fluxes through a sphere at radius r using the energy-momentum tensor. This will allow us to identify the decoupled fields at infinity and at the horizon, and in particular, the ingoing and outgoing decoupled waves at infinity. Such a flux is shown to be conserved in our background, by using the conservation law for the energy-momentum tensor, combined with the fact that the spatial integral of $T_t{}^t$ for each energy eigen-mode is constant. It is defined, evaluated at r, as

$$\mathcal{F}|_r = -\int_{S^n} d\Sigma\, T_t{}^r \tag{4.3.8}$$

where $d\Sigma$ is the volume element on a $t, r =$ constant hyper-surface. The energy-momentum tensor for the complex neutral Proca field is

$$T^{\mu\nu} = -\frac{1}{2}\left(W^{\dagger\mu\alpha}W^\nu_\alpha - \mu_p^2 W^{\dagger\mu}W^\nu + c.c.\right) - \frac{g^{\mu\nu}}{2}\mathcal{L} \,, \tag{4.3.9}$$

up to an irrelevant normalization. If we insert this in (4.3.8), assume a field configuration with a well defined energy/frequency ω, and make use of the equations of motion, then, for the non-trivial case of $\mu_p^2 \neq 0 \neq \kappa_s^2$, we obtain

$$\mathcal{F}|_r = \sum_\Lambda \frac{i\omega V \Upsilon_\Lambda^\dagger}{2r^2}\frac{d\Upsilon_\Lambda}{dr} + \sum_\Lambda \left\{ \frac{\kappa_s^2}{2r^2}\psi^\dagger\chi - \frac{1}{2\mu_p^2}\left[\frac{V}{r^n}\frac{d(r^n\xi^\dagger)}{dr} - \frac{\kappa_s^2\psi^\dagger}{r^2}\right]\left[i\omega\xi + \frac{\kappa_s^2\chi}{r^2}\right]\right\} + c.c \tag{4.3.10}$$

where Λ denotes the mode eigenvalues for the corresponding harmonic functions, and for convenience we define $\xi = d_r\psi + i\omega\chi$. Modes with different angular momentum eigenvalues are clearly decoupled, as are the transverse vector mode contributions in the first sum. The terms in the second sum couple two fields for fixed Λ. We can compute the flux at infinity and close to the horizon and express it in terms of the asymptotic coefficients in the corresponding

region. Focusing on a specific mode and in the coupled part of the flux (second sum in (4.3.10))

$$\mathcal{F}_{\infty}^{\text{coupled}} = |y_0^-|^2 - |y_0^+|^2 + |y_1^-|^2 - |y_1^+|^2 \equiv (\mathbf{y}^-)^\dagger \mathbf{y}^- - (\mathbf{y}^+)^\dagger \mathbf{y}^+ \ , \tag{4.3.11}$$

where y_i^s are linear combinations of the asymptotic coefficients a_i^s given in the Appendix, Eq. (A.0.5). This choice of y_i^s is already in a form close to decoupled, since we have separated the modulus square of the incident contribution from the reflected contribution, without interference terms. This form is invariant under separate unitary transformation of $\mathbf{y}^\pm$. Using the reflection matrix we obtain

$$\mathcal{F}_{\infty}^{\text{coupled}} = (\mathbf{y}^-)^\dagger \left(\mathbf{1} - \mathbf{R}^\dagger \mathbf{R}\right) \mathbf{y}^- \equiv (\mathbf{y}^-)^\dagger \mathbf{T}\, \mathbf{y}^- \ , \tag{4.3.12}$$

where we have defined a (hermitian) transmission matrix $\mathbf{T}$. Note that this matrix is composed of the transmission matrix given in Eq. (4.3.5), and it is a generalization of the transmission factor, defined in Eq. (4.3.7), to the coupled system. The transmission matrix can be diagonalized through a unitary transformation which is the remaining freedom we have for $\mathbf{y}^-$. In fact we can do even better, and diagonalize the reflection matrix $\mathbf{R}$ with a bi-unitary transformation using the arbitrary unitary $\mathbf{M}^\pm$ transformations. Then the fields are manifestly decoupled at infinity, both at the level of the reflection matrix and the transmission matrix. As a consequence, in the decoupled basis, an incident wave is reflected back in the same decoupled mode without interference with the other mode. Finally, the transmission factors are simply the eigenvalues of $\mathbf{T}$, since they are each associated with a decoupled component.

Furthermore, one can use the conservation law for the flux, to find an alternative expression for the transmission matrix, at the horizon (this will be useful to control numerical errors). The total flux at the horizon is

$$\mathcal{F}_{H}^{\text{coupled}} = \left(\mathbf{h}^-\right)^\dagger \mathbf{h}^- \ , \tag{4.3.13}$$

where the h_i^- coefficients are linear combinations of the two independent ν_i coefficients ($i = 0, 1$), given in the Appendix, Eqs. (A.0.6). Eq. (4.3.13) establishes the important point that the flux is positive definite, so the transmission factors must be positive definite (as expected since there is no superradiance in Schwarzschild spacetime). Finally, using the relation between $\mathbf{y}^-$

and $\mathbf{h}^-$ through* $\mathbf{S}^{--}$, we find

$$\mathbf{T} = (\mathbf{S}^{--}\mathbf{S}^{\dagger --})^{-1} \ . \tag{4.3.14}$$

Once we have obtained the transmission factors, the number and energy fluxes are given by the standard result

$$\frac{d\{N,E\}}{dtd\omega} = \frac{1}{2\pi}\sum_{\ell}\sum_{\zeta}\frac{\{1,\omega\}}{\exp(\omega/T_H)-1}d_\zeta \mathbb{T}_\zeta \ , \tag{4.3.15}$$

where ζ is a label running over the final set of decoupled scalar modes and the transverse mode, and d_ζ are the degeneracies of the corresponding spherical harmonics. Labeling the scalar and vector harmonic degeneracies by d_S and d_V respectively we have [104]

$$d_S = \frac{(n+2\ell-1)(n+\ell-2)!}{(n-1)!\ell!} \ , \tag{4.3.16}$$

$$d_V = \frac{(n+2\ell-1)(n+\ell-1)(n+\ell-3)!}{(\ell+1)(\ell-1)!(n-2)!} \ . \tag{4.3.17}$$

The Hawking temperature in horizon radius units is

$$T_H = \frac{n-1}{4\pi} \ . \tag{4.3.18}$$

4.4 Results

In this section we present a selection of numerical results to illustrate the behavior of the transmission factors and the corresponding Hawking fluxes. To integrate the coupled and decoupled radial equations, we first wrote test codes in MATHEMATICA and then a code in the C++ language, using the numerical integration routines of the Gnu Standard Library (GSL). Besides using different programming frameworks we have also tested different integration strategies which all agreed within relative numerical errors smaller than 0.1 %. In fact, most of our numerical points have a precision which is one order of magnitude better. To check numerical errors we have integrated the radial equations up to a large radius of typically $r = 10^4 r_H$ and varied this up to a factor of 3 to check the precision. Furthermore we have used the two expressions for the transmission factor from Eqs. (4.3.12) and (4.3.14) which agree within the quoted precision for almost all energies. The exception is for small energy, where the first definition converges poorly. This can be explained by a simple analysis of

*Note that the relation between $\mathbf{h}^-$ and $(\mathbf{M}^-)^{-1}\mathbf{y}^-$ can be made diagonal using $\mathbf{M}^-_H$, so the problem is also decoupled at the horizon.

propagation of errors combined with the fact that the $\mathbf{y}^{\pm}$ coefficients grow very fast as we decrease energy, thus requiring a very large precision for some fine cancellations to occur. The second expression is thus more natural in that limit since it does not need such cancellations and does not require such large precision.

We have generated several samples of transmission factors, some of which are displayed in Fig. 4.1. Hereafter, we shall denominate the partial waves associated to the different modes of the Proca field by ℓ_1, ℓ_2, ℓ_T and $\ell = 0$, where ℓ_1, ℓ_2 correspond to the two coupled modes described by Eqs. (3.1.5) and (3.1.6), ℓ_T to the decoupled mode described by Eq. (3.1.7) and $\ell = 0$ to the $\kappa_s = 0$ mode, described by Eq. (3.2.2). Moreover, partial waves associated to the Maxwell field shall be denoted by ℓ_E, and are described by Eq. (3.1.8).

In the top row panels of Fig. 4.1, we show the partial wave contributions for $n = 2, 3, 4$ in the zero mass limit. Some general properties are as follows. The $\mathbb{T}_\ell$ curve becomes shifted towards higher frequencies both as ℓ is increased, for n fixed, and as n is increased, for ℓ fixed. The former can be understood from standard geometrical optics arguments. Moreover, for this choice, there is always a numerical coincidence between one of the partial waves (ℓ_1) obtained from the two coupled fields and the electromagnetic partial wave ℓ_E. The $\ell = 0$ and ℓ_2 modes are always absent in the Maxwell theory, so they can be associated with the longitudinal polarization of the massive vector field. Similarly, the ℓ_T and ℓ_1 partial waves are associated with the transverse polarizations of the field. A qualitative dependence on dimension is that for $n = 2$, ℓ_T and ℓ_1 (or ℓ_E) modes are all equal. Curiously, this is in agreement with the fact that they describe the same number of transverse degrees of freedom as can be seen from the degeneracies (4.3.16) specialized for $n = 2$. This degeneracy is lifted for $n > 2$.

For non-zero mass (middle and bottom row panels of Fig. 4.1), the degeneracy observed for $n = 2$ in the massless limit is lifted. Also, we observe, for all n, that modes with higher ℓ partial waves (especially ℓ_1 modes) become a more dominant contribution at lower energies, as compared to lower ℓ partial waves of other modes. In particular for $\mu_p = 1$, the transmission factor for ℓ_1 becomes the largest for small energy. This effect of excitation of sub-dominant partial waves is well known to exist for example as we increase n (and we can also observe such effect in our plots) as well as with the introduction of BH rotation [46]. If this effect persists cumulatively on a rotating background, then we may have enhanced angular correlations for

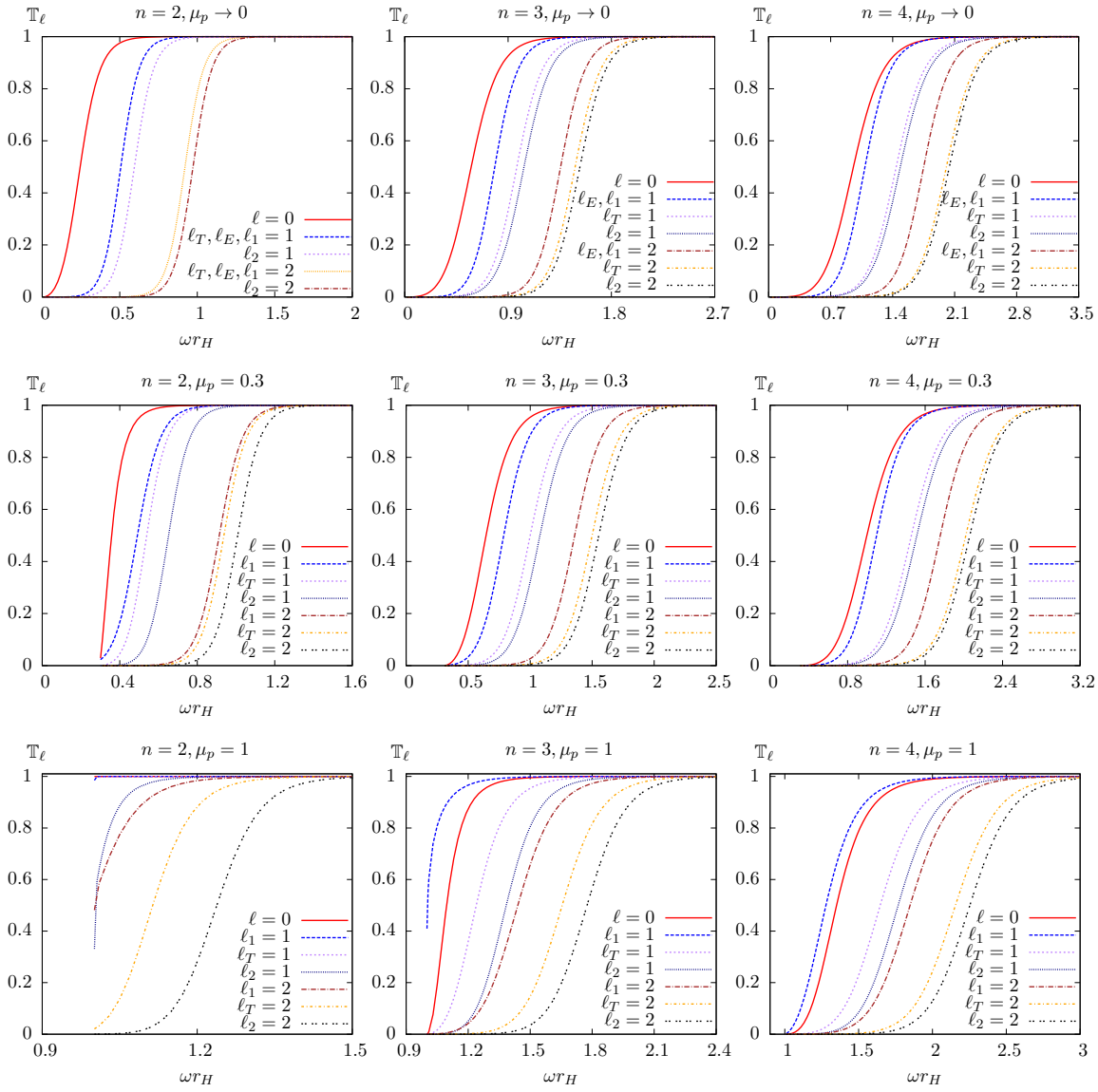

Figure 4.1: *Transmission factors:* The three rows of panels, show the first few partial waves contributing to the Hawking spectrum. Each row corresponds to a fixed mass and each column to a fixed dimension. In particular, the first row shows the small mass limit of the Proca theory in order to compare it with Maxwell's theory.

massive Proca fields emitted from the BH, since higher ℓ partial waves are less uniform.

Another outstanding point is that for large mass, when $n = 2, 3$, it can be seen that the transmission factor starts from a constant non-zero value at the threshold $\omega = \mu_p$ ($k = 0$), at least for small ℓ. We have checked that this does not happen for $n \geq 4$ for masses as large as $\mu_p = 10 \sim 15$, where the curves always asymptote smoothly to zero at $k = 0$. Note that the parameter in the radial equations is μ_p^2 so these are very large masses. A possible explanation for this phenomenon can be motivated from considerations about the range of the gravitational field in Rutherford scattering. In $n = 2$, the total cross-section for Rutherford scattering diverges, so the Newtonian gravitational potential is long ranged. This means that the effective size of the gravitational potential is infinite. The same happens in $n = 3$ but only at zero momentum $k = 0$. This indicates that a possible reason is that an incident wave at infinity with a very small momentum will still be sufficiently attracted by the gravitational field so that a constant non-zero fraction is still absorbed by the potential. In particular we note that some of the radial equations are similar in form to those obeyed by massive scalar and massive fermion fields, so the same effect exists for such fields. To our knowledge, this feature has not been noted or discussed in the literature. The only exception is the paper by Nakamura and Sato [150] in four dimensions, where it is claimed that the reflection factor for a scalar field always goes to 1 at $\omega = \mu_s$ (and thus the transmission factor goes to zero). Their result seems, however, inconsistent with Figs. 1, 2 and 3 of the paper by Page [151] (also in four dimensions), where the Hawking fluxes for massive fermions become constant at the $k = 0$ threshold (in agreement with our result).

Once we obtain the transmission factors, the computation of the Hawking fluxes (5.3.6) follows straightforwardly by summing up partial waves with the appropriate degeneracy factors (4.3.16). We have chosen to show the flux of number of particles. The flux of energy has similar features and is simply related by multiplying each point in the plots by ω.

In Fig. 4.2 we compare the Hawking fluxes of the Maxwell theory with the small mass limit of the Proca theory. For the particular case of $n = 2$ we have reproduced the results by Page [152] for the electromagnetic field and found very good agreement. All panels show a red solid curve corresponding to the total Hawking flux summed up over partial waves. The partial waves included in the sum are also represented, scaled up by the appropriate degeneracy factor. As

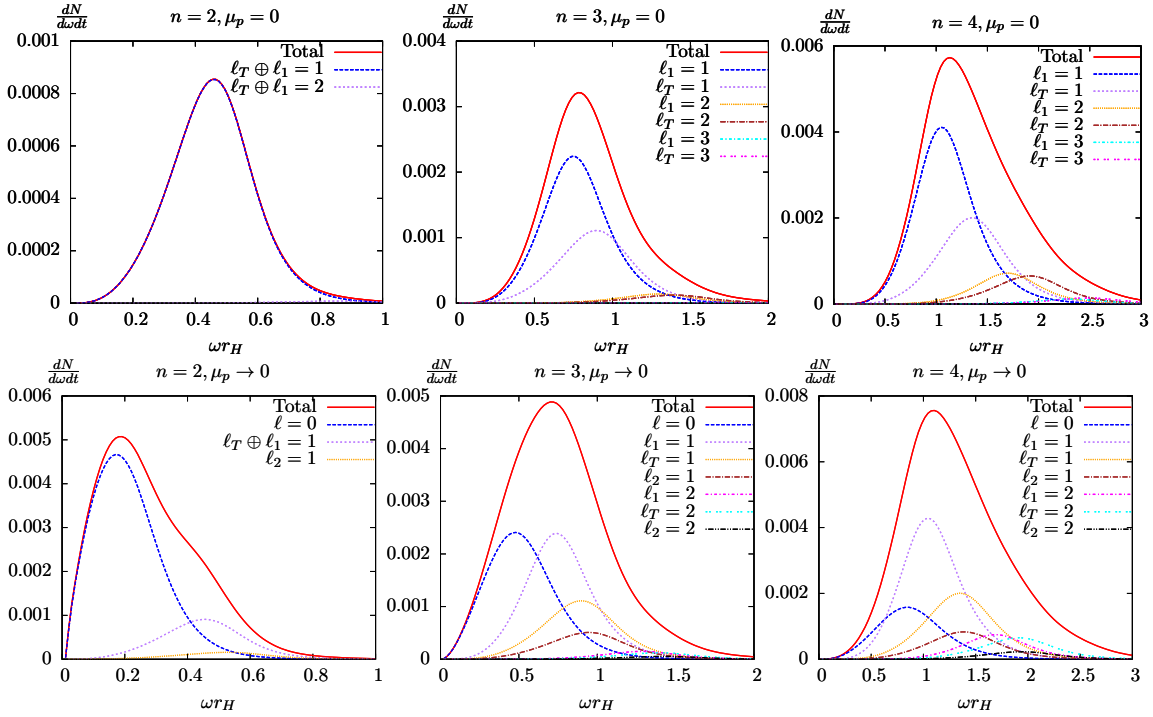

Figure 4.2: *Number fluxes for $\mu_p = 0$ (top panels) and $\mu_p \to 0$ (bottom panels):* The red solid curve of the top panels shows the Hawking flux of particles summed over the dominant partial waves for the Maxwell theory. The different partial waves are multiplied by the corresponding degeneracies. In the bottom panels the small (but non zero) μ_p limit of the Proca theory is shown for comparison. The $\oplus$ symbol denotes the addition of modes which are numerically equal.

claimed in the discussion of the transmission factors, as we increase n, partial waves with larger ℓ become more important for both Maxwell and Proca fields. One can clearly see that there is a large contribution to the total flux from the longitudinal degrees of freedom, since the vertical scales are larger for the Proca field. In particular the $\ell = 0$ mode enhances the spectrum greatly at small energies. Note that these extra contributions associated with the longitudinal degrees of freedom cannot in general (for arbitrary mass) be described by a scalar field, since there is always a contribution from the coupled modes ℓ_1, ℓ_2. That is, however, the approximation done so far in BH event generators, where the W and Z fields Hawking spectra in use are those of the electromagnetic field (for transverse polarizations) and a scalar field (for the longitudinal polarization). Thus, our methods can be readily applied to improve this phenomenological modeling.

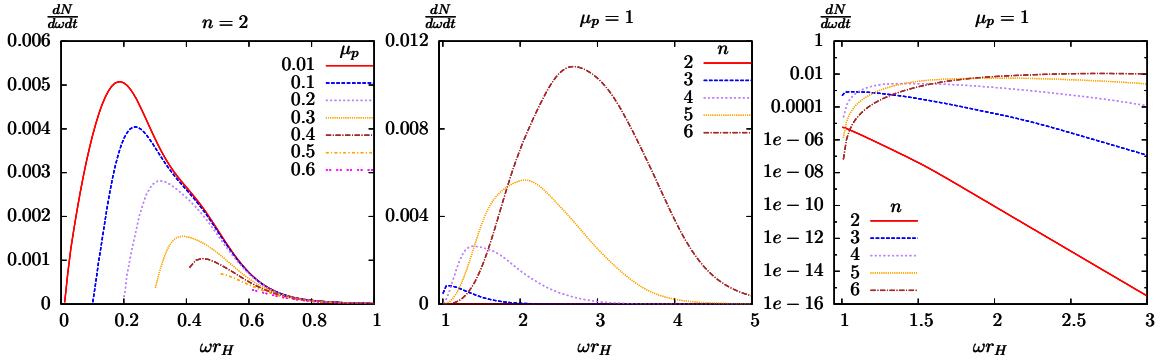

Figure 4.3: *Number fluxes for various μ_p and n:* (Left panel) Variation of the flux of particles for fixed $n = 2$ and variable mass. (Middle and right panels) Variation of the flux with n in a linear and logarithmic scale respectively. The logarithmic scale shows more clearly that the limiting flux at $k = 0$ is finite for $n = 2, 3$.

In Fig. 4.3 we show the variation of the total number flux with n and μ_p. The left panel shows the expected variation with μ_p: that the flux not only gets cutoff at the energy threshold $\omega = \mu_p$, but it is also suppressed with μ_p (the same holds for $n > 2$). This is the same behavior as found in [146, 147]. As pointed out already, in event generators massive vector particles are modeled using the Hawking fluxes for the Maxwell field and a massless scalar, with a cutoff at the mass threshold. In [146, 147] it was shown that simply imposing a sharp cut-off on the fluxes of massless scalars and fermions over-shoots the real amount of Hawking radiation emitted in the massive scalar and fermion channel. Qualitative inspection of our results suggests a similar effect for the W and Z channels in the evaporation. A quantitative comparison, however, requires a consideration of a Proca field confined to a thin brane, which will be studied in Chapter 5. The middle and right panels show variation with n. In addition to the well known large scaling of the area under the curve and the shift of the spectrum to larger energies, we can also see that more partial waves start contributing to the shape of the curve which becomes more wavy. This is particularly true because the degeneracy factors for fixed ℓ increase rapidly with n, which is a consequence of the larger number of polarizations available for a vector boson in higher dimensions. Finally, regarding $n = 2, 3$ we confirm the feature that the flux becomes a constant at $k = 0$. This can be seen more clearly in the right panel in a logarithmic scale where the lines for $n \geq 4$ curve down very sharply around that point, whereas for $n = 2, 3$ they tend to a constant.

4.5 Summary

In this chapter, we have studied Hawking radiation for a neutral Proca field, by solving the coupled wave equations as well as decoupled equations numerically, on a D-dimensional Schwarzschild BH. Our results exhibit distinctive features as we introduce the mass term, such as the lifting of the degeneracy of the two transverse modes in four dimensions, the appearance of longitudinal mode contributions (absent for Maxwell's theory) and in particular the s-wave. As we have shown, there is a large contribution from the longitudinal modes, to the Hawking fluxes.

One feature that appears not to have been discussed in the literature is that in four and five spacetime dimensions, the transmission factor has a non-vanishing value in the limit of zero spatial momentum. We also find the expected suppression with mass of the Proca field, but perhaps the most relevant feature is to notice the increasing importance of the longitudinal modes and larger ℓ partial waves.

Our results could be applied to improve the model used in the CHARYBDIS2 Monte Carlo event generator [45]. This simulates the production and decay of higher dimensional BHs in parton-parton collisions, a scenario which is being constrained at the second run of the LHC. It is therefore quite timely to improve the phenomenology of these models. Indeed our knowledge of Hawking evaporation process can still be improved greatly through the numerical study of various wave equations in BH backgrounds, which approximate the ones that could be produced at the LHC. This is illustrated by our results in this study, which alert for the importance of modelling the longitudinal modes correctly, instead of treating them as decoupled scalars as in current BH event generators.

Chapter 5

Hawking radiation for a Proca field: charged case

5.1 Introduction

In this chapter, we are going to study Hawking radiation for a charged Proca field, by solving the charged Proca equations derived in Chapter 3 numerically. This is a generalization of the study presented in Chapter 4, by adding charge both to the field and the BH, on the 3+1 dimensional SM brane. This charged brane background is motivated by TeV gravity scenarios, in which the SM particles are confined on a 4-dimensional brane, while gravity propagates in extra dimensions, see Section 1.1 for more details. As shown in [146], the Schwinger emission alone does not suffice to discharge the BH, which makes the study of Hawking radiation for charged BHs essential. The effects of charge on the Hawking evaporation process, for scalar and fermion fields, have been performed in [146, 147]. As a first motivation for this study, we are going to complete this picture by exploring the charged Proca fields.

Compared to the study for neutral Proca fields in Chapter 4, a new feature due to the charge of the background and of the field is the existence of superradiant modes. These modes are amplified through the extraction of Coulomb energy, as well as charge, from the charged BH. Furthermore, in a rotating background, the Proca field equation variables are not known to separate, which presents an extra difficulty added to the non decoupling of the modes, making

it difficult to study exactly the superradiance phenomenon – see [131, 132] for a recent study in the slow rotation approximation. Thus, as a second motivation for this study, the charged BH background with spherical symmetry, yields a setup where superradiance of a massive spin 1 field can be explored without any approximation, albeit numerically. Such analysis will be performed herein.

The structure of this chapter is organized as follows. In Section 5.2 we introduce the background geometry and study the near horizon and asymptotic behaviors of the coupled charged Proca equations. In Section 5.3 we discuss how to construct the scattering matrix from the electric current. The numerical results for the transmission factor and the associated Hawking fluxes are presented in Section 5.4 and we summarize our results in the last section. To keep the main part of this chapter compact and clear, some technical relations are left to Appendix B.

5.2 Boundary conditions and first order system

Before starting to deal with the Proca equations, we first present the following brane BH geometry

$$ds^2 = -V(r)dt^2 + \frac{1}{V(r)}dr^2 + r^2(d\theta^2 + \sin^2\theta d\varphi^2) \,, \tag{5.2.1}$$

with metric function

$$V(r) = 1 - \frac{M}{r^{n-1}} + \frac{Q^2}{r^2} \,, \tag{5.2.2}$$

where M and Q are the parameters related with BH bulk mass and brane charge. For numerical convenience, we choose units such that the outer horizon radius is $r_H = 1$, i.e. $M = 1 + Q^2$ at the outer horizon.

It is easy to map the line element in Eq. (5.2.1), to the general background geometry with the Einstein space given in Eq. (2.1.1). Then the charged Proca field equations we are interested herein, can be obtained by setting $n = 2$ in Eqs. (3.1.5), (3.1.6), (3.1.8) and (3.2.2)*.

The procedure to rewrite the second order wave equation for the coupled system into a first order form, to impose an ingoing boundary condition at the horizon, and to extract the

*Note that the explicit n appearing in these wave equations only depends on the dimension of the Einstein space. Therefore, we set $n = 2$ for the background in Eq. (5.2.1). But we keep n in general in the metric function (5.2.2) since gravity may propagate in the extra dimensions.

asymptotic expansion coefficients, is similar to what was done in Section 4.2. For clarity, we summarize the main steps in the reminder of this section.

To determine the transmission factors, we need to integrate the radial equations from the horizon to the far away region with ingoing boundary conditions. The standard procedure is to find a series expansion of the solution near the horizon, which can be used to initialize the solution (we do so at $r = 1.001$). Focusing on the coupled system $\{\psi, \chi\}$, if we define $y = r - 1$, Eqs. (3.1.5) and (3.1.6) become

$$\left[A(r)\frac{d^2}{dy^2} + B(r)\frac{d}{dy} + C(r)\right]\psi + E(r)\chi = 0 \,, \tag{5.2.3}$$

$$\left[\tilde{A}(r)\frac{d^2}{dy^2} + \tilde{B}(r)\frac{d}{dy} + \tilde{C}(r)\right]\chi + \tilde{E}(r)\psi = 0 \,, \tag{5.2.4}$$

where the polynomials $A, B, C, E, \tilde{A}, \tilde{B}, \tilde{C}, \tilde{E}$ are defined in Appendix B. Making use of Frobenius' method to expand ψ and χ, we insert the following expansions into Eqs. (5.2.3) and (5.2.4)

$$\psi = y^\rho \sum_{j=0}^{\infty} \mu_j y^j \,, \quad \chi = y^\rho \sum_{j=0}^{\infty} \nu_j y^j \,, \quad \rho = \frac{-i(\omega - qQ)}{(n-1) + (n-3)Q^2} \,, \tag{5.2.5}$$

where the sign of ρ was chosen to impose an ingoing boundary condition. We then obtain the recurrence relations (B.0.1) for the coefficients μ_j and ν_j found in the Appendix. A general solution close to the horizon can be parameterized by two free coefficients ν_0 and ν_1.

Similarly, to understand the asymptotic behavior of the waves at infinity we now expand ψ and χ as

$$\psi = e^{\beta r} r^p \sum_{j=0} \frac{a_j}{r^j} \,, \qquad \chi = e^{\beta r} r^p \sum_{j=0} \frac{b_j}{r^j} \,, \tag{5.2.6}$$

which, after insertion into Eqs. (3.1.5) and (3.1.6), yield

$$\beta = \pm ik \,, \qquad k = \sqrt{\omega^2 - \mu_p^2} \,, \qquad p = \pm i\varphi \,, \tag{5.2.7}$$

where $\varphi = \delta_{n,2}(\omega^2 + k^2)(1 + Q^2)/(2k) - qQ\omega/k$. Thus one can show that asymptotically

$$\psi \to \left(a_0^+ + \frac{a_1^+}{r} + \ldots\right) e^{i\Phi} + \left(a_0^- + \frac{a_1^-}{r} + \ldots\right) e^{-i\Phi} \,, \tag{5.2.8}$$

$$\chi \to \left[\left(-\frac{k}{\omega} + \frac{c^+}{r}\right) a_0^+ + \ldots\right] e^{i\Phi} + \left[\left(\frac{k}{\omega} + \frac{c^-}{r}\right) a_0^- + \ldots\right] e^{-i\Phi} \,, \tag{5.2.9}$$

where $\Phi \equiv kr + \varphi \log r$ and $c^{\pm}$ is defined in the Appendix, Eq. (**??**). Thus, as expected, each field is a combination of ingoing and outgoing waves at infinity. Asymptotically, the solution is parameterized by four independent coefficients $\left\{a_0^{\pm}, a_1^{\pm}\right\}$, two for each independent mode in the coupled system. In the same way as in Section 4.2, one can define a first order system of ODEs containing four radial functions $\{\chi^{\pm}, \psi^{\pm}\}$ which coincide with such coefficients at infinity, allowing for an easy extraction of the wave amplitudes. Our target system, which will be solved numerically in the remainder, is then

$$\frac{d\mathbf{\Psi}}{dr} = \mathbf{T}^{-1}\left(\mathbf{X}\mathbf{T} - \frac{d\mathbf{T}}{dr}\right)\mathbf{\Psi} \ , \tag{5.2.10}$$

with $\mathbf{\Psi}^T = (\psi_+, \psi_-, \chi_+, \chi_-)$. The definition of the matrices $\mathbf{X}$ and $\mathbf{T}$, and how they relate with (5.2.3) and (5.2.4) can be found in Appendix B.

5.3 Hawking fluxes

We shall now calculate the transmission factor for the coupled system as well as the Hawking fluxes generated from all the modes. In contrast to constructing a conserved flux from the energy-momentum tensor in Chapter 4 which was simple enough to extract the transmission factors, in the present case, we use the conserved electric current which is naturally defined for this charged field. One can show that such a current is given by

$$\mathcal{J}^{\alpha} = W^{\dagger\alpha\mu}W_{\mu} + \frac{1}{\sqrt{-g}}\partial_{\beta}\left(\sqrt{-g}W^{\dagger\beta}W^{\alpha}\right) - c.c. \tag{5.3.1}$$

The radial flux at r fixed is obtained by integrating the $\alpha = r$ component on the sphere. We note that only the first term in Eq. (5.3.1) (denoted from now on $\mathcal{J}_I^{\alpha}$) contributes, since the second term becomes a total derivative on the sphere.

The contribution for the flux of the coupled fields at infinity, is then found by simplifying the radial component of Eq. (5.3.1) using the equations of motion, and inserting the far away expansion at infinity

$$\mathcal{J}^{r,\infty}_{I-couple} = |y_0^-|^2 - |y_0^+|^2 + |y_1^-|^2 - |y_1^+|^2 \equiv (\mathbf{y}^-)^{\dagger}\mathbf{y}^- - (\mathbf{y}^+)^{\dagger}\mathbf{y}^+ \ , \tag{5.3.2}$$

where $y_i^s (s = \pm; i = 0, 1)$ are linear combinations of the asymptotic coefficients a_i^s given in the Appendix, Eq. (B.0.6). Using the reflection matrix ($\mathbf{R}$) defined in Chapter 4, we obtain

$$\mathcal{J}^{r,\infty}_{I-couple} = (\mathbf{y}^-)^{\dagger}\left(\mathbf{1} - \mathbf{R}^{\dagger}\mathbf{R}\right)\mathbf{y}^- \equiv (\mathbf{y}^-)^{\dagger}\mathbf{T}\,\mathbf{y}^- \ , \tag{5.3.3}$$

where we have defined a (hermitian) transmission matrix $\mathbf{T}$, which can be diagonalised to find the decoupled asymptotic fields.

Following the same procedure, one can also calculate the electric current at the horizon

$$\mathcal{J}^{r,H}_{I-couple} = \frac{1}{\omega - qQ} \left(\mathbf{h}^{-}\right)^{\dagger} \mathbf{h}^{-} \ , \tag{5.3.4}$$

where the h_i^- coefficients are linear combinations of the two independent ν_i coefficients ($i = 0, 1$), given in the Appendix, Eq. (B.0.7). It shows an important point in Eq. (5.3.4) that the current can be positive or negative. This is expected, because for a bosonic field, the electric coupling can trigger superradiance.

Furthermore, from the conservation law of the electric current, one can find an alternative expression for the transmission matrix. Using the scattering matrix ($\mathbf{S}^{--}$) defined in Chapter 4, we find

$$\mathbf{T} = \frac{1}{\omega - qQ} (\mathbf{S}^{--} \mathbf{S}^{\dagger --})^{-1} \ . \tag{5.3.5}$$

Once we have obtained the transmission factors, the number and energy fluxes are given by

$$\frac{d\{N, E\}}{dt d\omega} = \frac{1}{2\pi} \sum_{\ell,\zeta} \frac{(2\ell + 1)\{1, \omega\}}{\exp((\omega - qQ)/T_H) - 1} \mathbb{T}_{\ell,\zeta} \ , \tag{5.3.6}$$

where ζ labels the mode and T_H is the Hawking temperature which, in our units, is

$$T_H = \frac{(n-1) + (n-3)Q^2}{4\pi} \ . \tag{5.3.7}$$

5.4 Numerical Results

We now present a selection of numerical results for the transmission factor and the corresponding Hawking fluxes. In order to integrate the decoupled and coupled radial equations, we wrote independent codes in MATHEMATICA and in C++, finding agreement between the two codes. Using them we have generated a set of figures that we now describe.

In Fig. 5.1 transmission factors for different masses, spacetime dimensions and charges are shown to exhibit the superradiance phenomenon. As explained in Chapter 1, superradiant amplification of a bosonic field in a charged and/or rotating BH occurs since there is Coulomb and/or rotational energy that can be extracted without decreasing the BH area. The general

condition of superradiance is $\omega < m\Omega_H + q\Phi_H$; when this condition is verified, the transmission factor becomes negative and the scattered mode is amplified. In order to make the results clearer and more readable, here we just show the two coupled modes with $\ell = 1$, as an example. Other cases are qualitatively similar. In the left panel of Fig. 5.1, we show the superradiance dependence on the field charge for $n = 2$ (top row) and $n = 4$ (bottom row). It is clear that superradiant amplification is enhanced with growing field charge except in the small energy regime; in this regime one observes, at least for the cases plotted, that the amplification decreases with increasing field charge (this effect is more noticeable for higher dimensions, see bottom row). The middle panel of Fig. 5.1 shows the dependence on the background charge – the trend is the same as when the field charge is varied, i.e. a generic superradiance enhancement with the charge except for small energies. In the right panel of Fig 5.1, we show the superradiance dependence on the field mass; a suppression effect with increasing mass is observed, which is a generic behavior for the transmission factor (independently of the spin of the field or of being in the superradiant regime) [146, 147].

After we obtain the transmission factors, the Hawking fluxes (5.3.6) can be calculated directly. In the remainder we have chosen to show the flux of the number of particles. The flux of energy has similar features and can be simply calculated by multiplying each point with ω.

In Fig 5.2 we illustrate the number fluxes dependence on the field charge. On the left plots, we have kept the background charge parameter fixed (and positive), with $Q = 0.4$ and $n = 4$, varying the field charge q from -1 to 1. The plots show that there is a region at low energy, where the negative field charge flux is larger, whereas in the remaining part of the spectrum, positive charge emission is favored. It is also clear that if we integrate over the curves the emission of positive charge is always favored. This low energy behavior where negative charges are favored, only occurs for $n > 3$ as can be seen on the right panel, where the difference between the positive charge and negative charge flux spectrum is presented for various n. This inverted charge splitting effect was also observed for scalars and fermions [147], and it results from the interplay between the thermal factor and the transmission factor appearing in the expression for the number fluxes. Whereas the thermal factor always favors same charge emission, the transmission factor favors opposite charge emission and these factors dominate different parts of the spectrum. We have considered the same parameters as in [147], $Q = |q| = 0.3$, wherein scalars and fermions have been studied, to allow for an easy comparison.

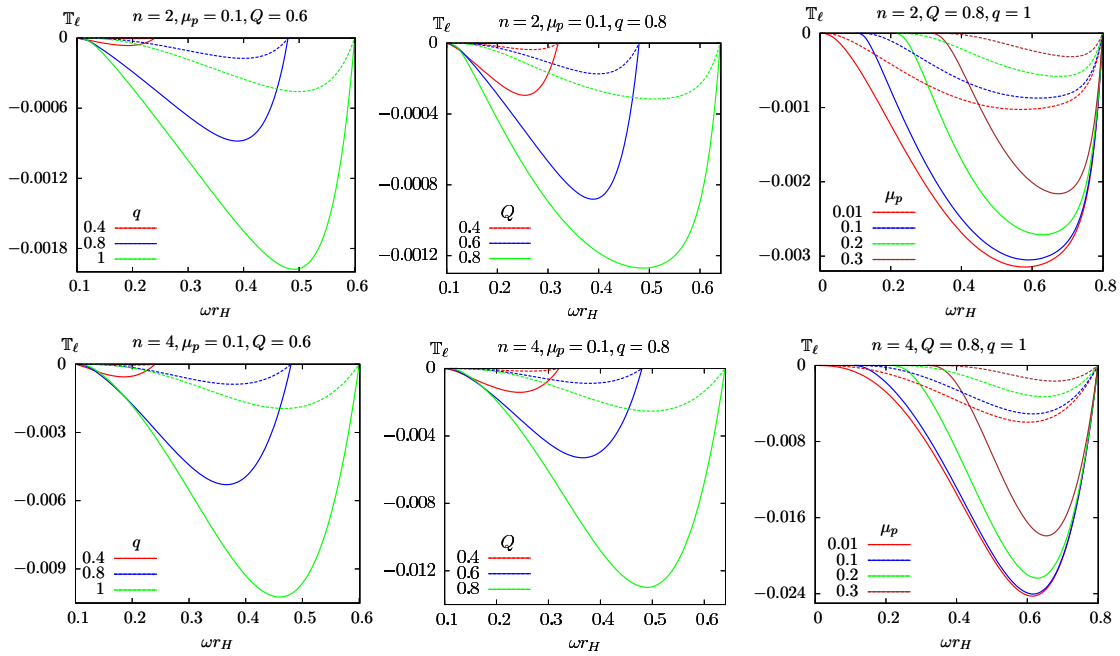

Figure 5.1: Negative transmission factors that show the superradiant amplification of the coupled modes with $\ell = 1$ for different parameters. The two coupled modes are represented with the same color (solid and dashed lines). The top and bottom rows differ in the spacetime dimension. (Left panel) Variation with the field charge q; (Middle panel) variation with the background charge Q; (Right panel) variation with the field mass.

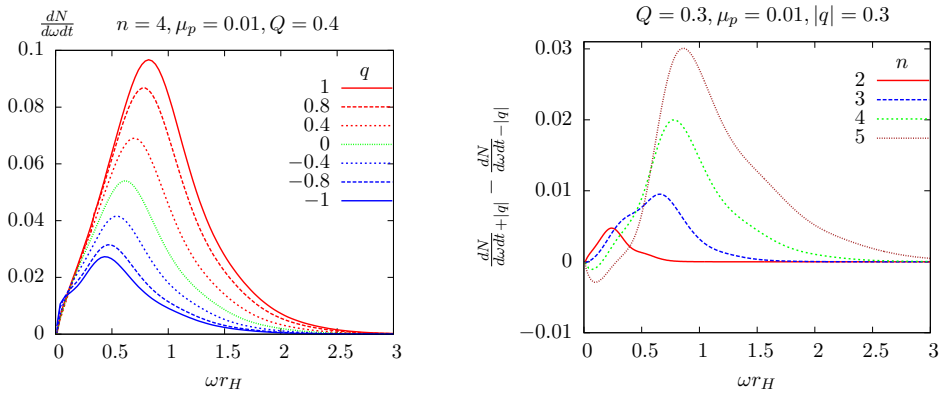

Figure 5.2: (Left panel) Variation of the number fluxes with field charge for fixed n and BH parameters in the small field mass limit. (Right panel) Variation of the difference between positive charge and negative charge flux with n.

In Fig. 5.3, we present the number flux dependence on the background charge for different field charge, in the same row, and different spacetime dimensions, in the same column. Consider first the $q = 0$ case (middle column); it shows that the fluxes are suppressed/maintained/enhanced with the increase of background charge for $n = 2/n = 3/n = 4$. To understand this behavior observe, from the definition of Hawking temperature, Eq. (5.3.7), that the Hawking temperature is decreased/maintained/increased with increasing background charge for $n = 2/n = 3/n = 4$, in these units. Since we are using horizon radius units, as we vary the charge parameter Q, we are actually varying the mass of the BH as well as the charge while keeping $r_H = 1$. Nevertheless, it is easy to see that, up to a stretching of the horizontal axis, if we fix the BH mass and vary the dimensionful charge, these conclusions for the variation of the height of the curves do not change since the number flux is dimensionless *. For higher temperature, one expects a larger flux of particles, which is indeed the behavior shown in the second column of Fig. 5.3. Turning on the field charge we observe a more involved behavior. For $n = 3$, in which the Hawking temperature does not vary with Q, we see in the first/third column and for sufficiently large energies a monotonic suppression/enhancement of the Hawking flux when the BH has the opposite/same charge as the field. This is in agreement with the discussion of the left panel of Figure 5.2. For $n = 2, 4$, varying Q one also varies the Hawking temperature and more complex patterns are observed. Another trend is that the number fluxes increase as the spacetime dimension increases, which may be understood from the existence of more modes that contribute to the transmission factor.

5.4.1 Mass effect and bulk/brane emission

In Figure 5.4, we perform a comparison of the effect of introducing a mass term for the various spins which are relevant for the Standard Model brane degrees of freedom. We have used the data of [147] for scalars and fermions. Note that for fermions we have multiplied the data by a factor of two to take into account the two helicities of the Dirac field, since here we are also considering all the three modes for the Proca field. The dashed curves are for increasingly

*The integrated flux however will not be the same for all background charges as expected, scaling as r_H^{-1} for fixed BH mass and varying charge.

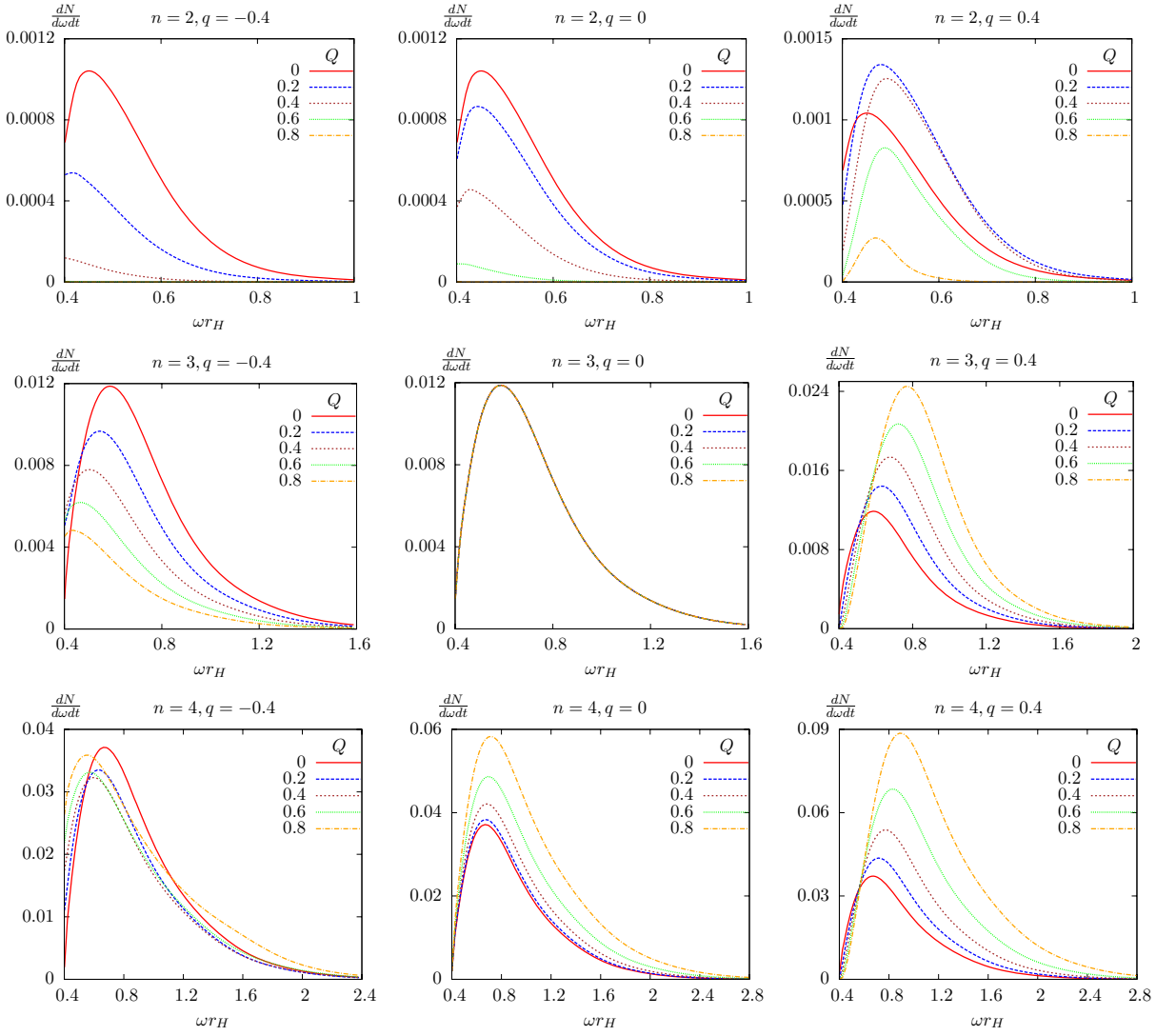

Figure 5.3: Number fluxes dependence on the background charge for different spacetime dimensions and field charge, with fixed field mass $\mu_p = 0.4$. We vary the field charge in the same row and vary the spacetime dimension in the same column.

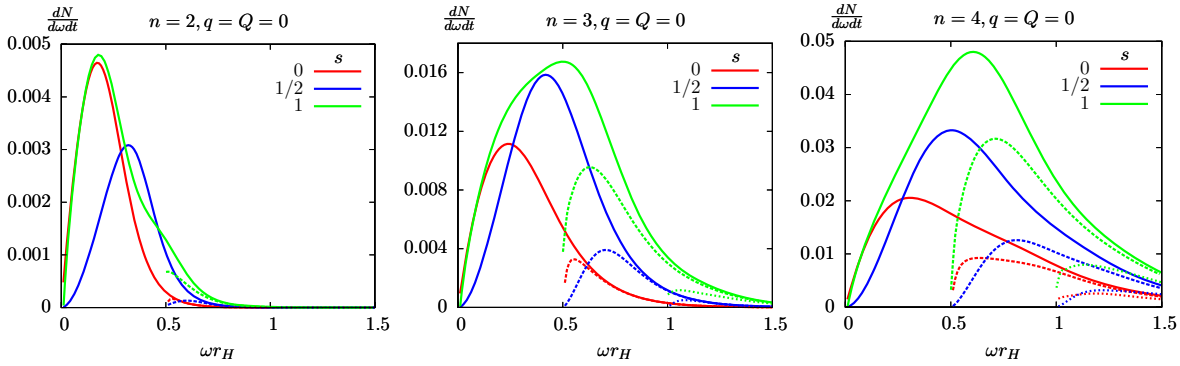

Figure 5.4: Variation of the number fluxes for neutral particles with different spins (scalar, fermion and Proca) on the brane. For each type of particles we consider three different masses ($\mu = 0$, 0.5 and 1), which can be identified by the starting point of the curve. Note we have included the two helicities for the fermion field and all the three modes for the Proca field (we have used a small mass $\mu_p = 0.01$ for the latter, instead of $\mu_p = 0$).

larger field mass (we have used the cases $\mu^* = 0$, 0.5 and 1, as can be seen from the threshold points where the curves start). For $D = n+2 = 4$ (left panel), we observe a striking similarity between the Proca ($s = 1$) flux with the scalar ($s = 0$) flux for $\mu = 0$ (except at the high energy tail), which is due to the dominance of the $\ell = 0$ mode. We can see this feature is always true at small energies for larger n (middle and right panels); as we increase n, however, higher modes of the Proca field enhance the flux as compared to scalars. The extra modes of the Proca field contributing at higher energy, also explain the fact that the mass suppression is not as large as for Dirac fermions or scalars, as we see from the dashed curves corresponding to $\mu = 0.5$ for example. The high energy behavior contrasts with the low energy behavior, where scalar and Proca fields are dominated by the s-wave, whereas Dirac fermions are suppressed since they do not allow an s-wave. At high energy, we observe tails which are in the ratio $1 : 2 : 3$ following the number of degrees of freedom for the scalar, fermion and Proca fields respectively. This is in agreement with the fact that all transmission factors tend to one at high energy.

In the remainder, we combine our results for the Proca field on the brane with those in Chapter 4 for a Proca field in the bulk, to analyze the relative bulk-to-brane emissivity in the

*In this subsection, the parameter μ, if not specified, referes to the mass for different spin fields, include scalar, fermion and Proca.

neutral case.

	$n=2$	$n=3$	$n=4$	$n=5$	$n=6$	$n=7$
$\mu_p=0.1$	1	0.46	0.38	0.41	0.53	0.83
$\mu_p=0.3$	1	0.49	0.40	0.42	0.55	0.86
$\mu_p=0.6$	1	0.59	0.47	0.49	0.62	0.95

Table 5.1: Bulk-to-Brane relative energy emission rates for massive neutral vector fields for different mass μ_p in terms of the spacetime dimension $D=2+n$.

The total energy rate (or number rate) emitted in Hawking radiation for a given field, is obtained by integrating the fluxes of Eq. (5.3.6) (or their counterparts in the bulk) over ω. The bulk-to-brane energy emissivity ratio, for massive neutral Proca fields of different mass is shown in Table 5.1 as a function of n. We have used the data in Chapter 4 to obtain the total emissivity for bulk fields, as well as the data presented here, for the brane emissivity. The entries of Table 5.1, show clearly that the emission of energy into brane-localized Proca particles is dominant, for n larger than two, which is consistent with the argument that BHs radiate mainly on the brane [153]. For fixed mass, as n increases, the bulk-to-brane energy emission ratio initially decreases, reaching a minimum value for an intermediate n. However, if one increases n further, the bulk-to-brane energy emission ratio increases again. Furthermore, we have also observed that the bulk-to-brane energy emission ratio increases with the field mass. A similar behavior was observed for scalar fields [136, 154]. Finally, we found that the bulk-to-brane energy emission ratio for the Proca field is larger than that for the scalar field for all n, being more noticeable for large n, say $n=6$ and $n=7$ (note the different notation for $D=2+n$ in this chapter as compared with [136, 154]).

5.5 Summary

In this chapter we have completed the analysis started in Chapter 4, by computing the transmission factor for a charged Proca field propagating in the background of a charged BH on a brane. Furthermore, this work completes the study of the effect of mass and charge for particles evaporating on the brane, for all spins relevant for the SM in brane world scenarios [146, 147].

One of the main, and novel features arising from considering a charged Proca field on a charged background is the existence of negative transmission factors, a signature of superradiant scattering, which we have presented and described. Our results are consistent with the condition of superradiance as allowed by the area theorem, and we found that generically increasing the field or background charge amplifies the effect (though some inversions are possible at small energies). As we explained in Chapter 1, it is worth commenting that although superradiant scattering is observed for both rotating and charged BHs, rotating BHs exhibit superradiant instabilities against massive scalar fields, and in particular against the Proca field [131, 132], whereas charged (non-rotating) BHs do not exhibit analogous instabilities against charged, massive bosonic fields. This will be explored for the Proca field in Chapter 6, by computing the frequencies of quasi-bound states, a study that can also teach us how long lived Proca hair around charged BHs can be.

An effect observed herein, is that similarly to scalars and fermions, there is an inverted charge splitting effect at small energies for more than one extra spacetime dimension, where particles with charge opposite to the BH are emitted dominantly. Nevertheless, for larger energies, the normal splitting order, favoring the emission of same charge particles as to discharge the BH is restored and overall (by integrating out the flux), this channel tends to discharge the BH. This effect has been suggested to be another signature that could be found in the energy spectrum of charged fermions [147]. Since fermions in the final state are also produced indirectly from the decay of vector bosons such as $W^{\pm}$ or the Z particles one may ask whether the effect survives. Here we have verified that the effect is present for $W^{\pm}$, so at least for the case when the final state decay products are a charged lepton $\ell^{\pm}$ and a neutrino, these contributions will certainly enhance the effect.

In the neutral case, we have performed two comparisons. First we have compared the effect of the mass and spin on the Hawking fluxes, for all spins in the SM. Our main findings are that the Proca field spectrum departs from being similar to a scalar field in four dimensions and becomes increasingly dominant for larger number of dimensions, peaking and extending towards larger energies. This also means that the mass suppression effect is smaller for the Proca field than it is for scalars and fermions. Second, we have compared the bulk-to-brane emission ratio for Proca fields, confirming brane dominance in general, and the suppression of brane dominance with increasing mass.

These results can be used to improve the modelling of BH evaporation in TeV gravity scenarios, in the BH event generators [45, 47] that are in use at the ATLAS and CMS experiments to put bounds on extra dimensions in this channel [28, 155–158].

Chapter 6

Marginal charged clouds around charged black holes

6.1 Introduction

Scattering processes for the Proca field were studied in Chapters 4 and 5. An interesting generalization is to study this field in the context of quasinormal modes and quasi-bound states. In fact, such studies have been performed for a neutral Proca field on a Schwarzschild BH [130], and on a slowly rotating Kerr BH [68]. In this chapter, we are going to study quasi-bound states for a charged Proca field (as well as a charged scalar field) on a Reissner-Nördstrom (RN) BH. This study is particularly interesting since we would like to know if the charge couplings between the background and the Proca field could balance the gravitational attraction, similarly to what occurs to scalar clouds.

Scalar clouds [16, 94, 159] are equilibrium configurations of a complex, massive scalar field in the background of a Kerr BH. They are stationary bound states, with a real frequency. These configurations are possible due to the existence of two qualitatively different types of quasi-bound states – i.e. bound field configurations with a *complex* frequency:

i) Time decaying quasi-bound states; this is the generic behavior expected for matter around a BH, due to the purely ingoing boundary condition at the horizon. Indeed, this is the only kind of quasi-bound state that can be found around Schwarzschild BHs.

ii) Time growing quasi-bound states; this occurs for Kerr BHs in the superradiant regime, i.e. when the real part of the frequency, ω, of the quasi-bound state obeys $\omega < m\Omega_H$, where m is the azimuthal harmonic index of the field mode and Ω_H is the horizon angular velocity of the Kerr BH. This yields an instability of Kerr BHs in the presence of any field for which quasi-bound states can be found in the superradiant regime.

Scalar clouds exist at the boundary between these two regimes, i.e. when $\omega = m\Omega_H$, which is compatible with the bound state condition $\omega < \mu$ for scalar fields with mass μ on the Kerr BH. Renewed interest concerning these clouds has been triggered by the recent observation that there are Kerr BHs with scalar hair [16,18,160], found as exact solutions of the Einstein-Klein-Gordon system, and which correspond to the nonlinear realization of these clouds.

It has long been known that charged, i.e. RN BHs can amplify charged scalar fields through superradiant scattering [53]. This is a process that has qualitative similarities with the superradiant scattering of (neutral) scalar fields by Kerr BHs. For the charged case, as explained in Section 1.3, there is no analogue of a charged superradiant instability for asymptotically flat charged BHs [84,85,161]. As such, one concludes that there will be no charged scalar clouds around RN BHs analogue to the ones discussed above for Kerr BH, i.e. as true bound states. An open question is whether the same holds for higher spin massive fields, where an effective potential analysis (which indicates if there is a potential well to support quasi-bound states) is not always straightforward. Here we study the charged Proca field around a RN BH, and show that similar statements to those for a scalar field hold.

Although no stationary bound states exist for charged scalar or Proca fields around RN BHs, we show in this chapter that stationary *marginally bound states* do exist. The first observation of such states for scalar case was reported in [93] in the double extremal limit wherein the BH charge tends to its mass $|Q| \to M$ and the field charge tends to its mass $|q| \to \mu$. It was noticed that, in this limit, the imaginary part of the quasi-bound states vanishes and the real part tends to the mass of the field. Moreover, in this limit, the scalar field does not trivialize and it can be interpreted as a collection of scalar particles at rest, outside the horizon, in a no-force configuration with the BH, due to a balance of electromagnetic and gravitational forces. These particles are only marginally bound to the BH and we shall therefore dub the corresponding field configuration as *marginal (charged) clouds*.

In fact we show that one needs not take a double extremal limit (as in [93]) to get marginal (charged) scalar clouds around RN BHs. It is enough that the *threshold condition*

$$qQ = \mu M \ , \tag{6.1.1}$$

is obeyed, clearly indicating that the equilibrium is due to a force balance. Moreover, we show that a completely analogous behavior is found for a charged Proca field around RN BHs. It is worth emphasizing that although these clouds are only marginally bound, arbitrarily long lived quasi-bound states exist close to the limit where these clouds appear, which, for many practical purposes, may be faced as eternal clouds.

The structure of this chapter is organized as follows. In Section 6.2 we review the background geometry as well as the field equations for the charged Proca and scalar fields. In particular, in Section 6.2.2, we analyze the effective potential for a decoupled mode of the Proca field, to illustrate some expected features of the result. In Section 6.3 we describe the numerical strategy to calculate the quasi-bound state frequencies for coupled and decoupled modes, summarize some known results in the small frequency limit and combine them to predict an approximation for the (hydrogen-like) real part of spectrum for the charged Proca field. In Section 6.4 we present numerical results illustrating the variation of the quasi-bound state frequencies with particle charge and mass as to identify the condition for long lived states. In Section 6.5 we demonstrate that there are indeed solutions when the threshold condition holds, which means that the imaginary part of the frequency vanishes. In a double extremal limit we even find closed form solutions for both the scalar (already discussed in [93]) and also the Proca case. Finally we conclude with a summary of our results in Section 6.6, in particular we discuss the possible existence of nonlinear realizations of these marginal clouds.

6.2 Charged Proca and scalar fields on a charged black hole

6.2.1 The Proca field

We consider first a Proca field W^μ with mass μ^*, which is charged under a $U(1)$ gauge symmetry associated with the gauge field A_μ. The field W^μ can describe W particles in the

*In this chapter, we use μ in general to stand for the mass both for the Proca fields and scalar fields, which were denoted by μ_p and μ_s, respectively, in previous chapters.

SM coupled to gravity and its Lagrangian density is given in Eq. (3.0.1). The background geometry for a $U(1)$ charged BH is given by the RN solution with line element

$$ds^2 = -U(r)dt^2 + \frac{1}{U(r)}dr^2 + r^2(d\theta^2 + \sin^2\theta d\varphi^2) \ , \tag{6.2.1}$$

where

$$U(r) = 1 - \frac{2M}{r} + \frac{Q^2}{r^2} \ .$$

M and Q are the BH mass and charge parameters, respectively. For numerical convenience, we change to units such that the outer horizon radius is at $r_H = 1$, i.e.

$$2M = 1 + Q^2 \ . \tag{6.2.2}$$

The field equations for a Proca field on an Einstein-symmetric (and in particular spherically symmetric) background have been derived in Eqs. (3.1.5), (3.1.6), (3.1.8) and (3.2.2). In the following we set $n = 2$ in those equations, and identify the metric function as $U(r)$. Then we obtain a system of two coupled modes (ψ, χ) obeying

$$\begin{aligned}
&\left[U^2\frac{d}{dr}\left(r^2\frac{d}{dr}\right) + (\omega r - qQ)^2 - U\left(\ell(\ell+1) + \mu^2 r^2\right)\right]\psi + \left[2iU\omega r - ir\left(\omega r - qQ\right)\frac{dU}{dr}\right]\chi = 0 \ , \\
&\left[U^2 r^2\frac{d^2}{dr^2} + (\omega r - qQ)^2 - U\left(\ell(\ell+1) + \mu^2 r^2\right)\right]\chi + \left[2iqQU - ir\left(\omega r - qQ\right)\frac{dU}{dr}\right]\psi = 0 \ ,
\end{aligned} \tag{6.2.3}$$

and a decoupled transverse mode Υ

$$\left[r^2 U\frac{d}{dr}\left(U\frac{d}{dr}\right) + (\omega r - qQ)^2 - \left(\ell(\ell+1) + \mu^2 r^2\right)U\right]\Upsilon = 0 \ , \tag{6.2.4}$$

where $\ell = 1, 2, \ldots$. There is also an exceptional mode for $\ell = 0$ which is described by a decoupled radial equation

$$\left[\frac{d}{dr}\left(\frac{Ur^4}{(\omega r - qQ)^2 - Ur^2\mu^2}\frac{d}{dr}\right) + \frac{r^2}{U} - \frac{qQr^2\left((\omega r - qQ)rU' - 2qQU\right)}{\left[(\omega r - qQ)^2 - Ur^2\mu^2\right]^2}\right]\psi^{(0)} = 0 \ . \tag{6.2.5}$$

The asymptotics of the solutions of such systems has been detailed in Chapter 4 and Chapter 5. Let us denote a generic field mode (coupled or not to others) by ψ_i. Then the near horizon asymptotics for all modes takes the form

$$\psi_i = (r-1)^{\mp i\frac{\omega - qQ}{1-Q^2}}\sum_{n=0}^{+\infty} a_i^{(n)}(r-1)^n \ , \tag{6.2.6}$$

where the minus sign corresponds to an ingoing boundary condition at the horizon. On the other hand, in the asymptotic region $r \to +\infty$ the expansion is

$$\psi_i = e^{i\Phi} \sum_{n=0}^{+\infty} \frac{c_{i,+}^{(n)}}{r^n} + e^{-i\Phi} \sum_{n=0}^{+\infty} \frac{c_{i,-}^{(n)}}{r^n} \tag{6.2.7}$$

with

$$\Phi \equiv kr + \varphi \log r \ ,$$
$$\varphi \equiv \frac{(\omega^2 + k^2)(1+Q^2) - 2qQ\omega}{2k} \ , \tag{6.2.8}$$
$$k \equiv \sqrt{\omega^2 - \mu^2} \ . \tag{6.2.9}$$

All the necessary expansion coefficients were provided in Chapters 4 and 5. As shown originally by Press and Teukolsky [162], if we consider initial data given on a compact support, the late time dynamics of generic linear perturbation is governed by a superposition of a discrete set of solutions in Fourier space. After imposing an ingoing boundary condition at the horizon, there are basically two types of solutions depending on the boundary conditions when $r \to +\infty$ (considering a mode oscillating as $e^{i\Phi}$, i.e. $\Re(k) > 0$ in the square root and assuming, without loss of generality, $\Re(\omega) > 0$):

- $\Im(k) < 0$: these are the quasinormal modes which describe time decaying oscillations. These modes are free to escape the BH potential and asymptotically grow exponentially [163] (for large r).

- $\Im(k) > 0$, these are quasi-bound states, i.e. they describe field configurations which are confined in the outside region of the BH and decay exponentially when $r \to +\infty$. They are possible if there is a confining potential well where the field can accumulate. The boundary condition for these states can thus be recast as

$$\lim_{r \to +\infty} \psi_i = 0 \ . \tag{6.2.10}$$

Quasi-bound states are very interesting in the presence of superradiance, since they provide the possibility of an instability as discussed in Chapter 1. If they exist within the superradiant regime, the field is able to extract energy from the BH which accumulates in the confining potential. This would be signaled by an exponential growth of the wave amplitude. The

condition for the instability to appear is $\omega_I \equiv \Im(\omega) > 0$, i.e. the time-dependence is

$$\psi_i \sim e^{-i\omega t} = e^{-i\omega_R t + \omega_I t} \ . \tag{6.2.11}$$

In the absence of instabilities (i.e. $\omega_I < 0$), the wave amplitude decays exponentially with a lifetime

$$\tau \equiv |\omega_I|^{-1} \ . \tag{6.2.12}$$

If $\omega_I \to 0$ is possible, then the state can be truly bound, or marginally bound if $\omega_R \to \mu \Leftrightarrow k_R \to 0$. Observe that in this exact limit the wavelength diverges so the state becomes delocalized. Actually, $\mu - \omega_R$ is basically the binding energy of the state; since this goes to zero, in the limit, the state becomes marginally bound. Moreover, one can have arbitrarily long lived quasi-bound states near this limit which have a large amplitude in a compact domain (similarly to true bound states – see the results in Section 6.4). If τ is very large, then the state may be effectively considered bound (rather than quasi-bound) for many practical purposes.

6.2.2 Effective potential for the transverse mode

A natural strategy to investigate the possibility of quasi-bound states to appear is to recast the radial equations for the fields in a Schrödinger like form with an effective potential. In the case of the Proca field, this is not so straightforward for the coupled system. However, the transverse mode Eq. (6.2.4), can be easily recast in a Schrödinger like form ($dr_\star \equiv dr/U$)

$$\left[-\frac{d^2}{dr_\star^2} + V_{\rm eff}\right] \Upsilon = 0 \ , \tag{6.2.13}$$

$$V_{\rm eff} = \left(\tfrac{\ell(\ell+1)}{r^2} + \mu^2\right) U - \left(\omega - \tfrac{qQ}{r}\right)^2 \ . \tag{6.2.14}$$

To classify the effective potential and investigate when a well forms, it is convenient to define a compactified coordinate $x \equiv 1 - 1/r \in [0,1]$ such that

$$V_{\rm eff}(x) = \sum_{k=0}^{4} b_k x^k \ , \tag{6.2.15}$$

where the coefficients b_k are

$$b_0 = -(\omega - qQ)^2 \ ,$$
$$b_1 = (1-Q^2)(\mu^2 + \ell(\ell+1)) - 2qQ(\omega - qQ) \ ,$$

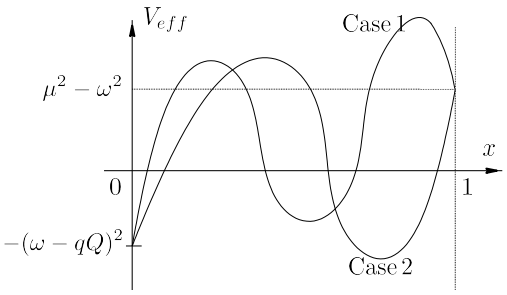

Figure 6.1: Schematic representation of the effective potential (in the compactified coordinate x) for the two possible cases where a well may form.

$$b_2 = -(2-3Q^2)\ell(\ell+1) + Q^2(\mu^2-q^2)\ , \tag{6.2.16}$$
$$b_3 = \ell(\ell+1)(1-3Q^2)\ ,$$
$$b_4 = \ell(\ell+1)Q^2\ .$$

Thus we are dealing with a quartic polynomial. Taking into account its values at the end points a well can only form for two possible configurations with three roots (shown schematically in Fig. 6.1). In case 1 the derivative $V'_{\rm eff}(x)$ must have three positive roots x_1, x_2, x_3. Then its form is $V'_{\rm eff}(x) = A(x-x_1)(x-x_2)(x-x_3)$. But we also know that

$$V'_{\rm eff}(x) \;=\; \sum_{k=0}^{3}(k+1)b_{k+1}x^k\ . \tag{6.2.17}$$

Equating the two forms we conclude that $x_1x_2x_3 = -b_1/(4b_4)$. We are interested in finding a well in the superradiant regime, $\omega < qQ$; but using Eqs. (6.2.16) we conclude that $-b_1/b_4 < 0$, which is inconsistent with the positivity of the roots of the derivative. Thus case 1 is not possible in the superradiant regime.

Case 2 on the other hand is defined by*

$$V'_{\rm eff}(1) > 0 \Leftrightarrow \mu^2 > \frac{2qQ\omega}{1+Q^2} \Leftrightarrow \mu M > qQ\frac{\omega}{\mu} \Leftrightarrow \frac{\omega}{\mu} < \sqrt{\frac{M}{r_H}}\ , \tag{6.2.18}$$

where in the last step we have used the superradiance condition $\omega r_H < qQ$. Except in the near-extremal case, Eq. (6.2.18) is not consistent with hydrogen-like spectrum. We have also made a numerical scan of the parameter space and found none of parameters satisfying the condition in Eq. (6.2.18).

*In this case we could not extract any other condition as for case 1.

This analysis indicates that no potential well is possible in the superradiant regime for the transverse modes. For the coupled system it is not simple to make a similar analysis, so we proceed in the following sections investigating the quasi-bound state frequencies numerically and attempting to flow the parameters into the superradiant regime.

We should note at this point that Furuhashi and Nambu [161] found a condition for bound states to exist for a charged scalar field, working in a small frequency and charge approximation, and using an analytic matching technique. They found the condition that $\mu M \gtrsim qQ$, which, from the applicability of their analysis, is not necessarily true for large parameters. We will find, however, a perfect agreement with this threshold condition for large parameters as well, therefore away from the applicability of the analytic matching approximation in [161].

6.2.3 The scalar field

In this study we have also solved the problem for a charged massive scalar field. In addition to being interesting on its own this also serves as a comparison to check some of the features we have found for the Proca field.

Discussions of the charged massive scalar field can be found, for example, in [46, 93, 146, 147] and in [161] where the rotating case was also analyzed. Here we only present the potential since the structure is very similar to the Υ mode of the Proca field. After decomposing the scalar field φ in spherical harmonics $\varphi = e^{-i\omega t}Y_\ell^m(\phi,\theta)R(r)/r$, the radial equation takes exactly the same Schrödinger like form as for Υ with a modified effective potential

$$V_{\rm eff}^{(\rm scalar)} = \left(\frac{\ell(\ell+1)}{r^2} + \mu^2 + \frac{1}{r}\frac{dU}{dr}\right)U - \left(\omega - \frac{qQ}{r}\right)^2 \ . \tag{6.2.19}$$

Then all the asymptotic analysis and boundary conditions follow our previous discussion, Eqs. (6.2.6) and (6.2.7), for the Proca field modes.

6.3 Numerical strategy

To find the quasi-bound state frequencies, we scan over ω on the complex plane. We first define a function of ω which returns the value of the solutions ψ_i at a large $r_{far} \sim (50 \sim 100)/k_R$ ($k_R = \Re(k)$), i.e. at a very large distance in multiples of the typical wavelength of the

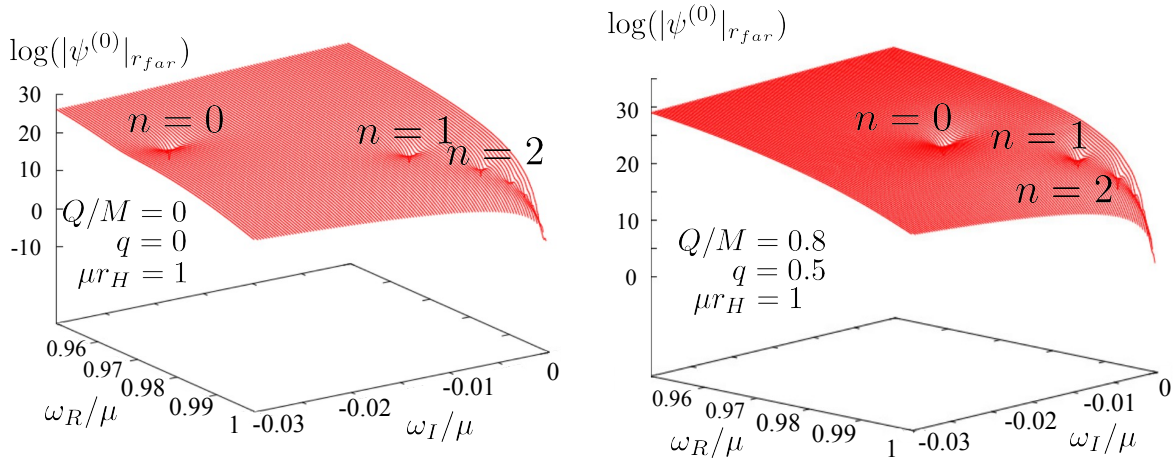

Figure 6.2: Magnitude of the $\psi^{(0)}$ mode at r_{far} (i.e. in the asymptotic far region), as a function of the complex frequency ω in the neutral limit (left) and for non-zero charges (right). The quasi-bound state frequencies occur at sharp dips indicated by the level numbers n.

wave. For each value of ω this is done by integrating the radial equations outwards from the horizon, with initial conditions given by the power series expansions Eq. (6.2.6) evaluated at $r = 1.001$, with typically twenty terms. This function is expected to be exponentially large for generic values of ω except in the vicinity of a quasi-bound state where it should be very small. Numerically, the quasi-bound state frequency is never attained exactly since there is always some numerical contamination of the exponentially growing solution. For example for a decoupled mode

$$\psi_i \sim c^{(0)}_{i,+} e^{ik_R r - |k_I| r} + \ldots + c^{(0)}_{i,-} e^{-ik_R r + |k_I| r} \ . \tag{6.3.1}$$

In the quasi-bound state limit, $c^{(0)}_{i,-} \to 0$. Numerically this corresponds to frequencies that minimize $|\psi_i|_{r_{far}}$. In Fig. 6.2 we show this quantity for the $\ell = 0$ decoupled mode in the neutral case (left) and in the charged case (right). The quasi-bound state frequencies are clearly seen as sharp dips in the surface plots (note that in the vertical axis the logarithm of the scalar field value is represented). We observe that turning on the charge, with $qQ > 0$, the real part of the frequency, ω_R, moves to values closer to the field mass, μ, and the (negative) imaginary part ω_I moves to values closer to zero.

For the coupled sector, the procedure is analogous if one recalls the scattering matrices defined in Chapter 4. First one notes that the general solution of a system of n coupled fields ψ_i,

with second order linear equations, can be represented by $2n$ integration constants. Those constants can be defined either at the event horizon or at infinity. The linearity of the system implies that a linear transformation relates the integration constants at the horizon, with those at infinity. We denote the ingoing and outgoing wave coefficients at the horizon (+/− respectively)

$$\vec{\mathbf{h}} = (\mathbf{h}^+, \mathbf{h}^-) = (h_i^+, h_i^-) \ ,$$

where $i = 1, 2$ for the current coupled system, and, similarly, the coefficients at infinity are defined

$$\vec{\mathbf{y}} = (\mathbf{y}^+, \mathbf{y}^-) = (y_i^+, y_i^-) \ .$$

The linear transformation is then represented as

$$\vec{\mathbf{y}} = \mathbf{S}\vec{\mathbf{h}} \quad \Leftrightarrow \quad \begin{pmatrix} \mathbf{y}^+ \\ \mathbf{y}^- \end{pmatrix} = \left(\begin{array}{c|c} \mathbf{S}^{++} & \mathbf{S}^{+-} \\ \hline \mathbf{S}^{-+} & \mathbf{S}^{--} \end{array}\right) \begin{pmatrix} \mathbf{h}^+ \\ \mathbf{h}^- \end{pmatrix} , \tag{6.3.2}$$

where the scattering matrix $\mathbf{S}$ depends on ω, ℓ, field couplings and the background. It encodes all the information on the scattering process and it can be constructed from specific combinations of modes with boundary conditions set at the horizon.

Similarly to the decoupled modes, we want to impose an ingoing boundary condition at the horizon i.e. $\mathbf{h}^+ = 0$. Then the solution coefficients far away are

$$\mathbf{y}^s = \mathbf{S}^{s-}\mathbf{h}^- \ . \tag{6.3.3}$$

We then must impose that the coefficients of the solution which grows exponentially fast vanish (in analogy to Eq. (6.3.1)), i.e. we need that there is a particular initial condition $\hat{\mathbf{h}}$ at the horizon such that $\mathbf{y}^- = 0$, i.e.

$$0 = \mathbf{S}^{--}\hat{\mathbf{h}}^- \ . \tag{6.3.4}$$

Thus we need to choose the eigenvector with zero eigenvalue of $\mathbf{S}^{--}$. The condition for this solution to be possible is then

$$\det \mathbf{S}^{--} = 0 \ , \tag{6.3.5}$$

which will occur at the quasi-bound state frequencies. Furthermore, one can check that (up to a normalization constant) the radial profile of the quasi-bound state solution is obtained

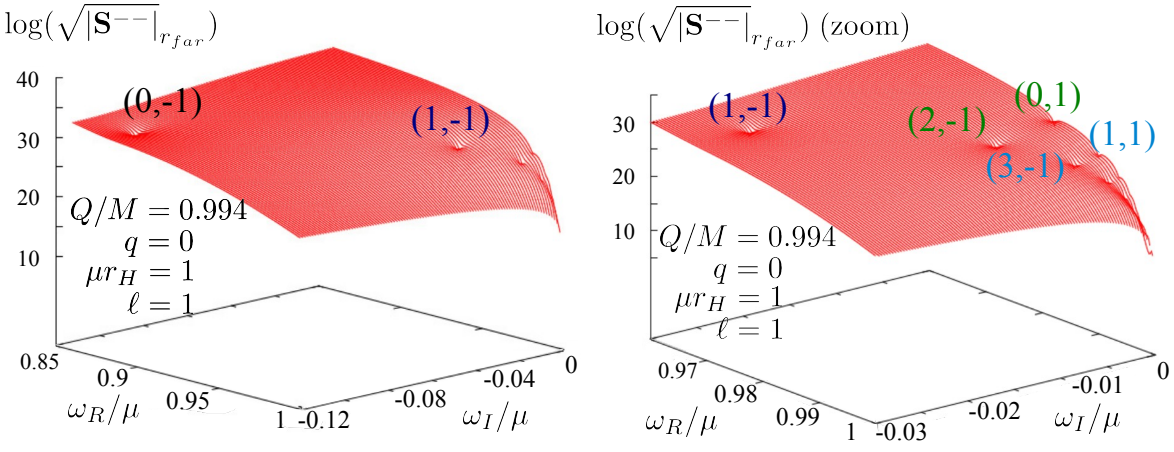

Figure 6.3: Magnitude of the determinant of $\mathbf{S}^{--}$ for the coupled system at r_{far} (i.e. in the asymptotic far region), as a function of the complex frequency ω in the neutral limit for $\ell = 1$. The various levels are indexed by (n, S) as discussed in the text. The right panel shows a zoom to better display the positions of a few higher levels.

using the following initial condition at the horizon

$$\begin{pmatrix} \hat{h}_1^- \\ \hat{h}_2^- \end{pmatrix} \propto \begin{pmatrix} -S_{12}^{--} \\ S_{11}^{--} \end{pmatrix} . \tag{6.3.6}$$

In practice, there is numerical contamination of exponentially growing eigenmodes, which means we must again employ a minimization condition (similarly to the decoupled modes)

$$\min_{\omega} \left[|\mathbf{S}^{--}|_{r_{far}} \right] . \tag{6.3.7}$$

In Fig. 6.3 we show an example of this quantity for $\ell = 1$ coupled modes with a non-zero background charge and a zoom around the corner where the higher frequency levels pile up (right). We discuss in more detail the effect of the field charge in Sections 6.4 and 6.6 so here we only highlight the differences compared with the decoupled cases. Once again the procedure is to find the local minimum for each valley found in the figure.

Since the search for the quasi-bound state frequencies reduces to a (local) minimization problem, one needs in general a good starting guess which is close enough to the valley. Several analytic estimates have been developed in the literature for small parameters. The general conclusion is that ω_R follows a hydrogen like spectrum. Of particular relevance to our

problem is the charged scalar spectrum approximation found in [161]:

$$\omega_R \simeq \mu \left[1 - \frac{1}{2}\frac{(\mu M - qQ)^2}{N^2}\right] \ , \ N = \ell + n + 1 \ , \tag{6.3.8}$$

with $n^* \in \mathbb{N}_0$. This approximation suggests that, as the charge is turned on to positive values, there is a critical value at[†] $\mu M = qQ$, after which we expect an exit from the quasi-bound state regime (since the exponentially decaying tail disappears at this threshold).

Also in the low energy limit, but in the neutral case ($q = Q = 0$), a low energy approximation was found for the Proca field in [130]. Their analytic approximations can in principle be generalized to our case by introducing a charge dependence. Even though in this study we have not developed such analytic matching calculation, we found an excellent agreement (for small parameters) with the following ansatz

$$\omega_R \simeq \mu \left[1 - \frac{1}{2}\frac{(\mu M - qQ)^2}{N^2}\right] \ , \ N = \ell + S + n + 1 \tag{6.3.9}$$

which results from shifting $\mu M \to \mu M - qQ$ in the formula of [130] as suggested by Eq. (6.3.8). Here $S = 0$ for the transverse modes and $S = 1, -1$ for the coupled modes (for the exceptional mode $\ell = 0$ there is only $S = 1$).

In Fig. 6.3 we indicate the labels (n, S) corresponding to this approximation, for the first few pairs of levels which arise in the coupled system. As expected, due to the degeneracy in N, i.e the same N can be obtained by adding different combinations of (n, S) for the same ℓ, the number of degrees of freedom is doubled. This can be observed in the existence of two distinct lines of valleys in the right panel. By continuity, this classification must hold also for larger parameters, so a natural strategy to obtain new frequencies is to perform a flow of the parameters in small steps from some reference quasi-bound state frequencies. This can be pictured as a flow of the valleys in the plots of Figs. 6.2 and 6.3.

The two parameters we will want to vary continuously are the field mass μ and charge q. Taking the mass μ as an example, let us assume we have obtained a high precision quasi-bound state frequency ω by minimization near a valley (with given mode labels $\{\ell, n, S\}$ and fixed μ, q, Q, M). Then by continuity the frequency for this mode at a nearby mass $\mu \to \mu + \delta\mu$ will shift by a small amount $\omega \to \omega + \delta\omega$ (all other parameters are fixed). If the step is small

[*] In the remaining part of this chapter, n refers to the overtone number.

[†] In this limit $\omega_R = \mu$ and in fact $\omega_I = 0$ (see [161]).

enough, we can use the previous ω as a first guess and refine it by minimization to obtain the new frequency. Thus, by using small steps, we can iterate this procedure to flow the frequencies as a function of a continuous parameter. The same procedure can be applied to flow the frequency with charge q.

Even though analytic approximations give a very useful guide to the dependence of the frequencies, and help understanding the labels of the various levels, in practice (especially for larger parameters) we determined various reference initial estimates for the frequencies of each state graphically (using plots such as Fig. 6.2) and then refined them through minimization before using as seeds to the flows. In Table 6.1, we provide a set of seed frequencies that were used as starting points to produce various of the plots in the results of Section 6.4 for the Proca field. Some scalar frequencies that were used to obtain scalar profiles to compare with the Proca field in the region of parameters where long lived states were found (see Sections 6.4 and 6.6) are shown in Table 6.2. All frequencies in these tables were obtained by refining initial estimates through minimization. The initial estimates were obtained graphically by zooming surfaces such as Figs. 6.2 and 6.3 around each valley. Once an initial estimate is found which is inside the valley, the minimization routines refine the result to the required precision. These high precision frequencies can be used to flow either the mass μ or the charge q in small steps, to other values as shown in the plots of Section 6.4.

6.4 Results

In this section, we present a selection of numerical results, focusing mostly on the positive charge coupling case. First, we note that we did not find any quasi-bound states in the superradiant region $\omega < qQ$. To understand why this is the case we analyze first Fig. 6.4 where we represent the variation of the frequencies with charge and mass couplings on a fixed background. In the top row of panels we represent the real part of the frequency (or more precisely $1 - \omega_R/\mu$). The thick curves correspond to the numerical results that we have generated through direct integration. We have requested a minimum relative precision of six digits (i.e. 10^{-6} of relative error). The thin solid lines (matching the color of the solid curves) correspond to the analytic guess, Eq. (6.3.9). In the bottom panels we represent the imaginary part which is always negative. We also indicate with vertical lines the value where

$Qr_H = 0$[a]

N	(ℓ, n, S)	$\mu^{-1}(\omega_R, \omega_I)$
1	$(1, 0, -1)$	$(0.95972157, -0.0037679893)$
2	$(1, 1, -1)$	$(0.99032863, -0.00062350043)$
	$(0, 0, 1)$	$(0.99031646, -0.00051223870)$
	$(1, 0, 0)$	$(0.99131023, -0.00001346974)$

$Qr_H = 0.3$ $(Q/M \simeq 0.55\ ,\ \mu M \simeq 0.27)$

N	(ℓ, n, S)	$\mu^{-1}(\omega_R, \omega_I)$
1	$(1, 0, -1)$	$(0.95270408, -0.0046419907)$
2	$(1, 1, -1)$	$(0.98838598, -0.00084694923)$
	$(0, 0, 1)$	$(0.98812624, -0.00095739793)$
	$(1, 0, 0)$	$(0.98953577, -0.00002375643)$

$Qr_H = 0.9$ $(Q/M \simeq 0.994\ ,\ \mu M \simeq 0.45)$

N	(ℓ, n, S)	$\mu^{-1}(\omega_R, \omega_I)$
1	$(1, 0, -1)$	$(0.87274751, -0.031112471)$
2	$(1, 1, -1)$	$(0.96469871, -0.011098631)$
	$(0, 0, 1)$	$(0.96824273, -0.016591447)$
	$(1, 0, 0)$	$(0.96354486, -0.001705819)$

Table 6.1: Some reference frequencies (found through minimization) used in the flow for the Proca field, with $\mu r_H = 0.5$ and $q = 0$. We indicate the background charge both in inverse horizon radius units, and also in BH mass units for comparison.

N	(ℓ, n)	$\mu^{-1}(\omega_R, \omega_I)$
1	$(0, 0)$	$(0.93713433, -0.083684629)$
2	$(0, 1)$	$(0.97694630, -0.016936300)$
	$(1, 0)$	$(0.96780454, -0.000797486)$

Table 6.2: Some reference frequencies (found through minimization) used in the flow for the scalar field, with $\mu r_H = 0.5$ and $q = 0$. We have focused on $Q/M = 0.994$ to compare with the Proca field.

[a]Note that the results shown in this table agree with the data used in [130], to all of the significant figures quoted.

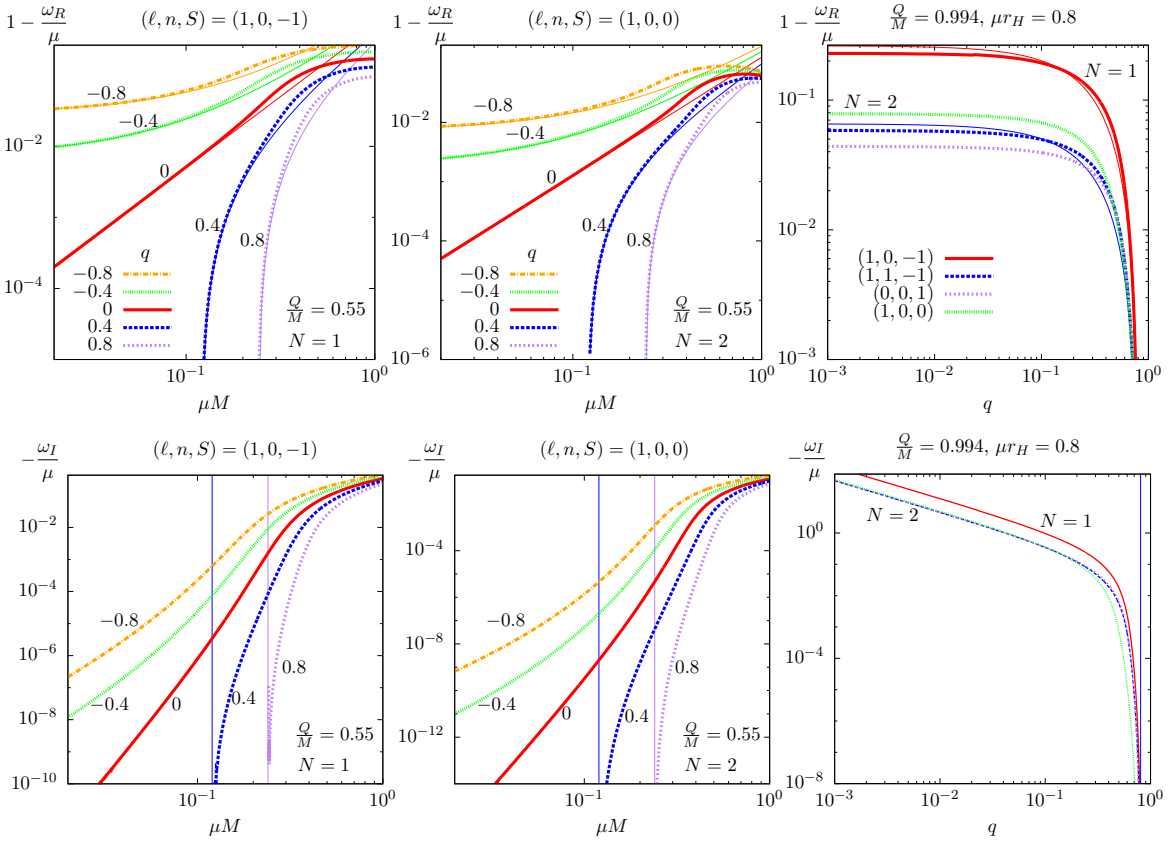

Figure 6.4: Variation of the quasi-bound state frequencies with field mass μ and charge q for the Proca field. In the top panels we represent curves for the real part ω_R whereas the corresponding curves for the imaginary part are in the bottom panels. The thick curves labeled in the key to the figures are obtained by numerical integration. The thin solid lines correspond to the analytic formula Eq. (6.3.9). The vertical lines give, for each case $\mu M = qQ$.

the threshold condition $\mu M = qQ$ is attained.

In the left panels we represent the fundamental mode frequency of the Proca system ($N = 1$) with various curves for different positive and negative field charge as a function of mass coupling μM. The middle panels are similar except that we represent a first excited state ($N = 2$). The main observations on these are:

- Generically, ω_I is negative and its modulus decreases for smaller mass.
- For negative field charge* q, as it goes to more negative values, $|\omega_I|$ grows for fixed mass, which means that τ decreases so the scalar mode should be quickly absorbed by the BH.
- For positive q, however, as we flow to smaller mass, there is a sharp threshold in ω_I precisely at $\mu M = qQ$, i.e. when the mass coupling balances out exactly the electromagnetic coupling. At this threshold $\tau \to +\infty$, which means that we can have arbitrarily long lived Proca quasi-bound states.
- Furthermore, at the threshold $\mu M = qQ$, the real part of the frequency also tends sharply to μ. This means that as we try to flow into the superradiant regime ($\omega < qQ$), we leave the quasi-bound state regime into the scattering regime, before reaching it. This explains the fact that we did not find any quasi-bound states in that regime.
- Finally, one can see a very good agreement between our guess, Eq. (6.3.9), (thin solid lines) not only for small mass, but also near the long lived state threshold even for larger mass and charge couplings.

These features are confirmed in the right panels of Fig. 6.4, where we have performed a flow of the charge q, with Q close to the extremal BH background limit, for all the $N = 1, 2$ modes of the Proca system. Here it can be seen more clearly that as the charge q is increased to larger positive values, there is a maximum value allowed which is given by $q_{max} = \mu M/Q$ (in the extremal limit this becomes $q = \mu$).

In Fig. 6.5 we display some examples of quasi-bound state radial profiles. In all panels we vary the field charge from zero up to a value close to the maximum allowed by the threshold

*Throughout we assume the convention that the BH charge is positive.

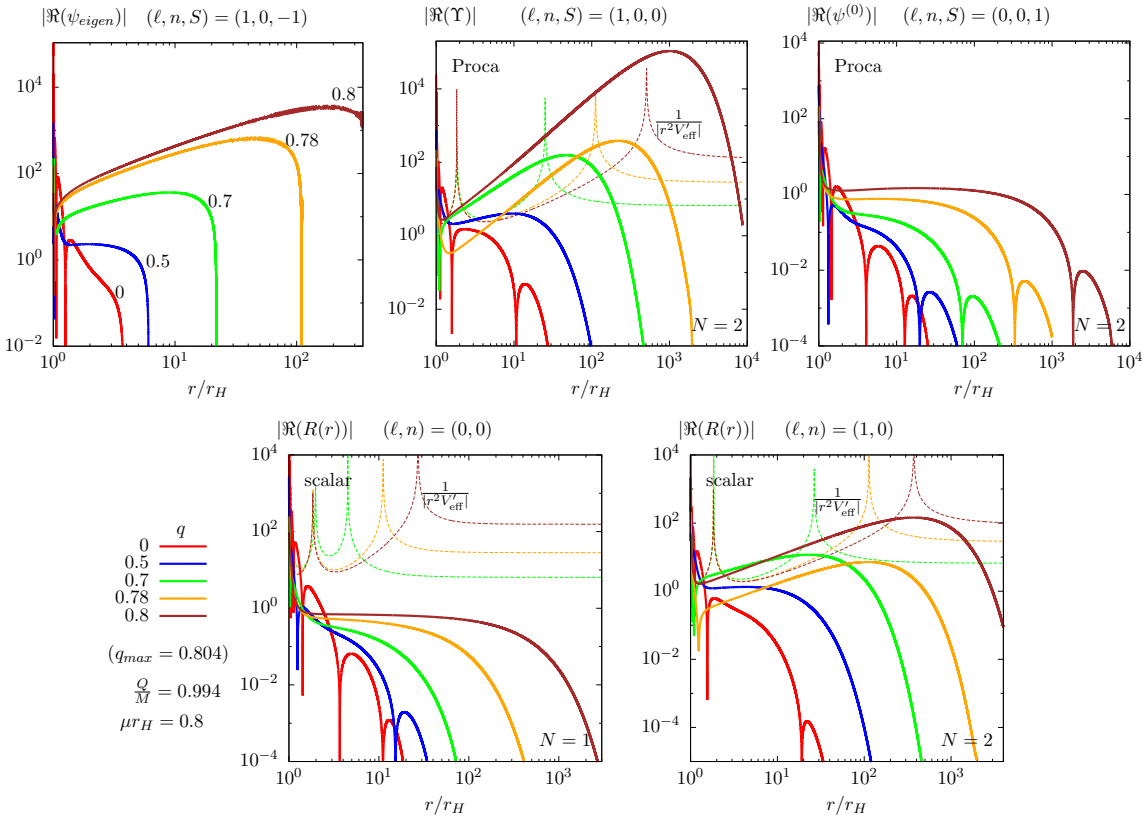

Figure 6.5: Radial profiles for some quasi-bound state modes for the Proca field (top row) and scalar field (bottom row) for comparison (key in the bottom row applies to all plots). We also indicate for some cases $|r^2 dV_{\rm eff}/dr|^{-1}$ whose poles indicate the local maximum and minimum of the effective potential (left and right peaks in each panel where it is represented in thin dashed lines). In the top left panel we also indicate the charge q associated with each curve (the same ordering applies to all other panels).

condition, to observe how the field binds around the BH close to that limit. The top row is for modes of the Proca field and we have also included, for comparison, some modes for the scalar field in the bottom row. Whenever an effective potential is known, we display the quantity $|r^2 dV_{\rm eff}/dr|^{-1}$ (i.e. the inverse derivative). The latter has poles, one at a local maximum of the effective potential near the horizon and another at a minimum (further away), which define the location of the potential well.

In the top left panel we display the fundamental mode of the Proca field. This mode is in the coupled system and it is the eigenvector with zero eigenvalue of the $\mathbf{S}^{--}$ matrix. It results from the linear combination of two exponentially growing solutions, so for large r the fine cancellation that must occur in the linear combination becomes numerically more difficult. This can be seen in the brown ($q = 0.8$) curve which starts oscillating due to numerical errors on the right tail region (in r). It is clear from the curves that as we approach the threshold charge the field spreads out to a larger radius and the oscillations close to the horizon (which are associated with the field's absorption by the BH) become less extended. This shows that the field configuration becomes more and more bound state like (rather than quasi-bound) since the field oscillations associated with absorption near the horizon become smaller in amplitude.

In the top middle panel we show an $N = 2$ level obtained from the transverse $S = 0$ equation. The features are similar to the left one except that the radial profile peaks more strongly. The peak is clearly correlated with the depth of the potential well where the field is more tightly bound, as seen in the dashed lines indicating the maximum and minimum of the potential.

The top right panel, shows the first $\ell = 0$ level. The main difference is that the curves in the bound region tend to be much more flat. This is due to the absence of orbital angular momentum for these states. In fact, in the bottom left panel we show the corresponding mode in the scalar case (for comparison) where exactly the same happens for $\ell = 0$.

In the scalar case (bottom row), similar features apply. In particular one can verify very clearly that the field profile in the long lived limit, extends inside the (increasingly wide) potential well.

6.5 Analytic solutions

We will now show that in the limit in which the imaginary part of the frequency goes to zero, there are indeed non-trivial solutions, which are the limiting behavior of the modes found numerically in the previous section. This follows closely the analysis in [93] but extends it, not only because we also consider the Proca field but also because we do not restrict ourselves to the double extremal limit considered therein.

From the results of Section 6.4, in the limit of the threshold condition

$$\mu M = qQ \Leftrightarrow qQ = \frac{(1+Q^2)}{2}\mu \,, \tag{6.5.1}$$

the frequency becomes real and equal to the field mass

$$\omega = \mu \,. \tag{6.5.2}$$

We replace these two conditions in the original equations, for both the Proca and the scalar field, and define $\rho \equiv r - 1$ and

$$\epsilon \equiv 1 - Q^2 \,. \tag{6.5.3}$$

If $\epsilon = 0$, then $Q^2 = 1$; going back to natural units, this means $Q = M$ and $\mu = q$. So this corresponds to a *double extremal limit*, i.e. an extremal limit for both the BH and the field. Thus ϵ parameterizes the deviation from the double extremal limit, but keeping the force balance condition given by Eq. (6.5.1). We will show that there are exact solutions for the Proca field when $\epsilon = 0$, an analogous situation to that observed in [93] for the scalar field case. But even for $\epsilon \neq 0$, as we will show later, non-trivial solutions of the Proca fields are existed.

With the definitions above, the equations for the Proca field simplify as follows. The transverse mode equation becomes

$$\left[\frac{d^2}{d\rho^2} + \left(\frac{1}{\rho} - \frac{2}{1+\rho} + \frac{1}{\epsilon+\rho}\right)\frac{d}{d\rho} - \frac{\ell(\ell+1)}{\rho(\epsilon+\rho)} + \left(\frac{\epsilon\mu(1+\rho)}{2\rho(\epsilon+\rho)}\right)^2\right]\Upsilon = 0 \,. \tag{6.5.4}$$

The $\ell = 0$ mode equation is in fact very similar

$$\left[\frac{d^2}{d\rho^2} + \left(\frac{1}{\rho} + \frac{2}{1+\rho} + \frac{1}{\epsilon+\rho}\right)\frac{d}{d\rho} - \frac{2-\epsilon}{\rho(1+\rho)(\epsilon+\rho)} + \left(\frac{\epsilon\mu(1+\rho)}{2\rho(\epsilon+\rho)}\right)^2\right]\psi^{(0)} = 0 \,. \tag{6.5.5}$$

The coupled system is now

$$\left[\frac{d^2}{d\rho^2}+\frac{2}{1+\rho}\frac{d}{d\rho}-\frac{\ell(\ell+1)}{\rho(\epsilon+\rho)}+\left(\frac{\epsilon\mu(1+\rho)}{2\rho(\epsilon+\rho)}\right)^2\right]\psi+i\mu\frac{4\rho^3+6\epsilon\rho^2+\epsilon^2(\rho-1)}{2\rho^2(\epsilon+\rho)^2}\chi=0\ ,$$
$$\left[\frac{d^2}{d\rho^2}-\frac{\ell(\ell+1)}{\rho(\epsilon+\rho)}+\left(\frac{\epsilon\mu(1+\rho)}{2\rho(\epsilon+\rho)}\right)^2\right]\chi-\frac{i\epsilon^2\mu(1+\rho)}{2\rho^2(\epsilon+\rho)^2}\psi=0. \tag{6.5.6}$$

Finally, for the scalar field we have

$$\left[\frac{d^2}{d\rho^2}+\left(\frac{1}{\rho}-\frac{2}{1+\rho}+\frac{1}{\epsilon+\rho}\right)\frac{d}{d\rho}-\frac{\ell(\ell+1)}{\rho(\epsilon+\rho)}+\left(\frac{\epsilon\mu(1+\rho)}{2\rho(\epsilon+\rho)}\right)^2+\frac{\epsilon(\rho-1)-2\rho}{\rho(1+\rho)^2(\epsilon+\rho)}\right]R=0\ . \tag{6.5.7}$$

We first consider the scalar field case with $\epsilon=0$, and obtain

$$R_\ell=(\rho+1)\left(A^{(R)}\rho^\ell+B^{(R)}\rho^{-\ell-1}\right)\ . \tag{6.5.8}$$

Then the scalar field can be written as a linear combination of harmonic functions*

$$\varphi=e^{-i\mu t}\sum_{\ell,m}Y_{\ell m}(\theta,\phi)\left(A^{(R)}\rho^\ell+B^{(R)}\rho^{-\ell-1}\right)\ . \tag{6.5.9}$$

To interpret the meaning of the modes (6.5.9), it is useful to rewrite the extremal RN BH, in isotropic coordinates

$$ds^2=-H^{-2}dt^2+H^2\delta_{ij}dx^idx^j\ ,\ A=(H^{-1}-1)dt\ , \tag{6.5.10}$$

where $H(x^i)$ is a harmonic function on Euclidean 3-space, i.e. $\Delta_{\mathbb{E}^3}H=0$. To describe a single extremal RN BH, H is taken to have a single pole localized at the origin, $H=1+M/|\mathbf{x}|$. But multi-centered solutions, of Majumdar-Papapetrou type [164, 165], are also possible if one chooses a harmonic function with multiple poles. Then one can solve the scalar field equation, by taking $\varphi(t,x^i)=e^{-i\mu t}U(x^i)$, with $\mu=q$ on the background in Eq. (6.5.10). The field equation thus becomes

$$\Delta U(\mathbf{x})=-4\pi\mu\delta^3(\mathbf{x}-\mathbf{x}')\ , \tag{6.5.11}$$

*One may observe that the harmonic modes with $e^{-i\mu t}$ can be transformed to be static by making a gauge transformation, $\varphi\to\varphi e^{i\xi}$ with $\xi=\mu t$, and $A_\mu\to A_\mu+q^{-1}\partial_\mu\xi$. This is also true for the Proca case, following the same transformation but $W_\mu\to W_\mu e^{i\xi}$. We would like to emphasize, however, that even without the above transformations, the energy momentum tensors for marginal scalar and Proca clouds are time independent, which imply that they are static.

with the solution $U(\mathbf{x}) = \mu/|\mathbf{x}-\mathbf{x}'|$, and where the δ function is introduced to describe that the field is localized at $\mathbf{x}'$ (not coincide with the BH horizon). In terms of spherical coordinates, (ρ, θ, ϕ), we have*

$$U(\mathbf{x}) = \frac{\mu}{|\mathbf{x}-\mathbf{x}'|} = \frac{4\pi\mu}{\rho'}\sum_{\ell,m}\frac{Y^*_{\ell m}(\theta',\phi')}{2\ell+1}F_\ell(\rho)Y_{\ell m}(\theta,\phi)\ , \tag{6.5.12}$$

where the function F_ℓ is constructed from two homogeneous solutions of Eq. (6.5.9)

$$F_l(\rho) \equiv \begin{cases} (\rho/\rho')^\ell, & \rho \leq \rho', \\ (\rho'/\rho)^{\ell+1}, & \rho \geq \rho'. \end{cases} \tag{6.5.13}$$

It is obvious that the solution in Eq. (6.5.12) is regular both at the horizon and at infinity, and describe scalar particles at some spatial location in equilibrium with the BH (due to a force cancellation).

Considering the Proca field equations and $\epsilon = 0$, we find exact general solutions which are qualitatively similar to the scalar solution:

$$\begin{aligned}
&\Upsilon = ((\rho+1)\ell+1)A^{(\Upsilon)}\rho^\ell + ((\rho+1)\ell+\rho)B^{(\Upsilon)}\rho^{-\ell-1}\ , \\
&\psi^{(0)} = \frac{1}{1+\rho}\left(A^{(0)}\rho + B^{(0)}\rho^{-2}\right)\ , \\
&\chi = A^{(\chi)}\rho^{\ell+1} + B^{(\chi)}\rho^{-\ell}\ , \\
&\psi = \frac{1}{1+\rho}\left[A^{(\psi)}\rho^{\ell+1} + \frac{B^{(\psi)}}{\rho^\ell} - i\mu\left(A^{(\chi)}\frac{\rho^{\ell+2}(3+\rho+\ell(2+\rho))}{(3+5\ell+2\ell^2)} - B^{(\chi)}\frac{\rho^{1-\ell}(\ell(2+\rho)-1)}{\ell(2\ell-1)}\right)\right].
\end{aligned} \tag{6.5.14}$$

We now apply a scalar-vector decomposition, using invariant tensors on the Euclidean 3-space, of the form

$$W_0 = H^{-1}\Psi\ , \qquad \vec{W} = \nabla\Phi + \vec{V}\ , \qquad \nabla\cdot\vec{V} = 0\ , \tag{6.5.15}$$

where $W_\mu = (W_0, \vec{W})$. All vectors and differential operators are now in Euclidean 3-space. Then, Φ becomes the non-dynamical mode which disappears due to the (gauged) Lorentz condition; this condition is a consequence of the Proca equations. As such, we have (as before) a longitudinal degree of freedom, Ψ, and two transverse degrees of freedom, $\vec{V}$. From

*This corrects a statement made in [87] and [93] that regular solutions at the horizon can be constructed from divergent partial waves. We would like to thank Sam Dolan for pointing out that only inhomogeneous solutions can be made regular at both boundaries.

the time and space components of the Proca equation, these obey a Laplace and a Maxwell-Faraday like equation, respectively:

$$\Delta\Psi = 0 \,, \qquad \nabla \times \vec{\beta} = -i\mu\nabla\Psi \,, \tag{6.5.16}$$

where we have defined

$$\vec{\beta} = \frac{1}{H^2}\nabla \times \vec{V} \,. \tag{6.5.17}$$

Clearly, the longitudinal mode equation can be solved by a point like source centered at any point

$$\Psi = \frac{A}{|\mathbf{x} - \mathbf{x}'|} \,, \tag{6.5.18}$$

and it serves as a source to the transverse modes. Furthermore, due to the linear structure, we can superpose any linear combination of solutions.

The bottom line we wish to emphasize is that the marginal (charged) Proca clouds exist in the double extremal limit and, as the scalar clouds, can be made regular at both boundaries. This can be achieved, as shown for scalar case, by constructing an inhomogeneous solution of the form (6.5.18) with $\mathbf{x}'$ not coinciding with the BH horizon, from two homogeneous solutions of each equation in (6.5.14).

When $\epsilon \neq 0$ we cannot find a closed form solution. Nevertheless, after asymptotically expanding the equations in the limit $\rho \gg 1$ we find

$$\begin{aligned}
\Upsilon &\to \rho\left(A^{(\Upsilon)}\rho^{J_{(0)}} + B^{(\Upsilon)}\rho^{-1-J_{(0)}}\right) \,, \\
\psi^{(0)} &\to \frac{1}{\rho}\left(A^{(0)}\rho^{J_{(+)}} + B^{(0)}\rho^{-J_{(+)}-1}\right) \,, \\
\chi &\to A_1\rho^{J_{(-)}} + B_1\rho^{-1-J_{(-)}} + A_2\rho^{J_{(+)}} + B_2\rho^{-1-J_{(+)}} \,, \\
\rho\,\psi &\to \hat{A}_1\rho^{2+J_{(-)}} + \hat{B}_1\rho^{1-J_{(-)}} + \hat{A}_2\rho^{2+J_{(+)}} + \hat{B}_2\rho^{1-J_{(+)}} \,,
\end{aligned} \tag{6.5.19}$$

where the hatted constants $\hat{A}_i,\ \hat{B}_i$ are proportional to $A_i,\ B_i$ (the constants are unimportant) and we have defined the effective total angular momentum

$$J_{(S)} \equiv \sqrt{\left(\frac{1}{2} + \ell + S\right)^2 - \left(\frac{\epsilon\mu}{2}\right)^2} - \frac{1}{2} \,. \tag{6.5.20}$$

For the scalar field

$$R \to \rho\left(A^{(R)}\rho^{J_{(0)}} + B^{(R)}\rho^{-1-J_{(0)}}\right) \,. \tag{6.5.21}$$

This result, justifies the existence of non-trivial solutions when the threshold condition $\mu M = qQ$ is obeyed, even away from double extremality.

6.6 Summary

In this chapter we have studied quasi-bound state for test field configurations of charged Proca and scalar fields in the background of the RN BH. We have found some interesting properties which are present for both types of fields and are likely to be generic for massive charged bosonic fields.

First, despite the existence of superradiant scattering of charged Proca fields by RN BHs as found in Chapter 5, we did not find any quasi-bound states in the superradiant regime, hence no superradiant instabilities due to charged Proca fields. This agrees with what occurs for charged scalar fields [84, 85, 161].

Second, we have found, considering $\mu M > qQ > 0$, that either decreasing the mass μ or increasing the charge q as to achieve the threshold condition $\mu M = qQ$, one gets arbitrarily long lived states, since the imaginary part of the quasi-bound state frequency tends to zero. When taking this limit the frequency becomes equal to the field mass $\omega \to \mu$, and so the states become marginally bound. Since they do not trivialize, we obtain configurations we have dubbed *marginal (charged) scalar and Proca clouds* around RN BHs. But observe that these clouds are qualitatively different from those found in the Kerr case [16, 94, 159], and recently extended to the Kerr-Newman case [166], which are real bound states.

By analyzing the behavior of the field profiles when approaching the threshold condition, the region where the field has a large amplitude agrees well with the region where a potential well is present. The width of the well typically increases when approaching the marginally bound limit meaning that the field is large on a wider region away from the BH horizon. Since the quasi-bound state is localized away from the horizon, the gravitational and electromagnetic field interactions which are responsible for supporting the bound state should be dominated by their asymptotic Newtonian and Coulombian limit respectively. Thus the threshold condition $\mu M = qQ$ should in fact correspond to a force balance condition between the Newtonian force and the electrostatic force.

Scalar clouds around Kerr BHs can be promoted to nonlinear hair. Indeed Kerr BHs with scalar hair exist that connect precisely to the Kerr solutions that allow the existence of the corresponding cloud [16, 18, 160]. One may therefore ask if the existence of these marginal

(charged) scalar and Proca clouds hints at the existence of nonlinear solutions of RN BHs with scalar or Proca hair. One possibility is along the lines of the discussion in [93], for the scalar case. It was observed therein that the marginal scalar clouds (albeit this terminology was not used therein) can be seen as the partial waves of a distribution of charged scalar particles in a no-force balance with the RN BH. This suggests the existence of multi-object nonlinear solutions – of Majumdar-Papapetrou type [164, 165], but not necessarily multiple BHs. One other possibility, however, is that since the clouds that are regular at the horizon are a linear combination of partial waves with $\ell \neq 0$, the corresponding nonlinear configurations will have non-zero angular momentum and thus will be a Kerr-Newman BH with charged scalar (or Proca) hair, a possibility already anticipated in [16, 166]. Of course, the existence (or nonexistence) of any of these possible solutions, can only be decided by a fully nonlinear analysis of the Einstein-(charged)-Klein-Gordon or Einstein-(charged)-Proca systems.

Part II

Scalar and Maxwell fields on asymptotically AdS spacetimes

Chapter 7

Superradiant instabilities in higher dimensions

7.1 Introduction

Superradiant instabilities are interesting phenomena with various applications from high energy physics to astrophysics, see a recent review [17] and references therein. Most of these studies focus on four dimensional spacetimes*, but a generic analysis for superradiant instabilities in higher dimensions is still missing. In order to perform such a study, we choose asymptotically AdS BHs, one of the confining mechanisms discussed in Section 1.3, in which bound states of perturbation fields can be supported.

The goal of this chapter is to present a complete study of superradiant instabilities triggered by a charged scalar field interacting with a D-dimensional Reissner-Nordström-anti-de Sitter (RN-AdS) BH. As a spin off we shall clarify a claim, made in [72], that, in $D = 5$, a subset of field modes – those with odd angular momentum quantum number, ℓ – do not develop superradiant instabilities. We shall show otherwise: that in fact *all* ℓ modes in *all* dimensions can develop superradiant instabilities.

In addition to the study of superradiant instabilities for a minimally coupled charged scalar field, other studies have been considered for charged AdS BHs. It was first observed in

*Exceptionally a few works were carried out in five dimensional spacetimes, see [72, 88], for example.

[167,168] that for BHs obtained within $\mathcal{N}=8$ supergravity* in $D=4$, *large* RN-AdS BHs are dynamically unstable due to the existence of a tachyonic mode in the scalar field perturbations. On the other hand, in purely Einstein-Maxwell theory in D dimensions, RN-AdS BHs have been argued to be stable against gravitational perturbations [169]. Thus the existence of scalar fields with some coupling to Maxwell fields is central to the instability of [167, 168].

A qualitatively different instability of RN-AdS BHs has been discussed in the context of holographic superconductors. It occurs in the presence of a massive scalar field that may or may not be charged and leads to the formation of scalar hair around the BH [170]. Unlike the superradiant instability, this other instability occurs even if the scalar field is not charged. In that case the, say, $D=4$ RN-AdS BH should be nearly extremal, which means its near horizon geometry has a two dimensional AdS factor; moreover, the scalar field should have a tachyonic mass above the Breitenlohner-Freedman bound [171, 172] of the four dimensional AdS space, but below the Breitenlohner-Freedman bound of the two dimensional AdS factor in the near horizon geometry of the BH. This is why the scalar field provides an instability to the BH geometry, but not to four dimensional AdS space.

In order to investigate the superradiant instability of a charged, massive scalar field in a D-dimensional RN-AdS background we shall employ both an analytical and a numerical method. First, we solve the charged Klein-Gordon equation using a matching method, and obtain a solution near the BH region and another one far away from the BH. This is done for small BHs, i.e. BHs obeying $r_+ \ll L$, where r_+ and L stand for the BH event horizon and the AdS radius, respectively. The analytical quasinormal frequency for small BHs is then obtained by matching the near and far solutions in an intermediate region. We find that the relation between ℓ and D plays a central role in determining the analytical quasinormal frequency formula. When $\ell=(p+\frac{1}{2})(D-3)$, where p is a non-negative integer, the matching method fails. The reason is that the near region solution and the far region solution have different functional dependence in terms of the radial coordinate, which makes our matching impossible. Such difficulty in employing the matching method also occurs for extremal BHs as discussed in [64], where an alternative point matching method was used. For all other values of ℓ and D, the matching method works and it may be used to show that a superradiance instability

*This is a theory containing four $U(1)$ gauge fields and three real scalar fields *non-minimally* coupled to the Maxwell fields.

exists for all ℓ modes, in a region of the parameters space.

After the (approximate) analytical analysis, then we solve the charged Klein-Gordon equation numerically both to check the analytical results and to explore the special case where the analytical method fails. We find good agreement between the two methods in the regime where both are valid. For the special case $\ell = (p+\frac{1}{2})(D-3)$, the numerical results show that the superradiant instability does exist.

The structure of this chapter is organized as follows. In Section 7.2 we introduce the background geometry and the scalar field equation. In Section 7.3 we solve the scalar field equation analytically using the matching method and obtain an analytical quasinormal frequency formula. We analyze this formula for different relations between ℓ and D, and show the reason why the matching method fails for the special case $\ell = (p + \frac{1}{2})(D - 3)$ in Section 7.4. To confirm our analytical results and to be able to investigate if there is a superradiant instability for that special case, we resort to a numerical method to solve the Klein-Gordon equation in Section 7.5. Conclusions are presented in the last section.

7.2 Background and field equation

We consider a D-dimensional RN-AdS BH with the line element

$$ds^2 = -f(r)dt^2 + \frac{1}{f(r)}dr^2 + r^2 d\Omega_n^2 \,, \tag{7.2.1}$$

where $d\Omega_n^2$ is the metric on the unit n-sphere. In the following it will be convenient to use $n = D-2$ rather than D to parameterize the spacetime dimension. The metric function $f(r)$ takes the form

$$f(r) = 1 - \frac{M}{r^{n-1}} + \frac{Q^2}{r^{2(n-1)}} + \frac{r^2}{L^2} \,, \tag{7.2.2}$$

where the parameters M, Q and L are related to the BH mass $\mathcal{M}$, charge $\mathbb{Q}$ and cosmological constant Λ through

$$M = \frac{16\pi G\mathcal{M}}{nS_n} \;, Q^2 = \frac{8\pi G\mathbb{Q}^2}{n(n-1)} \;, L^2 = -\frac{n(n+1)}{2\Lambda} \,,$$

and the area of a unit n-sphere is $S_n = \frac{2\pi^{\frac{n+1}{2}}}{\Gamma(\frac{n+1}{2})}$. The Hawking temperature is given by

$$T = \frac{1}{4\pi}\left[\frac{(n-1)M}{r_+^n} - \frac{2(n-1)Q^2}{r_+^{2n-1}} + \frac{2r_+}{L^2}\right] \,, \tag{7.2.3}$$

where the event horizon r_+ is determined as the largest root of $f(r_+) = 0$. For non-extremal BHs, we have $Q < Q_c$, where the critical charge Q_c corresponds to the maximal charge (i.e the charge of an extremal BH) and is given by

$$Q_c \equiv r_+^{n-1}\sqrt{1+\frac{n+1}{n-1}\left(\frac{r_+}{L}\right)^2}\,. \tag{7.2.4}$$

The electromagnetic potential of the charged BH is

$$A = \left(-\sqrt{\frac{n}{2(n-1)}}\frac{Q}{r^{n-1}} + C\right)dt\,,$$

where the choice of the constant C is a gauge choice. For instance, we should fix C as

$$C = \sqrt{\frac{n}{2(n-1)}}\frac{Q}{r_+^{n-1}}\,,$$

in order to have a vanishing electromagnetic potential at the event horizon, a choice used in the context of the AdS/CFT correspondence [173]. As argued in [75], however, this constant just shifts the real part of quasinormal frequency as $\mathrm{Re}(\omega) \to \mathrm{Re}(\omega) + qC$ (q is the field charge) without affecting the imaginary part of it. Therefore, as we are mostly interested in the superradiant instability, which is determined by the imaginary part of the quasinormal frequency, we take in the following $C = 0$.

For a charged massive scalar field, the corresponding Klein-Gordon (K-G) equation can be written as

$$\frac{1}{\sqrt{-g}}D_\mu\left[\sqrt{-g}g^{\mu\nu}D_\nu\right]\phi - \mu^2\phi = 0\,, \tag{7.2.5}$$

where $D_\mu = \partial_\mu - iqA_\mu$, q and μ are the field charge and mass, respectively. The scalar field ϕ can be decomposed in terms of spherical scalar harmonics due to the spherical symmetry of the background

$$\phi = \mathrm{e}^{-i\omega t}\mathrm{R(r)Y}(\theta_\mathrm{i})\,, \tag{7.2.6}$$

where $\mathrm{Y}(\theta_\mathrm{i})$ is a scalar spherical harmonic on the n-sphere. Substituting the metric in Eq. (7.2.1) and the field decomposition in Eq. (7.2.6) into the K-G equation (7.2.5), we have

$$\frac{\Delta}{r^{n-2}}\frac{d}{dr}\left(\frac{\Delta}{r^{n-2}}\frac{d\mathrm{R}}{dr}\right) - \left(\lambda+\mu^2r^2\right)\Delta\mathrm{R} + r^{2n}\left(\omega+qA_t\right)^2\mathrm{R} = 0\,, \tag{7.2.7}$$

with

$$\Delta \equiv r^{2(n-1)} - Mr^{n-1} + Q^2 + \frac{r^{2n}}{L^2}\,,$$

and the $n-$dimensional spherical harmonic eigenvalue λ is given by

$$\lambda \equiv \ell(\ell + n - 1) \ ,$$

where ℓ is the angular momentum quantum number.

For numerical convenience, we may rewrite Eq. (7.2.7) in terms of a new function X

$$f(r)^2 \frac{d^2\mathrm{X}}{dr^2} + f(r)f'(r)\frac{d\mathrm{X}}{dr} + \left[(\omega + qA_t)^2 - f(r)\left(\frac{\lambda}{r^2} + \mu^2 + \frac{nf'(r)}{2r} + \frac{n(n-2)f(r)}{4r^2}\right)\right]\mathrm{X} = 0 \ , \tag{7.2.8}$$

where $\mathrm{X} \equiv r^{n/2}\mathrm{R}$.

In order to determine the quasinormal frequency, by solving Eq. (7.2.8), one has to impose boundary conditions. Near the event horizon, we impose an ingoing boundary condition

$$\mathrm{X} \sim \mathrm{e}^{-i(\omega-\omega_0)r_*} \ , \tag{7.2.9}$$

where $\omega_0 \equiv -qA_t(r_+)$ and the tortoise coordinate r_* is defined by

$$\frac{dr_*}{dr} = \frac{1}{f(r)} \ .$$

At infinity, we impose a decaying boundary condition

$$\mathrm{X} \sim r^{-\frac{1}{2}(1+\sqrt{4\mu^2L^2+(n+1)^2})} \ , \tag{7.2.10}$$

then

$$\mathrm{R} \sim r^{-\frac{1}{2}(n+1+\sqrt{4\mu^2L^2+(n+1)^2})} \ . \tag{7.2.11}$$

For a massless field in D dimensions, the radial function goes, asymptotically as $\mathrm{R} \sim 1/r^{D-1}$, as expected for a normalizable massless scalar perturbation in D-dimensional AdS space.

7.3 Analytic calculations

In this section, we present the analytic calculations of quasinormal frequencies for a charged massive scalar field in a higher dimensional RN-AdS BH. Using a standard procedure, we shall divide the space outside the event horizon into two regions: the *near region*, defined by the condition $r - r_+ \ll 1/\omega$, and the *far region*, defined by the condition $r_+ \ll r - r_+$.

Then, in order to perform a matching of the two solutions we consider a low frequency condition, i.e. $r_+ \ll 1/\omega$, and match the two solutions in an *intermediate region* defined by $r_+ \ll r - r_+ \ll 1/\omega$. In the following analysis we focus on small AdS BH ($r_+ \ll L$). This allows us to treat the frequencies for the RN-AdS BH as a perturbation of the AdS normal frequencies.

7.3.1 Near region solution

For the near region analysis, we rewrite Eq. (7.2.7) as

$$(n-1)^2\,\Delta\frac{d}{dx}\left(\Delta\frac{d\mathrm{R}}{dx}\right)-\left(\lambda+\mu^2 r^2\right)\Delta\mathrm{R}+r^{2n}\Big(\omega+qA_t\Big)^2\mathrm{R}=0\,, \tag{7.3.1}$$

where $x\equiv r^{n-1}$. In the following we shall neglect the mass term in the first line of Eq. (7.3.1). This amounts to say that $r\ll\frac{\ell}{\mu}$, which is obeyed if the Compton wave length of the scalar particles is much larger than the BH horizon size and indeed becomes the near region condition if, moreover, the scalar particle Compton wave length is much smaller than the AdS radius. Observe that the condition $r\ll\frac{\ell}{\mu}$ fails for $\ell=0$ modes, but it turns out that even in that case the analytical results we shall obtain are in good agreement with the numerical results for sufficiently small mass (cf. Section 7.5). Under this approximation Eq. (7.3.1) becomes

$$(n-1)^2\Delta\frac{d}{dx}\left(\Delta\frac{d\mathrm{R}}{dx}\right)-\lambda\Delta\mathrm{R}+r_+^{2n}\Big(\omega+qA_t\Big)^2\mathrm{R}=0\,. \tag{7.3.2}$$

For convenience in the analytic calculations, one can define a new dimensionless variable

$$z\equiv\frac{x-x_+}{x-x_-}\,,$$

with $x_+=r_+^{n-1}$ and $x_-=r_-^{n-1}$, where r_+ and r_- refer to the event horizon and the Cauchy horizon, respectively. Then Eq. (7.3.2) can be transformed into

$$z\frac{d}{dz}\left(z\frac{d\mathrm{R}}{dz}\right)+\left[\bar{\omega}^2-\frac{\lambda}{(n-1)^2}\frac{z}{(1-z)^2}\right]\mathrm{R}=0\,, \tag{7.3.3}$$

with

$$\bar{\omega}\equiv\frac{x_+^{\frac{n}{n-1}}}{(n-1)(x_+-x_-)}\left(\omega-\sqrt{\frac{n}{2(n-1)}}\frac{qQ}{x_+}\right)\,. \tag{7.3.4}$$

Observe that $\bar{\omega}<0$ for $\omega<\sqrt{\frac{n}{2(n-1)}}\frac{qQ}{x_+}$. This will be shown below to correspond to the superradiant regime.

One may now obtain a solution for Eq. (7.3.3) with ingoing boundary condition in terms of a hypergeometric function:

$$\mathrm{R} \sim z^{-i\bar{\omega}}(1-z)^{\alpha} F(\alpha, \alpha - 2i\bar{\omega}, 1 - 2i\bar{\omega}; z) \,, \tag{7.3.5}$$

where

$$\alpha \equiv 1 + \frac{\ell}{n-1} \,. \tag{7.3.6}$$

In order to match the far region solution, one must expand the near region solution, Eq. (7.3.5), at large r. To achieve this we take the $z \to 1$ limit and use the properties of the hypergeometric function [174], then obtain

$$\mathrm{R} \sim \Gamma(1 - 2i\bar{\omega}) \left[\frac{\mathrm{R}^{\mathrm{near}}_{1/r}}{r^{n-1+\ell}} + \mathrm{R}^{\mathrm{near}}_{r} r^{\ell} \right] \,, \tag{7.3.7}$$

where

$$\begin{aligned} \mathrm{R}^{\mathrm{near}}_{1/r} &\equiv \frac{\Gamma(1-2\alpha)(r_+^{n-1} - r_-^{n-1})^{\alpha}}{\Gamma(1-\alpha)\Gamma(1-\alpha-2i\bar{\omega})} \,, \\ \mathrm{R}^{\mathrm{near}}_{r} &\equiv \frac{\Gamma(2\alpha-1)(r_+^{n-1} - r_-^{n-1})^{1-\alpha}}{\Gamma(\alpha)\Gamma(\alpha-2i\bar{\omega})} \,. \end{aligned} \tag{7.3.8}$$

Since the Gamma function has poles at negative integers, one observes that special care must be taken with the factor $\Gamma(1-2\alpha)/\Gamma(1-\alpha)$. Its analysis will play a role below.

7.3.2 Far region solution

In the far region, $r - r_+ \gg r_+$, the BH effects can be neglected ($M \to 0,\ Q \to 0$) so that

$$\Delta \simeq r^{2n} \left(\frac{1}{r^2} + \frac{1}{L^2} \right) \,.$$

Then Eq. (7.2.7) becomes

$$\left(1 + \frac{r^2}{L^2}\right) \frac{d^2\mathrm{R}}{dr^2} + \left(\frac{n}{r} + \frac{(n+2)r}{L^2} \right) \frac{d\mathrm{R}}{dr} + \left[\omega^2 \left(1 + \frac{r^2}{L^2}\right)^{-1} - \left(\frac{\lambda}{r^2} + \mu^2 \right) \right] \mathrm{R} = 0 \,. \tag{7.3.9}$$

Defining a new variable

$$y \equiv 1 + \frac{r^2}{L^2} \,,$$

Eq. (8.4.7) becomes

$$y\,(1-y)\,\frac{d^2\mathrm{R}}{dy^2} + \left(1 - \frac{n+3}{2}y\right) \frac{d\mathrm{R}}{dy} - \left[\frac{\omega^2 L^2}{4y} - \frac{\mu^2 L^2}{4} + \frac{\lambda}{4(1-y)} \right] \mathrm{R} = 0 \,. \tag{7.3.10}$$

The above equation has a hypergeometric equation structure, which can be shown explicitly through the transformation

$$\mathrm{R} = y^{\frac{\omega L}{2}}(1-y)^{\frac{\ell}{2}}F(a,b;c;y)\ ,$$

with parameters

$$\begin{aligned} a &\equiv \frac{n+1}{4} + \frac{\omega L}{2} + \frac{\ell}{2} + \frac{1}{2}\sqrt{\mu^2 L^2 + \left(\frac{n+1}{2}\right)^2}\ , \\ b &\equiv \frac{n+1}{4} + \frac{\omega L}{2} + \frac{\ell}{2} - \frac{1}{2}\sqrt{\mu^2 L^2 + \left(\frac{n+1}{2}\right)^2}\ , \\ c &\equiv 1 + \omega L\ . \end{aligned} \tag{7.3.11}$$

Then considering a decaying boundary condition at infinity given in Eq. (7.2.11), one finds a solution for Eq. (7.3.10) in the form

$$\mathrm{R} \sim (1-y)^{\frac{\ell}{2}} y^{\frac{\omega L}{2}-a} F(a, 1+a-c; 1+a-b; \frac{1}{y})\ . \tag{7.3.12}$$

To achieve the small r behavior of Eq. (7.3.12), making the transformation $\frac{1}{y} \to 1-y$ and using properties of the hypergeometric function [174], we obtain

$$\mathrm{R} \sim \Gamma(1+a-b)\left[\frac{\mathrm{R}^{\mathrm{far}}_{1/r}}{r^{n-1+\ell}} + \mathrm{R}^{\mathrm{far}}_{r} r^{\ell}\right]\ , \tag{7.3.13}$$

where

$$\mathrm{R}^{\mathrm{far}}_{1/r} \equiv \frac{\Gamma(\ell+\frac{n-1}{2})L^{n-1+\ell}}{\Gamma(a)\Gamma(1+a-c)}\ , \qquad \mathrm{R}^{\mathrm{far}}_{r} \equiv \frac{\Gamma(-\ell-\frac{n-1}{2})L^{-\ell}}{\Gamma(1-b)\Gamma(c-b)}\ . \tag{7.3.14}$$

The solution in Eq. (7.3.13) is for pure AdS. Regularity of the above solution at the origin ($r=0$) of AdS requires*

$$\Gamma(1+a-c) = \infty \ \Rightarrow 1+a-c = -N,$$

which gives the discrete spectrum

$$\omega_N L = 2N + \frac{n+1}{2} + \ell + \sqrt{\mu^2 L^2 + \left(\frac{n+1}{2}\right)^2}\ , \tag{7.3.15}$$

where N is a non-negative integer. Observe that the AdS frequencies remain real even for tachyonic modes when $0 > \mu^2 \geq -(n+1)^2/(4L^2)$. This is the well known Breitenlohner-Freedman bound already discussed in the introduction. In particular one may see that the

*We remark that, alternatively, one can also demand $\Gamma(a) = 0$, which gives the negative AdS spectrum. Without loss of generality, we only consider the positive spectrum here.

bound is more negative for higher dimensional spaces. This is the reason why one may violate the bound for two dimensional AdS but obey it for four dimensional AdS.

When the BH effects are taken into account, a correction to the frequency (which may be complex) will be generated

$$\omega = \omega_N + i\delta \ , \tag{7.3.16}$$

where the real part of δ is used to describe the damping of the quasinormal modes. Then, for small BHs, using the approximation $1/\Gamma(-N+\epsilon) \simeq (-1)^N N!\epsilon$ for small ϵ, the first term inside the bracket of Eq. (7.3.13) becomes

$$\mathrm{R}^{\mathrm{far}}_{1/r} = (-1)^{N+1} i\delta N! \frac{\Gamma(\ell+\frac{n-1}{2})L^{n+\ell}}{2\Gamma(a)} \ .$$

Finally, observe that there appears to be extra poles in $\mathrm{R}^{\mathrm{far}}_r$, Eq. (7.3.14), due to the Gamma function $\Gamma(-\ell-\frac{n-1}{2})$ for odd n. In the $\mathrm{R}^{\mathrm{far}}_r$ expression, however, due to Eq. (7.3.15), $\Gamma(1-b) = \Gamma(-\ell-\frac{n-1}{2}-N)$, which cancels the former poles.

7.3.3 Overlap region

To match the near region solution (7.3.7) and the far region solution (7.3.13) in the intermediate region, we impose the matching condition $\mathrm{R}^{\mathrm{near}}_r \mathrm{R}^{\mathrm{far}}_{1/r} = \mathrm{R}^{\mathrm{far}}_r \mathrm{R}^{\mathrm{near}}_{1/r}$. Then δ can be obtained perturbatively

$$\begin{aligned}\delta =& (-1)^N 2i \frac{(r_+^{n-1}-r_-^{n-1})^{2\alpha-1}}{N! L^{2\ell+n}} \frac{\Gamma(1-2\alpha)\Gamma(\alpha)}{\Gamma(2\alpha-1)\Gamma(1-\alpha)} \frac{\Gamma(a)}{\Gamma(1-b)\Gamma(c-b)} \frac{\Gamma(-\ell-\frac{n-1}{2})}{\Gamma(\ell+\frac{n-1}{2})} \\ & \times \frac{\Gamma(\alpha-2i\bar{\omega})}{\Gamma(1-\alpha-2i\bar{\omega})} \ .\end{aligned} \tag{7.3.17}$$

7.4 Analytical result analysis

To analyze Eq. (7.3.17), we shall simplify the Gamma functions therein. Firstly, the following combination, which is independent of the relation between ℓ and n, can be simplified as

$$\begin{aligned}\frac{\Gamma(a)}{\Gamma(1-b)\Gamma(c-b)} \frac{\Gamma\left(-\ell-\frac{n-1}{2}\right)}{\Gamma\left(\ell+\frac{n-1}{2}\right)} =& \frac{(-1)^N}{\Gamma\left(\ell+\frac{n-1}{2}\right)} \frac{\Gamma\left(N+\frac{n+1}{2}+\ell+\sqrt{\mu^2L^2+(\frac{n+1}{2})^2}\right)}{\Gamma\left(N+1+\sqrt{\mu^2L^2+(\frac{n+1}{2})^2}\right)} \\ & \times \prod_{k=1}^{N}\left(\ell+\frac{n-1}{2}+k\right) \ .\end{aligned}$$

Then one has to consider the following cases separately, because the simplification for the other Gamma functions in Eq. (7.3.17) depends on the relation between ℓ and n.

7.4.1 ℓ is an integer multiple of $(n-1)$

For this case we can write $\ell = p(n-1)$, where p is a non-negative integer. Then, the corresponding Gamma functions in Eq. (7.3.17) can be simplified to

$$\frac{\Gamma(1-2\alpha)\Gamma(\alpha)}{\Gamma(2\alpha-1)\Gamma(1-\alpha)} = \frac{(-1)^{p+1}}{2}\frac{(p!)^2}{(2p)!(2p+1)!}\,,$$

$$\frac{\Gamma(\alpha-2i\bar{\omega})}{\Gamma(1-\alpha-2i\bar{\omega})} = (-1)^{p+1}2i\bar{\omega}\prod_{k'=1}^{p}(k'^2+4\bar{\omega}^2)\,.$$

Therefore, Eq. (7.3.17) becomes

$$\begin{aligned}\delta =& -2\bar{\omega}\frac{(r_+^{n-1}-r_-^{n-1})^{1+\frac{2\ell}{n-1}}}{N!L^{2\ell+n}\Gamma\left(\ell+\frac{n-1}{2}\right)}\frac{(p!)^2}{(2p)!(2p+1)!}\frac{\Gamma\left(N+\frac{n+1}{2}+\ell+\sqrt{\mu^2L^2+(\frac{n+1}{2})^2}\right)}{\Gamma\left(N+1+\sqrt{\mu^2L^2+(\frac{n+1}{2})^2}\right)}\\ &\times\prod_{k=1}^{N}\left(\ell+\frac{n-1}{2}+k\right)\prod_{k'=1}^{p}(k'^2+4\bar{\omega}^2)\,.\end{aligned} \tag{7.4.1}$$

This equation shares a similar structure to the corresponding result in $D=4$. From the definition of $\bar{\omega}$ in Eq. (7.3.4), we find that in the superradiant regime, $\bar{\omega}<0$ which implies $\delta>0$. In this superradiant regime the wave function of the scalar field will grow with time which means the BH is unstable. Moreover, from Eq. (7.3.4), one may get a condition for the onset of the superradiant instability, i.e.

$$\frac{Q}{Q_c} > \sqrt{\frac{2(n-1)}{n}}\frac{\omega_N}{q}\,, \tag{7.4.2}$$

where ω_N is given in Eq. (7.3.15). For a massless field, Eq. (7.4.2) simplifies to

$$\frac{Q}{Q_c} > \sqrt{\frac{2(n-1)}{n}}\frac{2N+n+1+\ell}{qL}\,. \tag{7.4.3}$$

7.4.2 ℓ is not an integer multiple of $(n-1)$

For this case, the corresponding Gamma function in Eq. (7.3.17) can be simplified as

$$\frac{\Gamma(1-2\alpha)\Gamma(\alpha)}{\Gamma(2\alpha-1)\Gamma(1-\alpha)} = -\frac{1}{2\cos\frac{\pi\ell}{n-1}}\frac{\Gamma^2(1+\frac{\ell}{n-1})}{\Gamma(1+\frac{2\ell}{n-1})\Gamma(2+\frac{2\ell}{n-1})}\,.$$

If $\dfrac{\ell}{n-1} \neq p+\frac{1}{2}$, then $\cos\frac{\pi\ell}{n-1} \neq 0$, and the parameter δ becomes complex (not simply real as in the previous case). In this case the real part of δ reflects the instability, which is given by

$$\begin{aligned}\mathrm{Re}\delta = &-2\bar{\omega}\frac{(r_+^{n-1}-r_-^{n-1})^{1+\frac{2\ell}{n-1}}}{N!L^{2\ell+n}}\frac{\Gamma^4(1+\frac{\ell}{n-1})}{\Gamma(1+\frac{2\ell}{n-1})\Gamma(2+\frac{2\ell}{n-1})\Gamma(\ell+\frac{n-1}{2})}\prod_{k=1}^{N}(\ell+\frac{n-1}{2}+k)\\ &\times\frac{\Gamma(N+\frac{n+1}{2}+\ell+\sqrt{\mu^2L^2+(\frac{n+1}{2})^2})}{\Gamma(N+1+\sqrt{\mu^2L^2+(\frac{n+1}{2})^2})}\,,\end{aligned} \tag{7.4.4}$$

where we have expanded the terms $\Gamma(x-2i\bar{\omega})$ around small $\bar{\omega}$ to clearly distinguish the superradiant regime. Thus, when $\bar{\omega}<0$, we obtain $\mathrm{Re}\delta>0$ which implies that the BH is also unstable, and the corresponding onset of such instability is governed by Eq. (7.4.2) for a massive field and Eq. (7.4.3) for a massless field.

If $\frac{\ell}{n-1} = p+\frac{1}{2}$, the matching method fails; a similar situation occurs for extremal Kerr BHs [64]. In order to make this point clear, we can do the following analysis. First, from the definition of α in Eq. (7.3.6) and the condition $\frac{\ell}{n-1}=p+\frac{1}{2}$, one observes that the first expansion term inside the brackets of Eq. (7.3.7) is divergent, which means that we cannot expand Eq. (7.3.5) into Eq. (7.3.7) anymore when $\frac{\ell}{n-1}=p+\frac{1}{2}$. Alternatively, using a property of the hypergeometric function [174], we shall expand Eq. (7.3.5) as

$$\mathrm{R}\sim\Gamma(1-2i\bar{\omega})\left[-\frac{(r_+^{n-1}-r_-^{n-1})^{\alpha}\zeta}{\Gamma(1-\alpha)\Gamma(1-\alpha-2i\bar{\omega})\Gamma(2\alpha)}\frac{1}{r^{n-1+\ell}}+\frac{\Gamma(2\alpha-1)(r_+^{n-1}-r_-^{n-1})^{1-\alpha}}{\Gamma(\alpha)\Gamma(\alpha-2i\bar{\omega})}r^{\ell}\right]\,, \tag{7.4.5}$$

with

$$\zeta=\log\left(\frac{r_+^{n-1}-r_-^{n-1}}{r^{n-1}}\right)+\gamma+\psi(\alpha)-\psi(2\alpha)+\psi(\alpha-2i\bar{\omega})\,,$$

where γ is the Euler constant and $\psi(x)$ denotes the digamma function. Because the $\log r$ term is associated with distinct powers of r, it is impossible to match Eqs. (7.3.13) and (7.4.5). For this case, we have to resort to a numerical solution, which is discussed in the next section.

7.5 Numerical results

In order to confirm the above analytical results and to calculate the quasinormal frequencies for the special cases $\frac{\ell}{n-1}=p+\frac{1}{2}$ where the analytical method fails, we shall solve, in this section, Eq. (7.2.8) numerically. We use a direct numerical integration method to obtain the

quasinormal frequency of the BH. To do so, taking the boundary conditions near the horizon in Eq. (7.2.9) and at infinity in Eq. (7.2.10), we expand the radial function near the horizon as

$$\mathrm{X} \sim e^{-i(\omega-\omega_0)r_*} \sum_{j=0}^{\infty} \alpha_j (r-r_+)^j \ , \tag{7.5.1}$$

and at infinity as

$$\mathrm{X} \sim r^{-\frac{1}{2}(1+\sqrt{4\mu^2L^2+(n+1)^2})} \sum_{j=0}^{\infty} \frac{\beta_j}{r^j} \ . \tag{7.5.2}$$

The series expansion coefficients can be derived directly after inserting these expansions into Eq. (7.2.8). We use the series expansion near the horizon Eq. (7.5.1) to initialize the radial system Eq. (7.2.8) from a point r_s which is close to r_+ through the relation $r_s = (1+0.01)r_+$, and integrate the radial system outwards up to a radial value r_m. Similarly we can also use Eq. (7.5.2) as initial condition to integrate the radial system inward from $r_l = 1000r_+$ down to r_m. Then we have two solutions at an intermediate radius r_m, and these two solutions are linearly dependent if their Wronskian vanishes at r_m. Using a secant method one can solve $W(\omega, r_m) = 0$ iteratively to look for the quasinormal frequency of the BH. We also varied r_s, r_m and r_l to check the numerical accuracy.

We list some numerical results in Tables 7.1-7.5. Note that all physical quantities are normalized by the AdS radius L and we set $L = 1$. In the first three tables, we focus on the fundamental modes of massless fields because they are typically the most unstable modes. To check the mass effect on the validity of the analytical formulas, we also consider $\mu = 0.5$ and $\mu = 3.0$ in the last two tables. As a check of our numerical method, we have calculated the quasinormal frequencies for small Schwarzschild-AdS BHs and we obtained results which are in good agreement with those reported in [175].

In order to address the special case for which the analytical method fails, i.e when $\ell = (p+\frac{1}{2})(n-1)$, we chose $n = 3$ (five dimensional spacetime) and $\ell = 1$, corresponding to $p = 0$ in our condition. The results are shown in Table 7.1, with $r_+ = 0.1$, field mass $\mu = 0$ and field charge $q = 8$. It shows clearly that a superradiant instability appears when Q/Q_c satisfies the condition in Eq. (7.4.3). Moreover, we also list numerical results for the $\ell = 0$ mode in Table 7.1. It shows that the frequencies of the odd modes ($\ell = 1$) and even modes ($\ell = 0$) have a similar behavior; in other words, there is nothing special for odd modes.

To confirm the validity of the analytical quasinormal frequency formulas in Eqs. (7.4.1) and

Table 7.1: Frequencies of the fundamental modes with different ℓ for a BH with $r_+ = 0.1$, $q = 8$, $\mu = 0$ in $D = 5$.

Q/Q_c	ℓ=0	ℓ=1
0.1	3.958 - 1.335$\times 10^{-2}$ i	4.978 - 2.689$\times 10^{-4}$ i
0.3	3.997 - 6.435$\times 10^{-3}$ i	4.998 - 1.367$\times 10^{-4}$ i
0.5	4.030 - 1.522$\times 10^{-3}$ i	5.014 - 5.053$\times 10^{-5}$ i
0.7	4.058 + 1.996$\times 10^{-3}$ i	5.028 - 2.596$\times 10^{-6}$ i
0.8	4.070 + 3.198$\times 10^{-3}$ i	5.034 + 7.524$\times 10^{-6}$ i
0.9	4.081 + 3.954$\times 10^{-3}$ i	5.040 + 9.597$\times 10^{-6}$ i

(7.4.4), we also compare some analytical results with numerical data in Tables 7.2-7.5. In Table 7.2, we present analytical results obtained from Eq. (7.4.1) and numerical results with $r_+ = 0.01$, $q = 6$ for the $\ell = 0$ massless fundamental mode in five dimensional spacetimes. They show good agreement; the difference is smaller than 1%. In Table 7.3, we present analytical results obtained from Eq. (7.4.4) and numerical data for the $\ell = 1$ fundamental mode with $r_+ = 0.01$, $q = 10$, $\mu = 0$ in $D = 6$, and they show good agreement as well. From these two tables, we confirm the validity of the analytical matching method for $\mu = 0$. Results for non-zero mass are reported in Tables 7.4 and 7.5. Two conclusions may be drawn from these tables. First, as the mass increases the agreement between the analytical and numerical method becomes worse. This is expected in view of the discussion of the approximation employed in Section 7.3. Second, as the mass increases, the mode with $Q/Q_c = 0.9$ becomes stable. This is in agreement with Eq. (7.4.2) since, for the parameters in Table 7.5, superradiance is only expected for $Q/Q_c \gtrsim 1.1$.

7.6 Summary

We have studied the superradiant instability of small charged AdS BHs in D dimensions, in the presence of a charged scalar field. Very recently our result has been generalized to the D-dimensional singly rotating Myers-Perry BHs, where the same conclusion was drawn, i.e.

Table 7.2: Comparison of the frequencies for the $\ell = 0$ fundamental modes of a BH with $r_+ = 0.01$, $q = 6$, $\mu = 0$ in $D = 5$.

Q/Q_c	Im(ω) (numerical)	Im(ω) (analytical)
0.1	-1.053$\times 10^{-5}$	-1.0441$\times 10^{-5}$
0.3	-7.369$\times 10^{-6}$	-7.3230$\times 10^{-6}$
0.5	-4.222$\times 10^{-6}$	-4.2050$\times 10^{-6}$
0.7	-1.088$\times 10^{-6}$	-1.0870$\times 10^{-6}$
0.9	2.023$\times 10^{-6}$	2.0310$\times 10^{-6}$

Table 7.3: Comparison of the frequencies for the $\ell = 1$ fundamental modes of a BH with $r_+ = 0.01$, $q = 10$, $\mu = 0$ in $D = 6$.

Q/Q_c	Im(ω) (numerical)	Im(ω) (analytical)
0.1	-4.377$\times 10^{-11}$	-4.3678$\times 10^{-11}$
0.3	-2.830$\times 10^{-11}$	-2.8274$\times 10^{-11}$
0.5	-1.342$\times 10^{-11}$	-1.3418$\times 10^{-11}$
0.7	-1.538$\times 10^{-12}$	-1.5371$\times 10^{-12}$
0.8	2.283$\times 10^{-12}$	2.2846$\times 10^{-12}$
0.9	3.778$\times 10^{-12}$	3.7844$\times 10^{-12}$

the superradiant instability exist for all ℓ modes in *all* dimensions [176, 177].

First, we solved the Klein-Gordon equation for a charged scalar field in charged AdS BHs with a standard matching method. We found that the relation between the angular momentum quantum number ℓ and the spacetime dimension D plays an important role in determining the analytical quasinormal frequency formula. When $\ell = p(D-3)$, for a non-negative integer p, we found that the quasinormal frequencies of the small RN-AdS BHs have only an imaginary correction to the AdS normal frequencies. This is the case for all modes (i.e. all ℓ) in $D = 4$, even ℓ in $D = 5$, $\ell = 0, 3, 6, 9, \ldots$ in $D = 6$, $\ell = 0, 4, 8, 12, \ldots$ in $D = 7$ and so on.

A more subtle case occurs when $\ell = (p + \frac{1}{2})(D-3)$. For this case the matching method fails because a $\log r$ term appears in the near region solution – Eq. (7.4.5) – which cannot be matched to Eq. (7.3.13). Failure to observe this limitation has led to a claim that odd

Table 7.4: Comparison of the frequencies for the $\ell = 0$ fundamental modes of a BH with $r_+ = 0.01$, $q = 6$, $\mu = 0.5$ in $D = 5$.

Q/Q_c	Im(ω) (numerical)	Im(ω) (analytical)
0.1	-1.093$\times 10^{-5}$	-1.0844$\times 10^{-5}$
0.3	-7.711$\times 10^{-6}$	-7.6617$\times 10^{-6}$
0.5	-4.498$\times 10^{-6}$	-4.4797$\times 10^{-6}$
0.7	-1.300$\times 10^{-6}$	-1.2977$\times 10^{-6}$
0.9	1.878$\times 10^{-6}$	1.8842$\times 10^{-6}$

Table 7.5: Comparison of the frequencies for the $\ell = 0$ fundamental modes of a BH with $r_+ = 0.01$, $q = 6$, $\mu = 3.0$ in $D = 5$.

Q/Q_c	Im(ω) (numerical)	Im(ω) (analytical)
0.1	-2.379$\times 10^{-5}$	-2.3423$\times 10^{-5}$
0.3	-1.886$\times 10^{-5}$	-1.8637$\times 10^{-5}$
0.5	-1.399$\times 10^{-5}$	-1.3850$\times 10^{-5}$
0.7	-9.155$\times 10^{-6}$	-9.0632$\times 10^{-6}$
0.9	-4.321$\times 10^{-6}$	-4.2765$\times 10^{-6}$

ℓ modes in $D = 5$ did not exhibit superradiance [72]. Here we have shown otherwise that the superradiant instability indeed exists using a numerical method which is mandatory for analyzing this case, in view of the invalidity of the matching method. A similar conclusion applies to all cases defined by $\ell = (p + \frac{1}{2})(D - 3)$, i.e, odd ℓ in $D = 5$, $\ell = 2, 6, 10, 14, \ldots$ in $D = 7$ and so on. Observe that this case can only occur in odd dimensions.

Finally, all other cases have a complex correction to the AdS normal frequencies, i.e. the real part of the frequency is also shifted.

Our analytic results show good agreement with the numerical results in Section 7.5. In particular a central conclusion is that all ℓ modes in all dimensions, for sufficiently large field charge q display superradiance. Moreover, in $D = 4$, the dependence of the instability on the various parameters seems to be in qualitative agreement with the study of cavity BHs in $D = 4$ [90–92], and it would be interesting to make a more detailed comparison between the

two cases.

Let us close this study with two questions. First, is there a simple pattern for the behaviour of the frequencies as $D \to \infty$? A preliminary analysis could not unveil a simple formula. Finding such behavior would be relevant in view of the recent interest on General Relativity in the large D limit [178]. Second, can one follow this instability numerically into the non-linear regime? It has been recently shown that in four dimensions the end-point of the instability is a hairy charged AdS BH [83]. It would be interesting to generalize such study to higher dimensions, to display how the properties of hairy BHs depend on the spacetime dimension.

Chapter 8

Maxwell perturbations on Kerr-AdS black holes

8.1 Introduction

The global structure of asymptotically AdS spacetimes allows interesting novel features, as compared to asymptotically flat spacetimes. For instance, when a rotating BH exists in the bulk of an asymptotically AdS spacetime, superradiant instabilities can be triggered by a massless field, in contrast to the asymptotically flat case wherein such instabilities only arise for massive fields. Recently scalar [32] and gravitational perturbations [31] on Kerr-AdS BHs have been addressed, and have been shown to exhibit a rich physics.

In this chapter we complete the analysis of bosonic fields on this background by studying Maxwell perturbations. To do so, one has to assign physically relevant boundary conditions which depend on the specific problem. In the context of quasinormal modes in asymptotically AdS BHs, the most studied perturbations are those of scalar fields, for which *field vanishing* boundary conditions are usually imposed, see e.g. [32]. For other spin fields, the problem has only been partly addressed. The quasinormal modes for the Maxwell field and gravitational field on Schwarzschild-AdS BHs have been obtained using the Regge-Wheeler method [105], instead of the Teukolsky equation, in [179, 180], exploring the spherical symmetry of the background. Furthermore, these works impose field vanishing boundary conditions. For

non-spherically symmetric backgrounds, like in Kerr-AdS BHs, one must, however, use the Teukolsky formalism and, since this formalism uses a different set of variables, it is not obvious how to impose boundary conditions for non-zero spin fields. Recently, superradiant instabilities of the gravitational field on Kerr-AdS BHs have been studied [31] with boundary conditions chosen as to preserve the asymptotic global AdS structure of the background [118]. The general principle to impose boundary conditions for arbitrary spin fields on Kerr-AdS BHs, however, is still missing.

The AdS boundary may be regarded as a perfectly reflecting mirror, in the sense that no energy flux can cross it. We will take this viewpoint as our basic principle to impose boundary conditions for linear perturbations of asymptotically AdS spacetimes. It suggests taking *vanishing energy flux* (VEF) boundary conditions, which should be contrasted to the *field vanishing* boundary conditions we mentioned before. We will first illustrate how this simple physical principle, can lead to two different Robin boundary conditions, using the Maxwell field as an example.

These boundary conditions are then used to study quasinormal modes, superradiantly unstable modes, and vector clouds. To address superradiant instabilities triggered by the Maxwell field on Kerr-AdS BHs, we use both an analytical matching scheme as well as a numerical method to explore the problem. The former method provides an intuitive way to understand how these two boundary conditions produce different instabilities, in the small BH and slow rotation regime. The latter method provides a technique to understand the problem in a larger region of the parameter space. We find that Maxwell fields can trigger stronger instabilities than scalar fields [32] in the superradiant regime, for both boundary conditions.

Stationary clouds [94] are bound state solutions of test fields on a rotating background, at the linear level. They exist at the threshold of the superradiant instabilities triggered by that test field. Recently, a considerable number of studies of such clouds has appeared in the literature, mostly in asymptotically flat spacetimes [16, 94–96, 98, 159, 166, 181–187], but also in asymptotically AdS spacetimes [31, 73]. Most of these studies have addressed scalar field clouds* (even though *marginal* clouds have been considered for a charged Proca field on a

*Superradiance onset curves for gravitational perturbations on Kerr-AdS, which – as the existence lines for stationary clouds – identify the backgrounds supporting the zero-mode of the perturbation, have been studied in [31], and the corresponding "hairy" BH solutions have been constructed in [188].

charged BH background in Chapter 6). Here we perform a study of Maxwell clouds, which can exist around rotating BHs in asymptotically AdS spacetimes. As a comparison with the Maxwell clouds on Kerr-AdS BHs we also consider scalar clouds in the same background.

It was proposed in [16, 18] that the existence of stationary clouds of a given test field, as a *zero-mode* of the superradiant instability, indicates the existence of new families of "hairy" BH solutions, at fully nonlinear level, such as the Kerr BHs with scalar hair found (numerically) in [16], whose existence was recently formally proved [189]. It is an open issue if these hairy BHs may be formed dynamically, as the end point of the instability. Interesting evidence in this direction was reported recently [81] for the case of Reissner-Nordström BHs in a cavity, following the earlier discussion of superradiant instabilities in this setup [90–92]. The existence of Maxwell clouds on Kerr-AdS BHs has, therefore, the interesting implication that new families of solutions of charged rotating BHs exist, within the Einstein-Maxwell-AdS system, besides the well known Kerr-Newman-AdS family, and branching off from the latter.

The structure of this chapter is as follows. In Section 8.2 we present the Teukolsky equations for the Maxwell field on Kerr-AdS BHs. Then the corresponding boundary conditions are studied in Section 8.3, by requiring VEF. In Section 8.4, a standard analytical matching method is developed to study quasinormal modes in the small BH and slow rotation regime. In Section 8.5, we introduce two numerical methods, to solve the radial and angular Teukolsky equations, respectively, in a larger parameter space. In Section 8.6, we take the Schwarzschild-AdS BH as an example to show, even in this simpler case, that there is a new branch of quasinormal modes which has not been explored yet. In Section 8.7, numerical results for quasinormal modes, superradiant unstable modes and vector clouds are presented. As a comparison, scalar clouds are studied as well. We summarize our results in the last section.

8.2 Teukolsky equations of the Maxwell field

In the Newman-Penrose formalism, the Maxwell fields are described in terms of three complex scalars, two of which are independent. These two scalars are denoted by ϕ_0 and ϕ_2, and can be expanded as

$$\phi_0 = R_{+1}(r)S_{+1}(\theta)\ , \qquad \phi_2 = \frac{1}{2(\bar{\rho}^*)^2}R_{-1}(r)S_{-1}(\theta)\ , \tag{8.2.1}$$

where $\bar{\rho}^* = r - ia\cos\theta$, and the radial functions $R_{\pm1}$ obey Eqs. (2.2.28) and (2.2.30) while the angular functions $S_{\pm1}$ obey Eqs. (2.2.29) and (2.2.31).

In the following we present these equations (both the radial and angular equations) explicitly, governing a spin $s(s = \pm1)$ perturbation.

The radial equation is

$$\Delta_r^{-s}\frac{d}{dr}\left(\Delta_r^{s+1}\frac{dR_s(r)}{dr}\right) + H(r)R_s(r) = 0\ , \tag{8.2.2}$$

with

$$H(r) = \frac{\Xi^2K^2 - is\Xi K\Delta_r'}{\Delta_r} + 2is\Xi K' + \frac{s+|s|}{2}\Delta_r'' + \frac{a^2}{L^2} - \lambda\ ,$$

where K is given in Eq. (2.2.23). The angular equation is

$$\frac{d}{du}\left(\Delta_u\frac{dS_{lm}}{du}\right) + A(u)S_{lm} = 0\ , \tag{8.2.3}$$

with $u = \cos\theta$, and

$$A(u) = -\frac{K_u^2}{\Delta_u} - 4smu\frac{\Xi}{1-u^2} + \lambda - |s| - 2(1-u^2)\frac{a^2}{L^2}\ ,$$

where

$$K_u = \Big(\omega a(1-u^2) + (su-m)\Big)\Xi\ ,$$
$$\Delta_u = (1-u^2)\left(1 - \frac{a^2}{L^2}u^2\right)\ .$$

8.3 Boundary conditions

To solve a differential equation, such as the radial equation (8.2.2) or the angular equation (8.2.3), one has to impose physically relevant boundary conditions. For the angular equation (8.2.3), one usually requires its solutions to be regular at the singular points $\theta = 0$ and $\theta = \pi$. This determines uniquely the set of angular functions labeled by ℓ and m. For the radial equation (8.2.2), we have to impose conditions both at the horizon and at infinity. At the horizon, ingoing boundary conditions are imposed. At infinity, however, the boundary conditions are more subtle. For the often studied case of a scalar field on Kerr-AdS BHs, the boundary conditions typically imposed require the field itself to vanish [32, 180], when

looking for quasinormal modes. For the Maxwell field and in the Teukolsky formalism, the asymptotic boundary conditions have not been explored yet. In this section, we are going to discuss them for the general Kerr-AdS background.

We propose that in the Teukolsky formalism, when looking for quasinormal modes of the Maxwell field on Kerr-AdS BHs, VEF boundary conditions should be imposed, following the spirit that the AdS boundary is a perfectly reflecting mirror so that no energy flux can cross it. For the particular case of the electromagnetic field, these boundary conditions create an analogy between the AdS boundary and a perfect conductor. In fact the conductor condition for the Maxwell field has been considered in the Kerr-mirror system [17]. But the VEF boundary conditions, which for a scalar field can yield both standard Dirichlet and Neumann boundary conditions and for a Maxwell field can yield perfectly conducting boundary conditions, are a general principle for any spin field, based on a sound physical rationale.

The energy-momentum tensor for the Maxwell field is*

$$T_{\mu\nu} = F_{\mu\sigma}F^{\sigma}{}_{\nu} + \frac{1}{4}g_{\mu\nu}F^2 \ , \tag{8.3.1}$$

with the Maxwell tensor $F_{\mu\nu}$ [190]

$$F_{\mu\nu} = 2\left(\phi_1(n_{[\mu}l_{\nu]} + m_{[\mu}\bar{m}_{\nu]}) + \phi_2 l_{[\mu}m_{\nu]} + \phi_0\bar{m}_{[\mu}n_{\nu]}\right) + \text{c.c} \ ,$$

where square brackets on subscripts stand for anti-symmetrization, the tetrad $\{l_\mu, n_\mu, m_\mu, \bar{m}_\mu\}$ is given in Eq. (2.2.17), and c.c stands for complex conjugate of the preceding terms.

With the Maxwell scalars defined in Eq. (2.2.5), we are now able to calculate the radial energy flux $T^r{}_t$, by substituting all of the above ingredients into Eq. (8.3.1), which gives

$$T^r{}_t = T^r{}_{t,\,I} + T^r{}_{t,\,II} \ ,$$

where

$$T^r{}_{t,\,I} = \frac{1}{2\Xi}\left(4|\phi_2|^2 - \frac{\Delta_r^2}{\rho^4}|\phi_0|^2\right) \ , \tag{8.3.2}$$

while $T^r{}_{t,\,II}$ becomes irrelevant at infinity, so we do not show its expression here.
With the fields decomposition in Eq. (8.2.1), integrating $T^r{}_{t,\,I}$ over a sphere, we obtain the

*Note that the energy-momentum tensor for the Maxwell field used in Eq. (8.3.1) has a minus sign difference with the usual definition.

energy flux

$$\mathcal{F}|_r = \int_{S^2} \sin\theta d\theta d\varphi \, r^2 T^r{}_{t,\,I} = \frac{r^2}{2\,\Xi\,\rho^4}(|R_{-1}|^2 - \Delta_r^2|R_{+1}|^2) \,, \tag{8.3.3}$$

up to an irrelevant normalization, and where the angular functions $S_{\pm1}(\theta)$ are normalized to unity. To get the asymptotic boundary condition for R_{-1}, we expand Eq. (8.2.2) with $s=-1$ asymptotically as

$$R_{-1} \sim \; \alpha^- r + \beta^- + \mathcal{O}(r^{-1}) \,, \tag{8.3.4}$$

where α^- and β^- are two integration constants. In order to get the explicit form of the boundary conditions, the Starobinsky-Teukolsky identities are required. As we proved in Chapter 2, these identities can be written explicitly as

$$BR_{+1} = \left(\frac{d}{dr} - \frac{i\Xi K}{\Delta_r}\right)\left(\frac{d}{dr} - \frac{i\Xi K}{\Delta_r}\right) R_{-1} \,, \tag{8.3.5}$$

$$BR_{-1} = \Delta_r \left(\frac{d}{dr} + \frac{i\Xi K}{\Delta_r}\right)\left(\frac{d}{dr} + \frac{i\Xi K}{\Delta_r}\right) P_{+1} \,. \tag{8.3.6}$$

Keeping in mind the Starobinsky-Teukolsky identity (8.3.5), making use of the radial equation (8.2.2) with $s=-1$ and the asymptotic expansion in Eq. (8.3.4), at the asymptotic boundary, the energy flux in Eq. (8.3.3) becomes

$$\mathcal{F}|_{r,\infty} = B^2|\alpha^-|^2 - |(\lambda - 2\omega^2\Xi^2L^2)\alpha^- + 2i\beta^-\omega\Xi|^2 \,, \tag{8.3.7}$$

where an overall constant of proportionality has been ignored. In order to impose the VEF boundary conditions, i.e. $\mathcal{F}|_{r,\infty}=0$, we have

$$B^2|\alpha^-|^2 - |(\lambda - 2\omega^2\Xi^2L^2)\alpha^- + 2i\beta^-\omega\Xi|^2 = 0 \,. \tag{8.3.8}$$

Note that α^- and β^- are two independent integration constants; we can re-scale them so that the modulus in the above equation can be dropped*. Then it is easy to solve this quadratic equation and obtain the two solutions

$$\frac{\alpha^-}{\beta^-} = \frac{2i\omega\Xi}{B - \lambda + 2\omega^2\Xi^2L^2} \,, \quad \frac{\alpha^-}{\beta^-} = \frac{2i\omega\Xi}{-B - \lambda + 2\omega^2\Xi^2L^2} \,. \tag{8.3.9}$$

We have also proved in Appendix D that, the angular momentum flux of the Maxwell field vanishes asymptotically if the above boundary conditions are satisfied, similarly to the gravitational case [31].

*Indeed there still might be a phase factor between these two constants, but this phase factor can be fixed by calculating the normal modes.

For Schwarzschild-AdS BHs, Eq. (8.3.9) simplifies to

$$\frac{\alpha^-}{\beta^-} = \frac{i}{\omega L^2} \ , \quad \frac{\alpha^-}{\beta^-} = \frac{i\omega}{-\ell(\ell+1)+\omega^2 L^2} \ . \tag{8.3.10}$$

These are, apparently, two distinct Robin boundary conditions, but at this moment it is unclear if they lead to physically different modes or if they are isospectral.

We can also follow the same procedure to calculate boundary conditions for the Teukolsky equation with $s = +1$. Instead of using $R_{+1}(r)$, we use $P_{+1}(r)$ for convenience, which relates to $R_{+1}(r)$ through $P_{+1}(r) = \Delta_r R_{+1}(r)$. As before, we expand $P_{+1}(r)$ from Eq. (8.2.2) with $s = +1$ asymptotically

$$P_{+1} \sim \ \alpha^+ r + \beta^+ + \mathcal{O}(r^{-1}) \ , \tag{8.3.11}$$

where α^+ and β^+ are two integration constants. Using the Starobinsky-Teukolsky identity in Eq. (8.3.6), the asymptotic expansion in Eq. (8.3.11), the Teukolsky equation with $s = +1$ in Eq. (8.2.2) and the transformation $P_{+1}(r) = \Delta_r R_{+1}(r)$, then Eq. (8.3.3) gives the conditions

$$\frac{\alpha^+}{\beta^+} = -\frac{2i\omega\Xi}{B-\lambda+2\omega^2\Xi^2 L^2} \ , \quad \frac{\alpha^+}{\beta^+} = -\frac{2i\omega\Xi}{-B-\lambda+2\omega^2\Xi^2 L^2} \ , \tag{8.3.12}$$

after imposing the VEF boundary conditions. Comparing the two boundary conditions in Eq. (8.3.9) and in Eq. (8.3.12), we find that there is only a sign difference, or in other words, they are complex conjugate of each other. This is a consequence that $P_{+1}(r)$ and $R_{-1}(r)$ are proportional to complex conjugate functions of each other. We have checked that solving the radial equation (8.2.2) for $s = -1$ and $s = +1$ with the corresponding boundary conditions (8.3.9) and (8.3.12), for Schwarzschild-AdS BHs, the same quasinormal frequencies are obtained, which is consistent with the argument that these two Teukolsky equations encode the same information. Thus, for concreteness and without loss of generality, in the following we specify $s = -1$, and consider the corresponding boundary conditions.

8.4 Analytical matching

In this section, we present an analytical calculation of quasinormal frequencies for a Maxwell field on a Kerr-AdS BH, with the two Robin boundary conditions discussed in Section 8.3. Such calculations can be used to illustrate how these Robin boundary conditions generate unstable modes.

Making use of the standard matching procedure, we shall first divide the space outside the event horizon into two regions: the *near region*, defined by the condition $r - r_+ \ll 1/\omega$, and the *far region*, defined by the condition $r_+ \ll r - r_+$. Then we further require the condition $r_+ \ll 1/\omega$ so that an overlapping region exists where the solutions obtained in the near region and in the far region are both valid. In the following analysis we focus on small AdS BHs ($r_+ \ll L$) with slow rotation ($a \ll r_+$). The former condition allows treating the frequencies for the Kerr-AdS BH as a perturbation of the AdS normal frequencies; the latter condition together with $\omega r_+ \ll 1$, implying $\omega a \ll 1$ and $a \ll L$, allow approximating the angular equation for the spin-weighted AdS-spheroidal harmonics by the spin-weighted spherical harmonics, so that the separation constant becomes

$$\lambda \simeq \ell(\ell+1)\,, \quad \text{with } \ell = 1, 2, 3\,, \cdots\,, \tag{8.4.1}$$

where ℓ is the angular momentum quantum number.

8.4.1 Near region solution

In the near region, under the small BH, $r_+ \ll L$, and the slow rotation, $a \ll r_+$, approximations, Eq. (8.2.2) becomes

$$\Delta_r R'_{-1} + \left(\frac{(r_+ - r_-)^2 \hat{\omega}}{\Delta_r} - \lambda\right) R_{-1} = 0\,, \tag{8.4.2}$$

with

$$\hat{\omega} = \left(\bar{\omega} + \frac{i}{2}\right)^2 + \frac{1}{4}\,, \quad \bar{\omega} = (\omega - m\Omega_H)\,\Xi \frac{r_+^2 + a^2}{r_+ - r_-}\,,$$

where Ω_H is the angular velocity of the event horizon, given by Eq. (2.2.9). It is convenient to define a new dimensionless variable

$$z \equiv \frac{r - r_+}{r - r_-}\,,$$

to transform Eq. (8.4.2) into

$$z(1-z)\frac{d^2 R_{-1}}{dz^2} - 2z\frac{dR_{-1}}{dz} + \left(\frac{\hat{\omega}(1-z)}{z} - \frac{\lambda}{1-z}\right) R_{-1} = 0\,. \tag{8.4.3}$$

The above equation can be solved in terms of the hypergeometric function

$$R_{-1} \sim z^{1-i\bar{\omega}}(1-z)^{\ell}\, F(\ell+1, \ell+2-2i\bar{\omega}, 2-2i\bar{\omega}; z)\,, \tag{8.4.4}$$

where an ingoing boundary condition has been imposed.

The near region solution, Eq. (8.4.4), must be expanded for large r, in order to perform the matching with the far region solution below. To achieve this we take the $z \to 1$ limit, and obtain

$$R_{-1} \sim \Gamma(2-2i\bar{\omega}) \left[\frac{R^{\rm near}_{-1,1/r}}{r^\ell} + R^{\rm near}_{-1,r} r^{\ell+1} \right] , \tag{8.4.5}$$

by using the properties of the hypergeometric function [174], and where

$$\begin{aligned} R^{\rm near}_{-1,1/r} &\equiv \frac{\Gamma(-2\ell-1)(r_+-r_-)^\ell}{\Gamma(-\ell)\Gamma(1-\ell-2i\bar{\omega})} , \\ R^{\rm near}_{-1,r} &\equiv \frac{\Gamma(2\ell+1)(r_+-r_-)^{-\ell-1}}{\Gamma(\ell+1)\Gamma(\ell+2-2i\bar{\omega})} . \end{aligned} \tag{8.4.6}$$

8.4.2 Far region solution

In the far region, $r - r_+ \gg r_+$, the BH effects can be neglected ($M \to 0, a \to 0$) so that

$$\Delta_r \simeq r^2 \left(1 + \frac{r^2}{L^2} \right) .$$

Then Eq. (8.2.2) becomes

$$\Delta_r R'' _{-1}(r) + \left(\frac{K_r^2 + iK_r\Delta_r'}{\Delta_r} - 2iK_r' - \ell(\ell+1) \right) R_{-1}(r) = 0 , \tag{8.4.7}$$

with $K_r = \omega r^2$.

The general solution for Eq. (8.4.7) is

$$\begin{aligned} R_{-1} = r^{\ell+1}(r-iL)^{\frac{\omega L}{2}}(r+iL)^{-\ell-\frac{\omega L}{2}} \Big[& C_1 F\Big(+\omega L, 2\ell+2; \frac{2r}{r+iL} \Big) \\ & - 2^{-2\ell-1} C_2 \left(1 + \frac{iL}{r} \right)^{2\ell+1} F\Big(-\ell-1, -\ell+\omega L, -2\ell; \frac{2r}{r+iL} \Big) \Big] , \end{aligned} \tag{8.4.8}$$

where C_1, C_2 are two integration constants, and they will be constrained in the following to satisfy the boundary conditions.

The first boundary condition in Eq. (8.3.9), in the far region, becomes

$$\frac{\alpha^-}{\beta^-} = \frac{i}{\omega L^2} .$$

In order to impose this boundary condition, we first expand Eq. (8.4.8) at large r, in the form of Eq. (8.3.4); then one obtains the first relation between C_1 and C_2

$$\frac{C_2}{C_1} = -2^{2\ell+1} \frac{\ell}{\ell+1} \frac{F(\ell+1, \ell+1+\omega L, 2\ell+2; 2)}{F(-\ell, -\ell+\omega L, -2\ell; 2)} . \tag{8.4.9}$$

The second boundary condition in Eq. (8.3.9), in the far region, turns into

$$\frac{\alpha}{\beta} = \frac{i\omega}{-\ell(\ell+1)+\omega^2 L^2} \ .$$

To impose the second boundary condition above, again expanding Eq. (8.4.8) at large r, to extract α^- and β^-, then one gets the second relation between C_1 and C_2

$$\frac{C_2}{C_1} = 2^{2\ell+1}\left(\frac{\ell}{\ell+1}\right)^2 \frac{\ell+1+\omega L}{\ell-\omega L}\frac{\mathcal{A}_1}{\mathcal{A}_2} \ , \tag{8.4.10}$$

where

$$\begin{aligned}
\mathcal{A}_1 &= (\ell+1)F(\ell,\ell+1+\omega L,2\ell+2;2)+\omega L F(\ell+1,\ell+2+\omega L,2\ell+3;2) \ , \\
\mathcal{A}_2 &= \ell F(-\ell-1,-\ell+\omega L,-2\ell;2)-\omega L F(-\ell,-\ell+1+\omega L,1-2\ell;2) \ .
\end{aligned} \tag{8.4.11}$$

In order to match this solution to the near region solution, we expand Eq. (8.4.8) for small r, to obtain

$$R_{-1} \ \sim \ \frac{R^{\rm far}_{-1,1/r}}{r^\ell} + R^{\rm far}_{-1,r} r^{\ell+1} \ , \tag{8.4.12}$$

with

$$\begin{aligned}
R^{\rm far}_{-1,1/r} &\equiv -iLC_2 \ , \\
R^{\rm far}_{-1,r} &\equiv (-1)^\ell 2^{2\ell+1} L^{-2\ell} C_1 \ .
\end{aligned}$$

8.4.3 Overlap region

To match the near region solution Eq. (8.4.5) and the far region solution Eq. (8.4.12) in the intermediate region, we impose the matching condition $R^{\rm near}_{-1,r}R^{\rm far}_{-1,1/r} = R^{\rm far}_{-1,r}R^{\rm near}_{-1,1/r}$, then we obtain

$$\begin{aligned}
&\frac{\Gamma(-2\ell-1)}{\Gamma(-\ell)}\frac{\Gamma(\ell+1)}{\Gamma(2\ell+1)}\frac{\Gamma(\ell+2-2i\bar{\omega})}{\Gamma(1-\ell-2i\bar{\omega})}\left(\frac{r_+-r_-}{L}\right)^{2\ell+1} \\
&= \ i\,(-1)^\ell \frac{\ell}{\ell+1}\frac{F(\ell+1,\ell+1+\omega L,2\ell+2;2)}{F(-\ell,-\ell+\omega L,-2\ell;2)} \ ,
\end{aligned} \tag{8.4.13}$$

with the first boundary condition given by Eq. (8.3.9), and

$$\begin{aligned}
&\frac{\Gamma(-2\ell-1)}{\Gamma(-\ell)}\frac{\Gamma(\ell+1)}{\Gamma(2\ell+1)}\frac{\Gamma(\ell+2-2i\bar{\omega})}{\Gamma(1-\ell-2i\bar{\omega})}\left(\frac{r_+-r_-}{L}\right)^{2\ell+1} \\
&= \ i\,(-1)^{\ell+1}\left(\frac{\ell}{\ell+1}\right)^2 \frac{\ell+1+\omega L}{\ell-\omega L}\ \frac{\mathcal{A}_1}{\mathcal{A}_2} \ ,
\end{aligned} \tag{8.4.14}$$

with the second boundary condition given by Eq. (8.3.9).

Both Eqs. (8.4.13) and (8.4.14) can be solved perturbatively to look for the imaginary part of the quasinormal frequencies, in the small BH ($r_+ \ll L$) and slow rotation ($a \ll r_+$) approximations. In order to do so, we first look for normal modes. For a small BH, the left term in Eqs. (8.4.13) and (8.4.14) vanish at the leading order, then we have to require the right hand side of both equations to vanish as well. These conditions give the normal modes for pure AdS

$$F(\ell+1,\ell+1+\omega L,2\ell+2;2)=0 \;\;\Rightarrow\;\; \omega_{1,N}L=2N+\ell+2\,, \tag{8.4.15}$$

$$\mathcal{A}_1=0 \;\;\Rightarrow\;\; \omega_{2,N}L=2N+\ell+1\,, \tag{8.4.16}$$

where $N=0,1,2,\cdots$, and $\ell=1,2,3,\cdots$. The two sets of modes are, in this case, isospectral up to one mode.

When the BH effects are taken into account, a correction to the frequency will be introduced

$$\omega_j L=\omega_{j,N}L+i\delta_j\,, \tag{8.4.17}$$

where $j=1,2$ for the two different boundary conditions, and δ is used to describe the damping (growth) of the quasinormal modes, and we replace ωL appearing in the second line of Eqs. (8.4.13) and (8.4.14) by $\omega_1 L$ and $\omega_2 L$ in Eq. (8.4.17), respectively. Then, from each of these two equations, we obtain δ_j perturbatively, at leading order in a.

It turns out that the general expression for δ_j is quite complicated. As such, we only show here a few explicit examples. For $\ell=1$ and $N=0$, from Eq. (8.4.13), we obtain

$$\begin{aligned}\delta_1&=-\frac{16}{\pi}\frac{r_+^4}{L^4}+m\frac{16}{3\pi}\frac{ar_+^2}{L^3}+\mathcal{O}\left(\frac{a}{L},\frac{r_+^4}{L^4}\right)=-\frac{16}{3\pi}\frac{r_+^2}{L^2}\left(3\frac{r_+^2}{L^2}-m\frac{a}{L}\right)+\cdots\\&\simeq-\frac{16}{3\pi}\frac{r_+^4}{L^3}\left(\omega_{1,0}-m\Omega_H\right)+\cdots\,,\end{aligned} \tag{8.4.18}$$

where the angular velocity has been approximated by $\Omega_H\sim a/r_+^2$. It is manifest, from (8.4.18), that $\delta_1<0$ when $\omega_{1,0}>m\Omega_H$, while $\delta_1>0$ when $\omega_{1,0}<m\Omega_H$. Thus we find growing modes within the superradiant regime, as expected.

Keeping the same parameters as in the previous paragraph, i.e. $\ell=1$ and $N=0$, from Eq. (8.4.14), we obtain

$$\delta_2=-\frac{8}{3\pi}\frac{r_+^4}{L^4}+m\frac{4}{3\pi}\frac{ar_+^2}{L^3}+\mathcal{O}\left(\frac{a}{L},\frac{r_+^4}{L^4}\right)=-\frac{4}{3\pi}\frac{r_+^2}{L^2}\left(2\frac{r_+^2}{L^2}-m\frac{a}{L}\right)+\cdots$$

$$\simeq -\frac{4}{3\pi}\frac{r_+^4}{L^3}\left(\omega_{2,0} - m\Omega_H\right) + \cdots , \tag{8.4.19}$$

which also shows clearly that $\delta_2 < 0$ when $\omega_{2,0} > m\Omega_H$, but $\delta_2 > 0$ when $\omega_{2,0} < m\Omega_H$, signaling again superradiant instabilities.

Furthermore, for both cases, $\delta_1 = 0$ and $\delta_2 = 0$ give $\omega_{1,0} = m\Omega_H$ and $\omega_{2,0} = m\Omega_H$, which are the conditions to form clouds, with the two different boundary conditions.

8.5 Numerical method

When the BH parameters lie beyond the small size and slow rotation approximations considered in the last section, the analytical method fails and we have to solve the problem numerically. Since the radial equation (8.2.2) and the angular equation (8.2.3) are coupled through their eigenvalues, we have to solve both equations simultaneously. In this section, we describe the numerical method used to solve both equations.

The radial equation (8.2.2), will be solved with a direct integration method, which has been used in Chapters 4 and 5. To be complete, here we briefly outline the procedure.
We first use Frobenius' method to expand R_{-1} close to the event horizon

$$R_{-1} = (r - r_+)^\rho \sum_{j=0}^{\infty} c_j \, (r - r_+)^j \, ,$$

to initialize Eq. (8.2.2). The series expansion coefficients c_j can be derived directly after inserting these expansions into Eq. (8.2.2). The parameter ρ is chosen as

$$\rho = 1 - \frac{i(\omega - m\Omega_H)}{4\pi T_H} \, ,$$

so that an ingoing boundary condition is satisfied. The angular velocity Ω_H and the Hawking temperature T_H are given in Eq. (2.2.9) and Eq. (2.2.10).

At infinity, the asymptotic behavior of R_{-1} is given by Eq. (8.3.4). The expansion coefficients, α^- and β^-, can be extracted from R_{-1} and its first derivative. For that purpose, we define two new fields $\{\chi, \psi\}$, which asymptote respectively to $\{\alpha^-, \beta^-\}$ at infinity. Such a transformation can be written in the matrix form

$$\mathbf{V} = \begin{pmatrix} r & 1 \\ 1 & 0 \end{pmatrix} \mathbf{\Psi} \equiv \mathbf{T}\mathbf{\Psi} \, ,$$

by defining the vector $\mathbf{\Psi}^T = (\chi, \psi)$ for the new fields, and another vector $\mathbf{V}^T = (R_{-1}, \frac{d}{dr}R_{-1})$ for the original field and its derivative.

To obtain a first order system of ordinary differential equations for the new fields, we define another matrix $\mathbf{X}$, through

$$\frac{d\mathbf{V}}{dr} = \mathbf{X}\mathbf{V} \ , \tag{8.5.1}$$

which can be read off from the original radial equation (8.2.2) directly. Then the radial equation (8.2.2) becomes

$$\frac{d\mathbf{\Psi}}{dr} = \mathbf{T}^{-1}\left(\mathbf{X}\mathbf{T} - \frac{d\mathbf{T}}{dr}\right)\mathbf{\Psi} \ . \tag{8.5.2}$$

This is the final equation we are going to solve.

The angular equation (8.2.3), will be solved using a spectral method, to look for the separation constant λ. By observing Eq. (8.2.3) and considering the constraint on rotation $a < L$, one finds two regular singularities at $u = \pm 1$. To impose regular boundary conditions at these regular singularities, we require

$$S \ \sim \ \begin{cases} (1-u)^{\frac{|m+s|}{2}} & \text{when} \quad u \to 1 \ , \\ (1+u)^{\frac{|m-s|}{2}} & \text{when} \quad u \to -1 \ , \end{cases} \tag{8.5.3}$$

where as announced in Section 8.3, $s = -1$. These asymptotic behaviors can be factored out by defining a new function $\hat{S}$

$$S = (1-u)^{\frac{|m+s|}{2}}(1+u)^{\frac{|m-s|}{2}}\hat{S} \ . \tag{8.5.4}$$

Then the angular equation (8.2.3) becomes

$$Y(u)\hat{S} = \lambda\hat{S} \ , \tag{8.5.5}$$

where the operator $Y(u)$ can be obtained straightforwardly after inserting the transformation (8.5.4) into the angular equation (8.2.3).

We choose a Chebyshev grid as the collocation points to discretize the operator $Y(u)$, which becomes a matrix. Then Eq (8.5.5) becomes a linear algebraic equation, and λ is obtained by looking for the eigenvalues of the matrix $Y(u)$.

8.6 Warm up for Schwarzschild-AdS black holes

We shall now apply the VEF boundary conditions to Maxwell perturbations on Schwarzschild-AdS BHs, in the Teukolsky formalism. We show that even in this simpler case, there is a new branch of quasinormal modes which has not been explored yet.

As we mentioned in Section 8.1, the quasinormal modes for the Maxwell field on Schwarzschild-AdS BHs have been studied using the Regge-Wheeler formalism [180]. Here we will tackle the same problem in the Teukolsky formalism, imposing the boundary conditions discussed in Section 8.3. We find that:

- when the first of the two boundary conditions in Eq. (8.3.10) is imposed, we recover the results given in the literature [180, 191];
- when the second of the two boundary conditions in Eq. (8.3.10) is imposed, there is one new branch of quasinormal modes.

To be complete and for comparison, we will show both results in the following. In the numerical calculations all physical quantities are normalized by the AdS radius L, so we set $L = 1$. Also, observe that we use ω_1 (ω_2) to represent the quasinormal frequency corresponding to the first (second) boundary conditions.

The numerical method we are using here has already been illustrated in Section 8.5. Since the angular function in this case becomes the standard spherical harmonics, we do not need to solve the angular equation numerically. The results are as follows.

In Table 8.1, we list a few fundamental ($N = 0$) quasinormal frequencies of ω_1 (with $\ell = 1$) and ω_2 (with $\ell = 2$), for different BH sizes. As observed in Section 8.4, the normal modes displayed in Eqs. (8.4.15) and (8.4.16), are isospectral under the mapping

$$\ell_2 \leftrightarrow \ell_1 + 1 \ , \tag{8.6.1}$$

except for one mode for the ω_2 branch. Here ℓ_1 and ℓ_2 refer to the angular momentum quantum number in the spectrum of ω_1 and ω_2. The presence of a BH, however, breaks the isospectrality. To show this, we present in Table 8.1, the two sets of quasinormal frequencies, with $\ell_1 = 1$ and $\ell_2 = 2$, respectively. One observes that the degeneracy between ω_1 and ω_2

Table 8.1: Quasinormal frequencies of the Maxwell field on Schwarzschild-AdS. Some fundamental modes are shown, for different BH sizes r_+ and for the two sets of modes.

r_+	$\omega_1(\ell=1)$	$\omega_2(\ell=2)$
0.2	2.6384 - 5.7947$\times 10^{-2}$ i	2.9403 - 1.0466$\times 10^{-4}$ i
0.5	2.2591 - 0.6573 i	2.7804 - 0.07549 i
0.8	2.1758 - 1.2870 i	2.6923 - 0.2721 i
1.0	2.1630 - 1.6991 i	2.6647 - 0.4061 i
5.0	0 - 8.7948 i	0 - 5.0528 i
10	0 - 15.5058 i	0 - 13.8198 i
50	0 - 75.0958 i	0 - 74.7533 i
100	0 - 150.048 i	0 - 149.876 i

gets broken, especially in the small BH and intermediate BH regimes. For large BHs, these two modes are, again, almost isospectral, which seems to be a general feature for any type of perturbation [180, 191]. Furthermore, for large BHs, the real part of the frequency for either of the sets vanishes, while the imaginary part scales linearly with the BH size r_+. This scaling can be equally stated in terms of the Hawking temperature, which relates to the BH size through $T_H = 3r_+/(4\pi L^2)$ for large BHs, supporting the arguments given in [192], where a similar linear relation was found for scalar fields. We remark that the numerical data for ω_1 displayed in Table 8.1 coincides with the numerical results presented in [179, 180], at least within 4 significant digits, which can be used as a check for our numerical method.

For small BHs, it can be shown using a perturbative analytical matching method given in Section 8.4, that the real part of the frequencies approaches the normal modes of empty AdS [175], given by Eqs (8.4.15) and (8.4.16) for the two different boundary conditions. On the other hand, the imaginary part for both modes approaches zero as

$$-\omega_{j,I} \propto r_+^{2\ell+2} \ ,$$

which also seems to be a general feature for any type of perturbations [193]. In Fig. 8.1, left panel, we display the numerical data (thick lines) for the fundamental modes of each branch against the leading behavior obtained from the perturbative matching method in Section 8.4. We find a good agreement for small r_+, which is another check for our numerical method.

In Table 8.2, we consider intermediate size BHs to exemplify the effect of the angular mo-

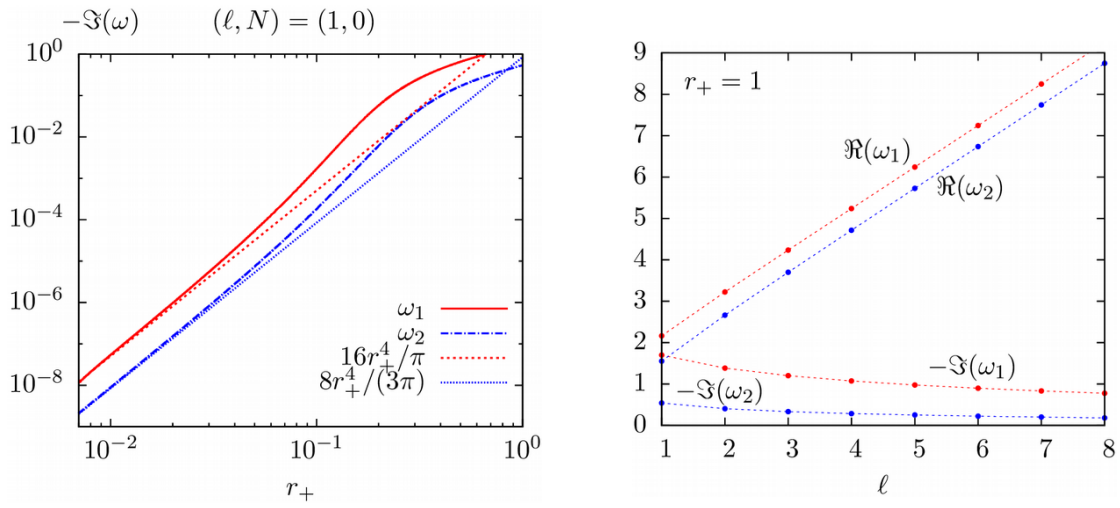

Figure 8.1: *Left:* Comparison of the imaginary part for quasinormal frequencies between the analytical approximation of small BHs (thin dashed lines) and the numerical data (thick lines) for the fundamental modes of each branch of solutions. *Right:* Effect of the angular momentum quantum number ℓ on the quasinormal frequencies for intermediate size BHs with $r_+ = 1$, and $N = 0$. The red line is for ω_1 and the blue line is for ω_2.

mentum quantum number ℓ on the frequencies*. As one can see, for both modes, the real (imaginary) part of the quasinormal frequencies increases (decreases) in magnitude as ℓ increases. These behaviors are more clearly shown in the right panel of Fig. 8.1. Observe that the increase of the real part of the frequency with ℓ is qualitatively similar to the one observed for empty AdS.

Finally, let us remark that, in the above, we have focused on fundamental modes because, on the one hand, our main interest has been to explore the new set of modes which arises even for $N = 0$ and, on the other hand, these low lying modes are expected to dominate the late time behavior of time evolutions.

8.7 Quasinormal modes and superradiant instabilities

In this section, we now turn on rotation, to study superradiant instabilities for the Maxwell field on a Kerr-AdS BH. With the numerical strategies described in Section 8.5, and the

*We have checked that the effect of varying ℓ is qualitatively similar for small BHs.

Table 8.2: Same as Table 8.1, but fixing now the BH size to be $r_+ = 1$. Some fundamental modes are shown, considering different angular momentum quantum number ℓ.

ℓ	ω_1	ω_2
1	2.16302 - 1.69909 i	1.55360 - 0.541785 i
2	3.22315 - 1.38415 i	2.66469 - 0.406058 i
3	4.23555 - 1.20130 i	3.69923 - 0.334088 i
4	5.23994 - 1.07445 i	4.71659 - 0.286828 i
5	6.24294 - 0.97775 i	5.72784 - 0.252025 i
6	7.24598 - 0.89976 i	6.73632 - 0.224622 i
7	8.24941 - 0.83447 i	7.74335 - 0.202110 i
8	9.25327 - 0.77838 i	8.74952 - 0.183072 i

boundary conditions given in Eq. (8.3.9), the eigenvalues $\{\omega, \lambda\}$ of the coupled system in Eqs. (8.5.2) and (8.5.5) can be obtained iteratively. This is achieved by starting with an initial guess for ω or λ, which are roots of a characteristic equation, and then polishing the solution until $\{\omega, \lambda\}$ become stable. The initial values for ω or λ can be chosen from the results in Schwarzschild-AdS BHs [194] or $\ell(\ell+1)$, respectively.

Note that we use ω_1 (ω_2) to represent the quasinormal frequency and λ_1 (λ_2) to stand for the separation constant, corresponding to the first (second) boundary conditions.

A few selected eigenvalues for ω and λ are tabulated in Tables 8.3−8.7, with two boundary conditions for various BH sizes. Since it is a generic feature for superradiant instabilities that lower order modes exhibit a stronger instability, we focus on the lowest fundamental modes, characterized by $N = 0$, $\ell = 1$ and $m = 0, \pm 1$.

In Tables 8.3 and 8.4 we consider a small BH with size $r_+ = 0.1$. The first observation from these two tables is that superradiant instabilities exist for both boundary conditions, with positive m; this is because only positive m modes can meet the superradiance condition, assuming positive frequencies.

The effect of varying the rotation parameter on both eigenvalues, for different values of m with fixed $\ell = 1$, are shown in Figs. 8.2−8.5. In Fig. 8.2, the real part of the frequency is shown. An immediate first impression from Fig. 8.2, is that it seems the rotation impacts differently on the $m = -1$ modes, for the two boundary conditions. Checking carefully the numerical data

Table 8.3: Quasinormal frequencies and separation constants of the Maxwell field with the first boundary condition, for $\ell = 1$ fundamental modes, on a Kerr-AdS BH with size $r_+ = 0.1$.

(ℓ, m)	a	ω_1	λ_1
(1, 0)	0	2.8519 - 1.7050×10^{-3} i	2
	0.01	2.8505 - 1.7295×10^{-3} i	2.0005 - 5.9147×10^{-7} i
	0.05	2.8151 - 2.5818×10^{-3} i	2.0133 - 2.1677×10^{-5} i
	0.1	2.6740 - 2.2847×10^{-2} i	2.0480 - 7.1650×10^{-4} i
(1, 1)	0.01	2.8436 - 9.5962×10^{-4} i	1.9149 + 2.8541×10^{-5} i
	0.05	2.7837 + 5.5800×10^{-4} i	1.5879 - 8.0057×10^{-5} i
	0.1	2.6493 + 2.0481×10^{-3} i	1.2278 - 5.6148×10^{-4} i
(1, -1)	0.01	2.8572 - 2.7984×10^{-3} i	2.0859 - 8.4666×10^{-5} i
	0.05	2.8422 - 1.7571×10^{-2} i	2.4296 - 2.7419×10^{-3} i
	0.1	2.7398 - 1.2611×10^{-1} i	2.8269 - 4.0538×10^{-2} i

Table 8.4: Quasinormal frequencies and separation constants of the Maxwell field with the second boundary condition, for $\ell = 1$ fundamental modes, on a Kerr-AdS BH with size $r_+ = 0.1$.

(ℓ, m)	a	ω_2	λ_2
(1, 0)	0	1.9533 - 1.8240×10^{-4} i	2
	0.01	1.9529 - 1.8329×10^{-4} i	2.0003 - 4.2946×10^{-8} i
	0.05	1.9452 - 2.0829×10^{-4} i	2.0071 - 1.2092×10^{-6} i
	0.1	1.9160 - 1.0036×10^{-3} i	2.0276 - 2.2602×10^{-5} i
(1, 1)	0.01	1.9436 - 7.9809×10^{-5} i	1.9417 + 2.3800×10^{-6} i
	0.05	1.8989 + 1.9474×10^{-4} i	1.7156 - 2.8302×10^{-5} i
	0.1	1.8292 + 7.8282×10^{-4} i	1.4552 - 2.1958×10^{-4} i
(1, -1)	0.01	1.9622 - 3.2541×10^{-4} i	2.0589 - 9.8188×10^{-6} i
	0.05	1.9900 - 2.1380×10^{-3} i	2.2975 - 3.2933×10^{-4} i
	0.1	1.9987 - 1.9186×10^{-2} i	2.5914 - 6.0286×10^{-3} i

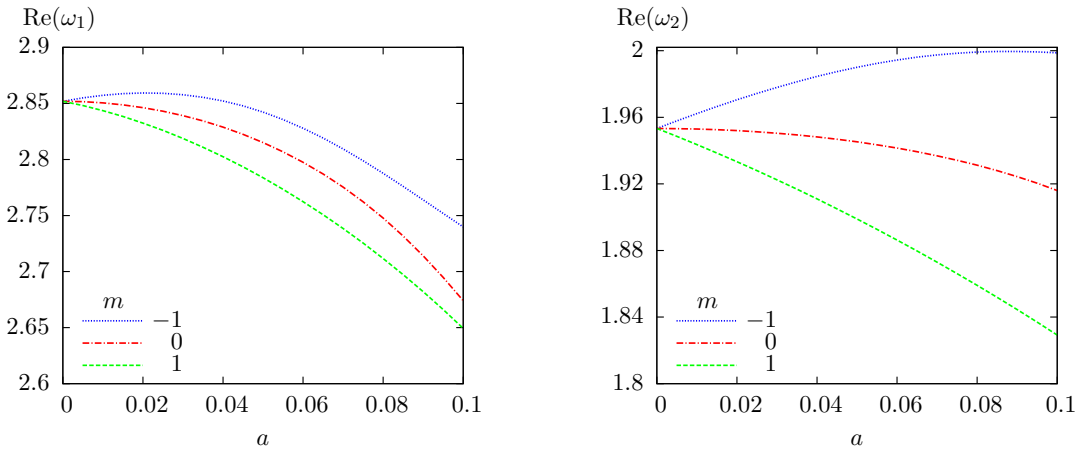

Figure 8.2: Variation of Re(ω) with varying rotation parameter, for fixed $r_+ = 0.1$ and $\ell = 1$ but for different values of m. The left panel is for the first boundary condition while the right panel is for the second boundary condition.

for Re(ω_2), however, we find that its value decreases sightly when a is approaching 0.1. Thus, for $m = -1$ and for both boundary conditions, Re(ω) starts by increasing with increasing rotation but then decreases. For the other two values of m, Re(ω) always decreases with increasing rotation.

In Fig. 8.3, the imaginary part of the frequency is shown, for both boundary conditions. Im(ω) increases with increasing rotation when $m = 1$, eventually becoming positive, signaling the presence of superradiant unstable modes.

In Fig. 8.4 and Fig. 8.5, we show the real and imaginary part of the separation constant, respectively, for both boundary conditions. The real part increases with increasing rotation both when $m = -1$ and $m = 0$, albeit only slightly in the latter case, and decreases with the rotation when $m = 1$. As for the imaginary part, for $m = 1$, it increases with the rotation initially in a small range; but it starts decreasing afterwards. For the other two values of m, the imaginary part of the separation constants always decrease with the rotation. We also note that Im(λ), for $m = 0$, with the first boundary condition decays faster than its counterpart with the second boundary condition. From these first four figures, we conclude that the effect of varying the rotation on the eigenvalues is qualitatively similar for the two boundary conditions. In the following, therefore, we only show the rotation effect on the eigenvalues with the first boundary condition, when considering other BH sizes.

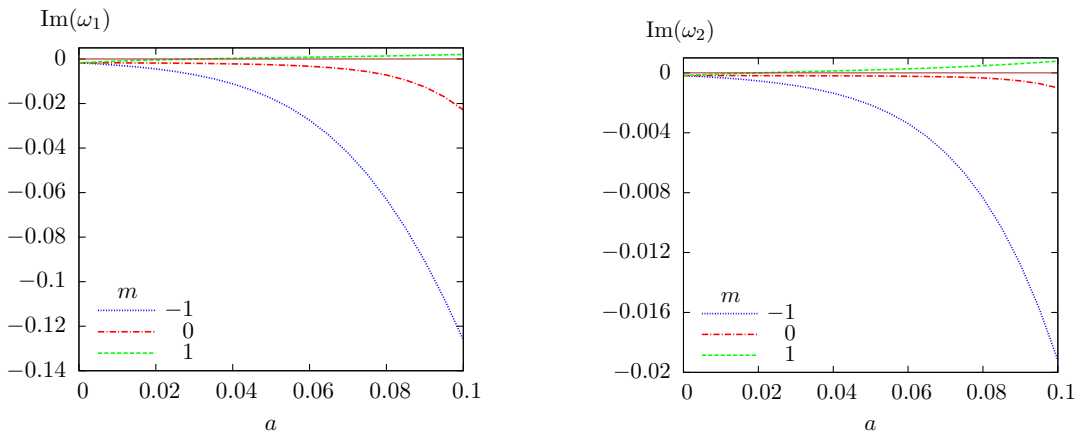

Figure 8.3: Variation of Im(ω) with varying rotation parameter, for fixed $r_+ = 0.1$ and $\ell = 1$ but for different values of m. The left panel is for the first boundary condition while the right panel is for the second boundary condition. The brown solid thin line corresponds to Im(ω)=0, to exhibit more clearly superradiant instabilities.

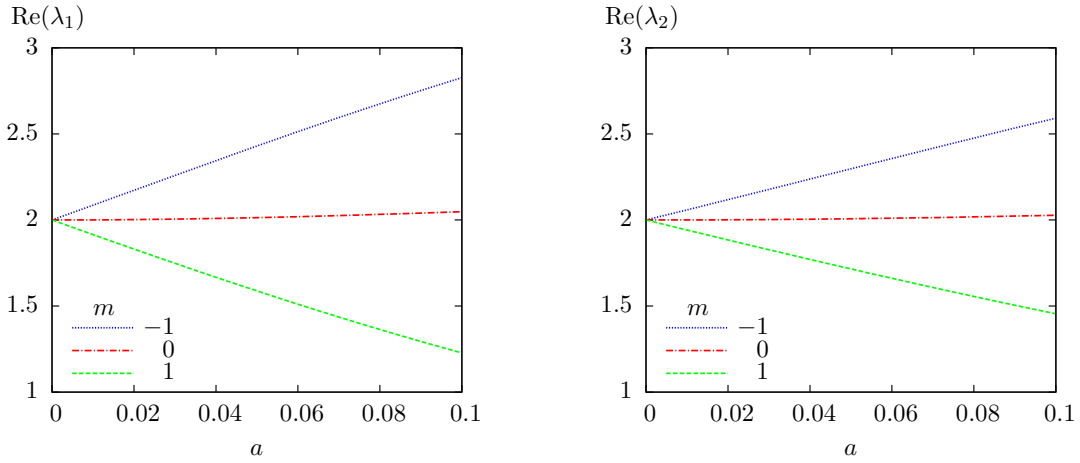

Figure 8.4: Variation of Re(λ) with varying rotation parameter, for fixed $r_+ = 0.1$ and $\ell = 1$ but for different values of m. The left panel is for the first boundary condition while the right panel is for the second boundary condition.

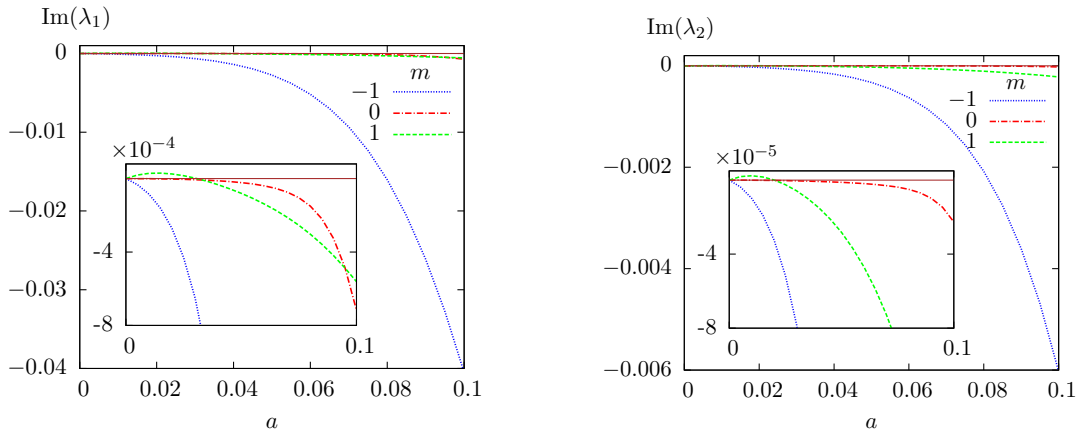

Figure 8.5: Variation of Im(λ) with varying rotation parameter, for fixed $r_+ = 0.1$ and $\ell = 1$ but for different values of m. The left panel is for the first boundary condition while the right panel is for the second boundary condition. Again, the brown solid thin line corresponds to Im(λ)=0, to exhibit that the sign of Im(λ) changes when the superradiant instability occurs (seen in the insets).

We continue our study by varying the BH size. In Tables 8.5 and 8.6 we list a few selected eigenvalues for $r_+ = 0.3$. The interesting feature that now emerges is that superradiant instabilities only occur for the second boundary condition. This implies that the second boundary condition may produce unstable modes in a larger parameter space. This feature will be shown more clearly in the parameter space for the vector clouds. The effect of varying the rotation on the eigenvalues is shown in Figs. 8.6−8.7, with the first boundary condition. In Fig. 8.6, it displays that, Re(ω) increases with increasing rotation for the $m = -1$ mode but decreases for both $m = 0$ and $m = 1$ modes, while Im(ω) increases with increasing rotation for the $m = 1$ mode but decreases for both $m = 0$ and $m = -1$ modes. The behaviors of the separation constant, shown in Fig. 8.7, are similar to the counterparts in the $r_+ = 0.1$ case*.

The results for $r_+ = 1$ are presented in Table 8.7 and Figs. 8.8−8.9. From Table 8.7 one observes that there is no superradiant instability for any of the boundary conditions.

In Fig. 8.8, we present the real and imaginary parts of the frequency for the first boundary condition and $r_+ = 1$. Re(ω) increases with rotation for the $m = -1$ mode, decreases with rotation for the $m = 1$ mode, and increases sightly with rotation for the $m = 0$ mode. The

*Notice that for the $m = 1$ mode, Im(λ) starts decreasing with rotation around $a \simeq 0.25$.

Table 8.5: Quasinormal frequencies and separation constants of the Maxwell field with the first boundary condition, for $\ell = 1$ fundamental modes, on a Kerr-AdS BH with size $r_+ = 0.3$.

(ℓ, m)	a	ω_1	λ_1
(1, 0)	0	2.4481 - 0.2291 i	2
	0.1	2.4093 - 0.2768 i	2.0397 - 7.8286$\times 10^{-3}$ i
	0.2	2.3071 - 0.4480 i	2.1373 - 4.5479$\times 10^{-2}$ i
	0.3	2.2136 - 0.7769 i	2.2476 - 1.5300$\times 10^{-1}$ i
(1, 1)	0.1	2.3197 - 0.1512 i	1.3185 + 4.1838$\times 10^{-2}$ i
	0.2	2.1325 - 0.1120 i	0.7889 + 5.6598$\times 10^{-2}$ i
	0.3	1.8707 - 7.4377$\times 10^{-2}$ i	0.4681 + 5.1126$\times 10^{-2}$ i
(1, -1)	0.1	2.5468 - 0.3994 i	2.7643 - 0.1276 i
	0.2	2.6884 - 0.7162 i	3.5705 - 0.4764 i
	0.3	2.9588 - 1.2044 i	4.4377 - 1.2239 i

Table 8.6: Quasinormal frequencies and separation constants of the Maxwell field with the second boundary condition, for $\ell = 1$ fundamental modes, on a Kerr-AdS BH with size $r_+ = 0.3$.

(ℓ, m)	a	ω_2	λ_2
(1, 0)	0	1.8152 - 3.8034$\times 10^{-2}$ i	2
	0.1	1.8092 - 4.7641$\times 10^{-2}$ i	2.0252 - 1.0134$\times 10^{-3}$ i
	0.2	1.7921 - 8.8195$\times 10^{-2}$ i	2.0949 - 6.9871$\times 10^{-3}$ i
	0.3	1.7875 - 1.8395$\times 10^{-1}$ i	2.1957 - 2.9422$\times 10^{-2}$ i
(1, 1)	0.1	1.7265 - 1.5809$\times 10^{-2}$ i	1.4841 + 4.4473$\times 10^{-3}$ i
	0.2	1.6328 - 2.8939$\times 10^{-3}$ i	1.0447 + 1.4994$\times 10^{-3}$ i
	0.3	1.5304 + 5.2612$\times 10^{-3}$ i	0.7048 - 3.6993$\times 10^{-3}$ i
(1, -1)	0.1	1.9063 - 8.8702$\times 10^{-2}$ i	2.5624 - 2.7793$\times 10^{-2}$ i
	0.2	2.0270 - 1.9387$\times 10^{-1}$ i	3.1487 - 1.2392$\times 10^{-1}$ i
	0.3	2.2192 - 3.6493$\times 10^{-1}$ i	3.7662 - 3.4830$\times 10^{-1}$ i

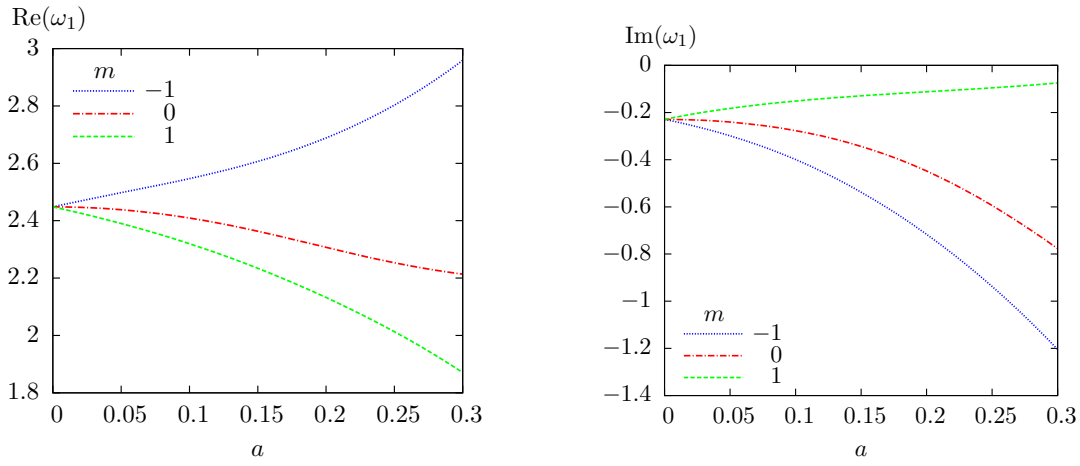

Figure 8.6: Variation of ω with varying rotation parameter, for different values of m. The BH size is fixed as $r_+ = 0.3$ and the first boundary condition has been imposed. The left panel is for Re(ω) while the right panel is for Im(ω).

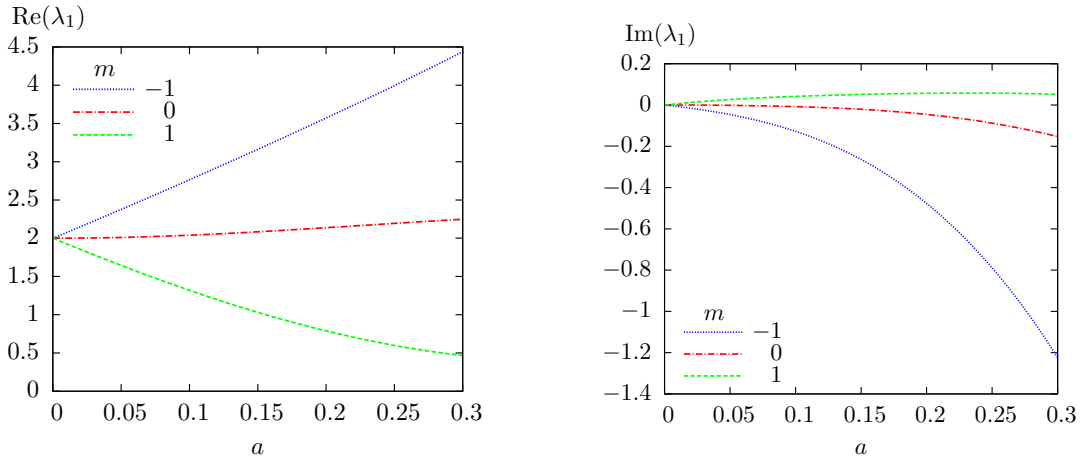

Figure 8.7: Variation of λ with varying rotation parameter, for different values of m. The BH size is fixed as $r_+ = 0.3$ and the first boundary condition has been imposed. The left panel is for Re(λ) while the right panel is for Im(λ).

Table 8.7: Quasinormal frequencies and separation constants of the Maxwell field with the two different Robin boundary conditions, for $\ell = 1$ fundamental modes, on a Kerr-AdS BH with size $r_+ = 1$.

(ℓ, m)	a	ω_1	λ_1	ω_2	λ_2
(1, 0)	0	2.1630 - 1.6991 i	2	1.5536 - 0.5418 i	2
	0.1	2.1672 - 1.7274 i	2.0162 - 4.4059$\times 10^{-2}$ i	1.5627 - 0.5510 i	2.0186 - 1.0131$\times 10^{-2}$ i
	0.2	2.1805 - 1.8146 i	2.0580 - 0.1757 i	1.5909 - 0.5795 i	2.0727 - 4.0857$\times 10^{-2}$ i
	0.3	2.2067 - 1.9686 i	2.1067 - 0.3931 i	1.6416 - 0.6297 i	2.1574 - 9.2910$\times 10^{-2}$ i
(1, 1)	0.1	1.9512 - 1.5858 i	1.4111 + 0.4430 i	1.4277 - 0.4948 i	1.5675 + 0.1404 i
	0.2	1.7679 - 1.5195 i	0.9445 + 0.7797 i	1.3209 - 0.4643 i	1.2046 + 0.2445 i
	0.3	1.6048 - 1.4929 i	0.5998 + 1.0384 i	1.2273 - 0.4463 i	0.9151 + 0.3204 i
(1, -1)	0.1	2.4169 - 1.8746 i	2.7065 - 0.5962 i	1.7067 - 0.6116 i	2.4983 - 0.1905 i
	0.2	2.7349 - 2.1390 i	3.5193 - 1.4235 i	1.8996 - 0.7147 i	3.0586 - 0.4532 i
	0.3	3.1548 - 2.5377 i	4.4164 - 2.6136 i	2.1522 - 0.8684 i	3.6770 - 0.8235 i

behavior of $\mathrm{Im}(\omega)$ is almost the opposite, since $\mathrm{Im}(\omega)$ decreases with rotation for both $m = 0$ and $m = -1$ modes, but for the $m = 1$ mode, it increases first and then starts to decrease around $a \simeq 0.33$. Comparing Fig. 8.9 with Fig. 8.8, shows that the effect of rotation on λ (both real part and imaginary part) mimics closely that on ω, except for $\mathrm{Im}(\lambda)$ of the $m = 1$ mode, which always increases with the rotation parameter.

8.8 Stationary vector and scalar clouds

Stationary clouds are bound state solutions with real frequency of test fields around a rotating background, computed at the linear level. The existence of clouds indicates nonlinear hairy BH solutions [16, 18], but the converse needs not be true [195, 196]. In order to find such solutions, we demand $\omega = m\Omega_H$; in other words, stationary clouds are the zero modes of superradiance. Imposing this condition leads to a constraint on the BH parameters: BHs are quantized in the sense that only BHs with specific parameters can support a cloud with a given set of "quantum" numbers. This quantization defines *existence lines* in the BH parameter space. In the practical implementation of our numerical calculations, we use the same method as before, with the condition $\omega = m\Omega_H$, to look for the rotation parameter. Note that all the

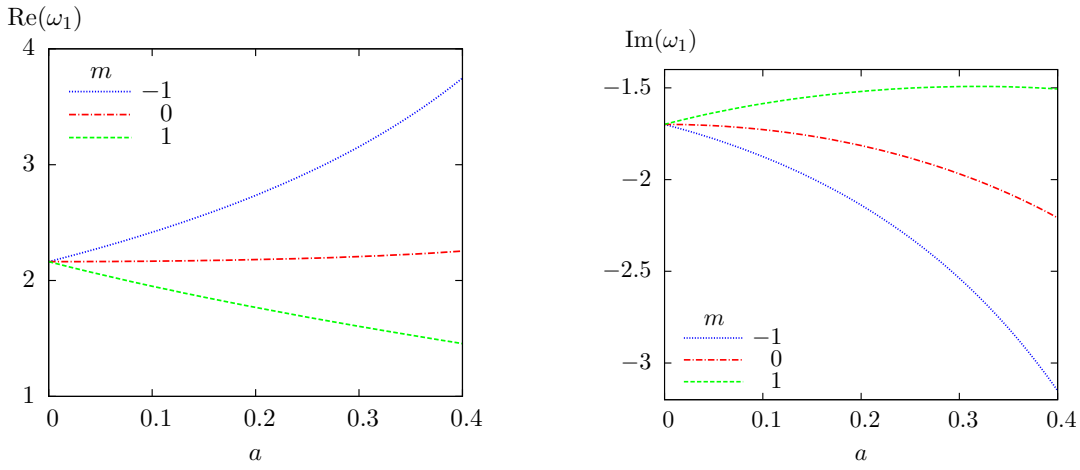

Figure 8.8: Variation of ω with varying rotation parameter, for different values of m. The BH size is fixed as $r_+ = 1$ and the first boundary condition has been imposed. The left panel is for Re(ω) while the right panel is for Im(ω).

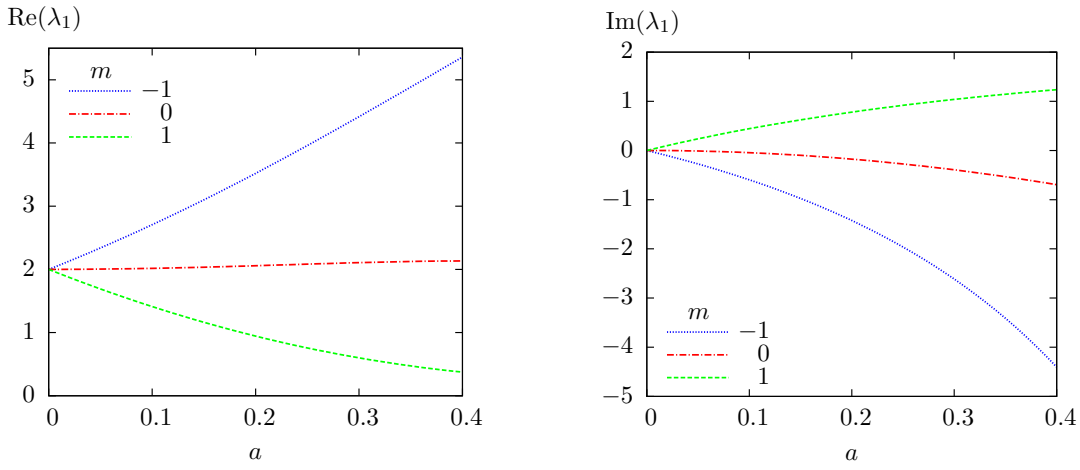

Figure 8.9: Variation of λ with varying rotation parameter, for different values of m. The BH size is fixed as $r_+ = 1$ and the first boundary condition has been imposed. The left panel is for Re(λ) while the right panel is for Im(λ).

results presented in this subsection are for fundamental modes, characterized by $N = 0$.

The vector clouds we have obtained shall be presented in a parameter space spanned by R_+ and $\hat{\Omega}_H$, where

$$R_+ = \sqrt{\frac{r_+^2 + a^2}{\Xi}} \,, \qquad \hat{\Omega}_H = \Omega_H \Xi + a \,, \tag{8.8.1}$$

in which $\hat{\Omega}_H$ has been defined in Eq. (2.2.15). The reason to use this pair of parameters, instead of r_+ and Ω_H, is as follows. Ω_H, as defined in Eq. (2.2.9), is the horizon angular velocity measured relatively to a rotating frame at infinity, while $\hat{\Omega}_H$, defined in Eq. (2.2.15) (also in Eq. (8.8.1)), is the horizon angular velocity measured with respect to a non-rotating observer at infinity. The latter one is more relevant in BH thermodynamics [119]. In the practical calculations, one can use either of them since they are simply related by Eq. (8.8.1). As one may check, $\hat{\Omega}_H$ is a monotonic function of a, in terms of R_+, but not of r_+. Also there is an intuitive geometric meaning for R_+, which is the areal horizon radius.

In Fig. 8.10, the existence lines for some examples of vector clouds are displayed (left panel) together with the corresponding separation constants (right panel). In the left panel, the red solid line corresponds to extremal BHs, and regular BHs only exist below this extremality line. The first three existence lines (with $\ell = m = 1, 2, 3$) for the first boundary condition, and the first two existence lines (with $\ell = m = 1, 2$) for the second boundary condition, are presented by dotted and dot dashed lines, respectively. These lines start from bound state solutions (normal modes), denoted by orange dots in Fig. 8.10, of the Maxwell field on empty AdS, i.e.

$$\hat{\Omega}_{H,1\,|R_+=0} = 1 + \frac{2}{\ell} \,, \qquad \hat{\Omega}_{H,2\,|R_+=0} = 1 + \frac{1}{\ell} \,. \tag{8.8.2}$$

These are obtained by equating the superradiance condition*, $\omega = m\Omega_H$, to the normal mode conditions in Eqs. (8.4.15) and (8.4.16), together with $m = \ell$, and $N = 0$. Observe, in particular, that although the two sets of normal modes in AdS are isospectral, the existence lines for the two boundary conditions only coincide as $R_+ \to 0$, when taking $\ell = 1$ for the first boundary condition and $\ell = 2$ for the second.

An existence line with a particular $\ell = m$, separates the superradiantly stable Kerr-AdS BHs (to the left side of the existence line) and the superradiantly unstable ones (to the right side of

*Ω_H is the same as $\hat{\Omega}_H$ in pure AdS.

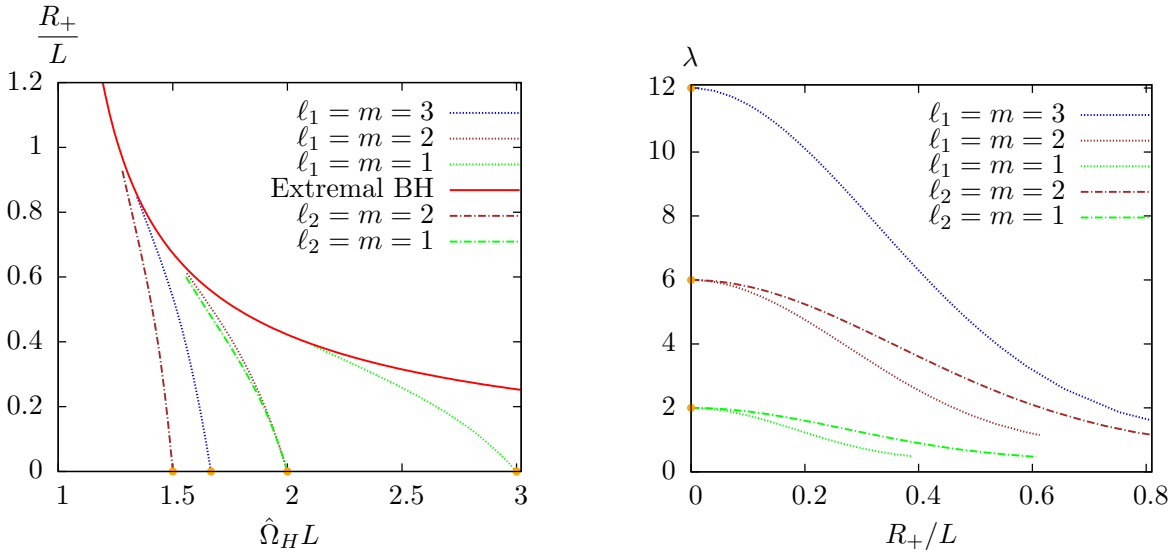

Figure 8.10: Vector clouds (left panel) and the corresponding separation constants (right panel) in R_+ versus $\hat{\Omega}_H$ and λ versus R_+ plots, respectively. $\ell_1(\ell_2)$ refer to the results obtained by imposing the first (second) boundary condition.

the existence line), against that particular mode. Therefore, as one may observe from the left panel of Fig. 8.10, the stable region in the parameter space against the mode, say $\ell = m = n$, where n is some integer, with the second boundary condition is also stable against all the modes with the first boundary condition from $\ell = m = 1$ up to $\ell = m = n+1$. From the data in this figure, together with the relation between R_+ and r_+, Eq. (8.8.1), it can be concluded that: with the first boundary condition, BHs with $r_+ \leq 0.25$ are superradiantly unstable against the $\ell = m = 1$ fundamental mode; while with the second boundary condition, BHs with $r_+ \leq 0.34$ are superradiantly unstable against the $\ell = m = 1$ fundamental mode. These observations also explain the fact that the superradiant instability only appears for modes with the second boundary condition in Table 8.6.

As a comparison with the Maxwell stationary clouds reported above, we have also computed stationary scalar clouds, by solving the massless Klein-Gordon equation on Kerr-AdS BHs, with VEF boundary condition which in this case is the same as the usual field vanishing boundary condition. For this case there is a single set of modes. The results for the scalar clouds are exhibited in Fig. 8.11, in terms of the same parameters R_+ and $\hat{\Omega}_H$.

In the left panel of Fig. 8.11, the red solid line stands, as before, for extremal BHs, so that

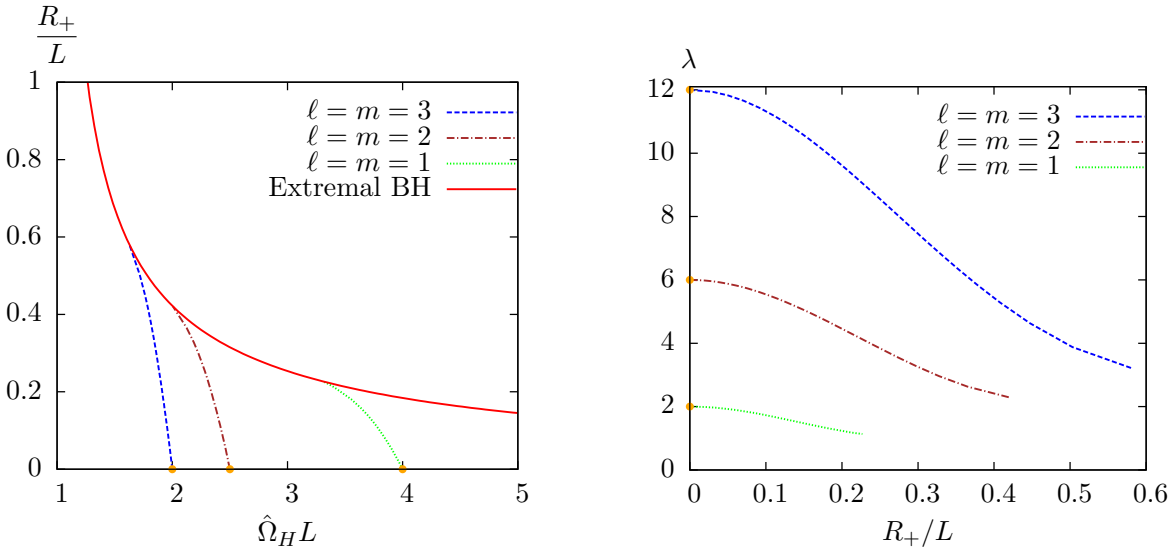

Figure 8.11: Scalar clouds (left panel) and the corresponding separation constants (right panel) in R_+ versus $\hat{\Omega}_H$ and λ versus R_+ plots, respectively.

regular BHs only exist below this line. The first three existence lines, corresponding to the modes with $\ell = m = 1, 2, 3$, are described by dotted, dot dashed and dashed lines, respectively. The corresponding separation constants are also shown in the right panel of Fig. 8.11. The orange dots in both panels indicate again the normal modes and eigenvalues of the angular function in pure AdS, which are

$$\hat{\Omega}_{H,\text{scalar}} = 1 + \frac{3}{\ell}\,, \qquad \lambda = \ell(\ell+1)\,. \tag{8.8.3}$$

Again, the existence line with a particular $\ell = m$, divides the parameter space into two regions: BHs in the left region are superradiantly stable while BHs in the right region are superradiantly unstable, against that particular mode.

Comparing Figs. 8.10 and 8.11 it becomes clear that the existence lines for stationary vector clouds appear to the *left* of the existence line of a stationary scalar cloud with the same quantum numbers. Thus, there are BHs that are stable against the scalar mode but become unstable against the vector mode. In a sense, vector superradiance is stronger. Qualitatively, this conclusion agrees with the computation of the amplification factors for scalar and vector modes in superradiant scattering, in asymptotically flat spacetimes.

8.9 Summary

The behavior of test fields on an asymptotically AdS spacetime depends sensitively on the boundary conditions, since such spacetimes contain a timelike boundary. The AdS boundary is often regarded as a perfectly reflecting mirror in the sense that no flux (both energy flux and angular momentum flux) can cross it. Various types of boundary conditions in asymptotically AdS spacetimes have been explored, in particular consistent with this simple requirement. We took this requirement as the *guiding principle* to impose boundary conditions on test fields. Following this principle, two boundary conditions were found for Maxwell fields on asymptotically AdS spacetimes, of which only one had been previously discussed on the Schwarzschild-AdS background. These two boundary conditions were then used to study quasinormal modes, superradiant unstable modes and vector clouds for the Maxwell field on Kerr-AdS BHs.

To find quasinormal modes and superradiant modes, we have solved the Teukolsky equations both analytically and numerically. In the small BH and slow rotation regime, an analytical matching method was applied to exhibit how these two boundary conditions work and how they produce superradiant instabilities. A numerical method was then used to explore the parameter space away from the small BH and slow rotation approximations. We found that for small BHs characterized by $r_+ = 0.1$, unstable superradiant modes appear with both boundary conditions. Increasing the BH size, as exemplified for $r_+ = 0.3$, superradiant instabilities only appear with the second boundary condition, and eventually disappear for both boundary conditions, as exemplified when $r_+ = 1$. Our analysis also shows that superradiant instabilities for the Maxwell field may exist for (moderately) larger BH sizes, when comparing with the scalar case, for which superradiant instabilities appear in the regime $r_+ \leq 0.16$ [32].

To study stationary vector clouds, which can occur for massless fields in AdS due to the box-like global structure, we have solved the Teukolsky equations at the onset of the superradiant instability, i.e. for $\omega = m\Omega_H$. We found that both boundary conditions can yield vector clouds, and that these clouds are bounded by the extremal BHs, as for the scalar clouds on asymptotically flat Kerr BHs [16, 94, 159]. This behaviour differs from that observed for gravitational perturbations, for which only one of the sets of clouds are bounded by the extremal BHs [31]. The existence of clouds at the linear level indicates nonlinear hairy BH

solutions [16, 18], so it would be interesting to find the nonlinear realization of these vector clouds. There is already a well-known exact BH family within the Einstein-Maxwell-AdS system: the Kerr-Newman-AdS family. It will then be interesting to understand the interplay between this well known family and the new family of "hairy" BHs.

Chapter 9

Conclusions and outlook

In this final chapter we draw our conclusions, and address some open questions.

This thesis covers studies of Hawking radiation and superradiance, for scalar and vector fields in the probe limit, using perturbative methods.

In Chapter 3, we have studied the wave equations of a Proca field on spherically symmetric higher dimensional spacetimes. Such background was chosen to avoid the non-separation of variables for the Proca equations in a rotating spacetime; while still being an interesting setup in TeV gravity models. Using the Kodama-Ishibashi formalism, we achieved separation of variables, and obtained a set of coupled equations, as well as some decoupled ones.

These equations were used to study Hawking radiation, for a neutral Proca field on a D-dimensional Schwarzschild black hole in Chapter 4 and a charged Proca field on a brane charged black hole in Chapter 5. We have designed a numerical strategy to solve the coupled equations and showed that the coupled systems may be treated with an **S**-matrix type formalism which allows decoupling in the asymptotic regions. This **S**-matrix was used to define a transmission matrix the eigenvalues of which give us the transmission factors. Then the Hawking fluxes were calculated using the standard formulas. For a neutral Proca field, we found distinctive features by introducing the mass term, such as the lifting of the degeneracy of the two transverse modes in four dimensions, the appearance of longitudinal modes and in particular the s-wave. When both background and Proca field charges were included, we observed the existence of superradiant modes, and a charge splitting effect for small energies

and for two or more extra dimensions. We also compared the Proca bulk-to-brane ratio of energy emission, showing that most of the energy is emitted on the brane.

In Chapter 6, we have studied quasi-bound states for both the charged massive scalar field and the charged Proca field in Reissner-Nordström black holes. We established that no such states exist in the superradiant regime for the Proca field, a similar behavior to that known for the scalar field. For both fields, however, decaying quasi-bound states with an arbitrary small imaginary part of the frequency exist and thus which are arbitrarily long lived. In the limit of vanishing imaginary part of the frequency, the fields did not trivialize and we dubbed the corresponding configurations as marginal scalar or Proca clouds, since they were only marginal bound.

A problem which is still open is the study of the Proca field in the Kerr black hole without any approximations. Indeed, this problem has been partially addressed for slow rotation [131,132]. This is still interesting because of the following open questions: (1) is it possible to construct a modified Newman-Penrose formalism to deal with linear perturbations for massive fields in general? (2) Is it possible to establish a numerical method to solve the type of two dimensional partial differential equation arising in this problem?

In Chapter 7, we have studied superradiant instabilities for a charged scalar field in a D-dimensional Reissner-Nordström-AdS black hole. By employing an analytic matching method and a numerical method, we proved that superradiant instabilities do exist for all ℓ modes in higher dimensions. Inspired by the large D general relativity [178], it would also be interesting to develop another analytic treatment to look for superradiant modes.

In Chapter 8, we have studied Maxwell perturbations on Kerr-AdS black holes. From the viewpoint that the AdS boundary may be regarded as a perfectly reflecting mirror, we proposed *vanishing energy flux* boundary conditions which are physically motivated. Imposing such conditions, we obtained a set of two Robin boundary conditions even for a Schwarzschild-AdS black hole, where only one of them has been reported in the literature. Applying these two boundary conditions to Kerr-AdS black holes, we have studied superradiant instabilities, and observed that the new branch of quasinormal modes may be unstable in a larger parameter space. Our results also showed that superradiant instabilities for the Maxwell field may exist for (moderately) larger black hole size, when comparing with the scalar case.

To study stationary vector clouds, we have solved the Teukolsky equations at the onset of the superradiant instability. We found that both boundary conditions can yield vector clouds, which are characterized by existence lines in the parameter space. These lines are bounded by pure AdS spaces and the extremal black holes, which differs from that observed for gravitational perturbations, for which only one of the sets of clouds are bounded by the extremal black holes [31]. The existence of clouds at the linear level indicates nonlinear hairy black hole solutions, so the open question is to find the nonlinear realization of these vector clouds. There is already a well-known exact black hole family within the Einstein-Maxwell-AdS system: the Kerr-Newman-AdS family. It will then be very interesting to study properties of the new type of "hairy" black hole solutions, and understand the interplay between the Kerr-Newman-AdS black holes and the new family of "hairy" black holes.

Appendix A

Functions and matrices for the neutral Proca case

This appendix contains details on the functions, recurrence relations and matrices, used in Chapter 4.

The functions appeared in Eqs. (4.2.1) and (4.2.2) are ($\kappa_s^2 = \ell(\ell+n-1)$)

$$
\begin{aligned}
M(r) &\equiv \sum_{m=0}^{2n-1} \alpha_m y^m = r\left(r^{n-1}-1\right)^2 \ , \\
N(r) &\equiv \sum_{m=0}^{2n-2} \beta_m y^m = n\left(r^{n-1}-1\right)^2 \ , \\
P(r) &\equiv \sum_{m=0}^{2n-1} \gamma_m y^m = -(\kappa_s^2+\mu_p^2 r^2)\left(r^{2n-3}-r^{n-2}\right)+\omega^2 r^{2n-1} \ , \\
Q(r) &\equiv \sum_{m=0}^{2n-2} \sigma_m y^m = i\omega r^{n-1}\left(2r^{n-1}-n-1\right) \ , \\
\tilde{M}(r) &\equiv \sum_{m=0}^{2n} \tilde{\alpha}_m y^m = r^2\left(r^{n-1}-1\right)^2 \ , \\
\tilde{N}(r) &\equiv \sum_{m=0}^{2n-1} \tilde{\beta}_m y^m = (n-2)r\left(r^{n-1}-1\right)^2 \ , \\
\tilde{P}(r) &\equiv \sum_{m=0}^{2n} \tilde{\gamma}_m y^m = -\left(\kappa_s^2+\mu_p^2 r^2\right)\left(r^{2n-2}-r^{n-1}\right)+\omega^2 r^{2n}-(n-2)\left(r^{n-1}-1\right)^2 \ , \\
\tilde{Q}(r) &\equiv \sum_{m=0}^{n} \tilde{\sigma}_m y^m = -i\omega(n-1)r^n \ .
\end{aligned}
$$

The recurrence relations are

$$\begin{aligned}
\mu_0 &= \nu_0 \ , \\
\mu_1 &= -\frac{(\rho(\rho-1)\alpha_3 + \rho\beta_2 + \gamma_1 + \sigma_1)\,\nu_0 + \sigma_0\nu_1}{\rho(\rho+1)\alpha_2 + \gamma_0} \ , \\
\mu_j &= \frac{\omega^2 + (n-1)^2(\rho+j)(\rho+j-1)}{D_j} f_j + \frac{i\omega(n-1)}{D_j}\tilde{f}_j \ , \\
\nu_j &= \frac{\omega^2 + (n-1)^2(\rho+j)(\rho+j-1)}{D_j} \tilde{f}_j + \frac{i\omega(n-1)}{D_j} f_j \ ,
\end{aligned} \tag{A.0.1}$$

with

$$\begin{aligned}
D_j &= (n-1)^2\omega^2 + \left(\omega^2 + (n-1)^2(\rho+j)(\rho+j-1)\right)^2 \ , \\
f_j &= -\sum_{m=1}^{j} \left[\left(\alpha_{m+2}(\rho+j-m)(\rho+j-m-1) + \beta_{m+1}(\rho+j-m) + \gamma_m\right)\mu_{j-m} + \sigma_m\nu_{j-m} \right] , \\
\tilde{f}_j &= -\sum_{m=1}^{j} \left[\left(\tilde{\alpha}_{m+2}(\rho+j-m)(\rho+j-m-1) + \tilde{\beta}_{m+1}(\rho+j-m) + \tilde{\gamma}_m\right)\nu_{j-m} + \tilde{\sigma}_m\mu_{j-m} \right] .
\end{aligned}$$

The coefficients used in the asymptotic expansion in the text are

$$c^{\pm} = \frac{i}{2\omega}\left[-\kappa_s^2 + \frac{n(2-n)}{4} + (2\omega^2 - \mu_p^2)\left(\delta_{2,n} + \delta_{3,n}\right) + \left(\pm i\frac{\mu_p^2}{2k} - \left(\frac{\mu_p^2}{2k}\right)^2 \right)\delta_{2,n} \right] \ . \tag{A.0.2}$$

The matrices used in the text are as follows

$$\mathbf{T} = \frac{1}{r^{\frac{n-2}{2}}} \begin{pmatrix}
\frac{e^{i\Phi}}{r} & \frac{e^{-i\Phi}}{r} & e^{i\Phi} & e^{-i\Phi} \\
\frac{ike^{i\Phi}}{r} & -\frac{ike^{-i\Phi}}{r} & \left[ik + \frac{i\varphi - \frac{n-2}{2}}{r}\right]e^{i\Phi} & -\left[ik + \frac{i\varphi + \frac{n-2}{2}}{r}\right]e^{-i\Phi} \\
0 & 0 & \left(-\frac{k}{\omega} + \frac{c^+}{r}\right)e^{i\Phi} & \left(\frac{k}{\omega} + \frac{c^-}{r}\right)e^{-i\Phi} \\
0 & 0 & \left[-\frac{ik^2}{\omega} + \frac{ikc^+ - \frac{k}{\omega}(i\varphi - \frac{n-2}{2})}{r}\right]e^{i\Phi} & -\left[\frac{ik^2}{\omega} + \frac{ikc^- + \frac{k}{\omega}(i\varphi + \frac{n-2}{2})}{r}\right]e^{-i\Phi}
\end{pmatrix} , \tag{A.0.3}$$

$$\mathbf{X} = \begin{pmatrix}
0 & 1 & 0 & 0 \\
-\frac{P}{M} & -\frac{N}{M} & -\frac{Q}{M} & 0 \\
0 & 0 & 0 & 1 \\
-\frac{\tilde{Q}}{\tilde{M}} & 0 & -\frac{\tilde{P}}{\tilde{M}} & -\frac{\tilde{N}}{\tilde{M}}
\end{pmatrix} , \tag{A.0.4}$$

and the 2-vectors

$$\mathbf{y}^{\pm} = \begin{pmatrix} \sqrt{\frac{\kappa_s^2 k}{\omega}} a_0^{\pm} \\ \sqrt{\frac{\omega k}{\mu_p^2}} \left[(\pm i\varphi - \frac{n-2}{2} + i\omega c^{\pm} \mp ik\delta_{n,2}) a_0^{\pm} \pm ika_1^{\pm} \right] \end{pmatrix} , \tag{A.0.5}$$

$$\mathbf{h}^{-} = \begin{pmatrix} \sqrt{\kappa_s^2} \nu_0 \\ \underline{i\omega(\mu_1 - \rho(\frac{n}{2}\nu_0 + \nu_1 - \mu_1)) + \kappa_s^2 \nu_0} \\ \mu_p \end{pmatrix} . \tag{A.0.6}$$

Appendix B

Functions and matrices for the charged Proca case

This appendix contains details on the functions and matrices used to rewrite the second order radial differential equations into a first order form, and recurrence relations used to initialize these radial differential equations close to the event horizon. This was used in Chapter 5.

The functions that used in the text are (where $\kappa_s^2 = \ell(\ell+1)$):

$$A(r) \equiv \sum_{m=0}^{2n+1} a_m y^m = r\left[r^n - (1+Q^2)r + Q^2 r^{n-2}\right]^2 \ ,$$

$$B(r) \equiv \sum_{m=0}^{2n} b_m y^m = 2\left[r^n - (1+Q^2)r + Q^2 r^{n-2}\right]^2 \ ,$$

$$C(r) \equiv \sum_{m=0}^{2n+1} c_m y^m = (\omega r - qQ)^2 r^{2n-1} - (\kappa_s^2 + \mu_p^2 r^2) r^{n-1}\left[r^n - (1+Q^2)r + Q^2 r^{n-2}\right] \ ,$$

$$E(r) \equiv \sum_{m=0}^{2n} e_m y^m = iqQr^{n-1}\left[(1+Q^2)(n-1)r - 2Q^2 r^{n-2}\right] + i\omega r^n\left[2r^n - (1+Q^2)(n+1)r + 4Q^2 r^{n-2}\right] \ ,$$

$$\tilde{A}(r) \equiv \sum_{m=0}^{2n} \tilde{a}_m y^m = \left[r^n - (1+Q^2)r + Q^2 r^{n-2}\right]^2 \ ,$$

$$\tilde{B}(r) \equiv 0 \ ,$$

$$\tilde{C}(r) \equiv \sum_{m=0}^{2n} \tilde{c}_m y^m = (\omega r - qQ)^2 r^{2n-2} - \left(\kappa_s^2 + \mu_p^2 r^2\right) r^{n-2}\left[r^n - (1+Q^2)r + Q^2 r^{n-2}\right] \ ,$$

$$\tilde{E}(r) \equiv \sum_{m=0}^{2n-2} \tilde{e}_m y^m = iqQr^{n-1}\left[(n-3)(1+Q^2)+2r^{n-1}\right] - i\omega r^{n-1}\left[(1+Q^2)(n-1)r - 2Q^2 r^{n-2}\right] \ .$$

The recurrence relations are

$$\begin{aligned}
\mu_0 &= \nu_0 \ , \\
\mu_1 &= -\frac{\left[a_3\rho(\rho-1)+b_2\rho+c_1+e_1\right]\nu_0 + e_0\nu_1}{a_2\rho(\rho+1)+c_0} \ , \\
\mu_j &= \frac{\tilde{a}_2(\rho+j)(\rho+j-1)+\tilde{c}_0}{D_j} f_j - \frac{e_0}{D_j}\tilde{f}_j \ , \\
\nu_j &= \frac{a_2(\rho+j)(\rho+j-1)+c_0}{D_j}\tilde{f}_j - \frac{\tilde{e}_0}{D_j} f_j \ ,
\end{aligned} \tag{B.0.1}$$

with

$$\begin{aligned}
D_j &= \left[a_2(\rho+j)(\rho+j-1)+c_0\right]\left[\tilde{a}_2(\rho+j)(\rho+j-1)+\tilde{c}_0\right] - \tilde{e}_0 e_0 \ , \\
f_j &= -\sum_{m=1}^{j}\left[\left(a_{m+2}(\rho+j-m)(\rho+j-m-1)+b_{m+1}(\rho+j-m)+c_m\right)\mu_{j-m} + e_m\nu_{j-m}\right] \ , \\
\tilde{f}_j &= -\sum_{m=1}^{j}\left[\left(\tilde{a}_{m+2}(\rho+j-m)(\rho+j-m-1)+\tilde{c}_m\right)\nu_{j-m} + \tilde{e}_m\mu_{j-m}\right] \ .
\end{aligned}$$

The coefficients used in the asymptotic expansion in the text are

$$\begin{aligned}
c^{\pm} =& \frac{i}{2\omega}\Big[-\kappa_s^2 + Q^2(\mu_p^2-2\omega^2) - \frac{q^2Q^2\mu_p^2}{k^2} \mp i\frac{qQ\omega}{k} + (2\omega^2-\mu_p^2)(1+Q^2)\delta_{3,n} \\
&+ \Big(\pm i\frac{\mu_p^2(1+Q^2)}{2k} - \Big(\frac{\mu_p^2(1+Q^2)}{2k}\Big)^2 + (1+Q^2)^2(2\omega^2-\mu_p^2) \\
&+ \frac{qQ\omega(1+Q^2)(\mu_p^2-2k^2)}{k^2}\Big)\delta_{2,n}\Big] \ .
\end{aligned}$$

The relation between the new first order radial functions $\mathbf{\Psi}$ used in (5.2.10), and the 4-vector $\mathbf{V}^T = (\psi, d_r\psi, \chi, d_r\chi)$ for the original fields and derivatives is found from Eqs. (5.2.8), (5.2.9) and their derivatives. The corresponding r-dependent matrix transformation $\mathbf{T}$ is defined

$$\mathbf{V} = \mathbf{T}\mathbf{\Psi} \ , \tag{B.0.2}$$

and its form is

$$\mathbf{T} = \begin{pmatrix} \frac{e^{i\Phi}}{r} & \frac{e^{-i\Phi}}{r} & e^{i\Phi} & e^{-i\Phi} \\ \frac{ike^{i\Phi}}{r} & -\frac{ike^{-i\Phi}}{r} & \left[ik + \frac{i\varphi}{r}\right] e^{i\Phi} & -\left[ik + \frac{i\varphi}{r}\right] e^{-i\Phi} \\ 0 & 0 & \left(-\frac{k}{\omega} + \frac{c^+}{r}\right) e^{i\Phi} & \left(\frac{k}{\omega} + \frac{c^-}{r}\right) e^{-i\Phi} \\ 0 & 0 & \left[-\frac{ik^2}{\omega} + \frac{ikc^+ - \frac{ik\varphi}{\omega}}{r}\right] e^{i\Phi} & -\left[\frac{ik^2}{\omega} + \frac{ikc^- + \frac{ik\varphi}{\omega}}{r}\right] e^{-i\Phi} \end{pmatrix} , \tag{B.0.3}$$

On another hand, the original system (3.1.5) and (3.1.6), can be written in a first order form

$$\frac{d\mathbf{V}}{dr} = \mathbf{X}\mathbf{V} , \tag{B.0.4}$$

where the matrix $\mathbf{X}$ is

$$\mathbf{X} = \begin{pmatrix} 0 & 1 & 0 & 0 \\ -\frac{C}{A} & -\frac{B}{A} & -\frac{E}{A} & 0 \\ 0 & 0 & 0 & 1 \\ -\frac{\tilde{E}}{\tilde{A}} & 0 & -\frac{\tilde{C}}{\tilde{A}} & 0 \end{pmatrix} , \tag{B.0.5}$$

and the 2-vectors

$$\mathbf{y}^{\pm} = \begin{pmatrix} \sqrt{\frac{\kappa_s^2 k}{\omega^2}} a_0^{\pm} \\ i\sqrt{\frac{k}{\mu_p^2}} \left[\left(\pm\varphi + \omega c^{\pm} \mp k(1+Q^2)\delta_{n,2} \pm \frac{kqQ}{\omega} \right) a_0^{\pm} \pm k a_1^{\pm} \right] \end{pmatrix} , \tag{B.0.6}$$

$$\mathbf{h}^{-} = \begin{pmatrix} \sqrt{t}\nu_0 \\ \sqrt{\frac{\mu_p^2}{\mu_p^4 + q^2Q^2}} \left(-i\kappa_s^2 \nu_0 + (\omega - qQ)d \right) \end{pmatrix} , \tag{B.0.7}$$

with

$$t = \frac{\kappa_s^2}{\mu_p^4 + q^2Q^2} \left[(\omega - qQ) \left(qQa + b\mu_p^2 + 2i\rho\mu_p^2\alpha + \frac{2qQ\mu_p^2}{\beta} \right) - \kappa_s^2 \mu_p^2 \right] ,$$

$$d = \left[\left(1 + \rho - \frac{iqQ}{\mu_p^2}\rho \right) (a + ib) + \left(1 + \frac{iqQ}{\mu_p^2} \right) \left(\frac{iqQ}{\beta} - \alpha\rho \right) \right] \nu_0 + (1 + 2\rho) \left(\frac{iqQ}{\mu_p^2} - 1 \right) \nu_1 ,$$

$$a = \frac{qQ}{\omega - qQ} , \qquad b = \frac{qQ(2 + n(n-3)(1+Q^2))}{\beta^2} - \frac{2\omega\alpha}{\beta} + \frac{\kappa_s^2 + \mu_p^2}{\omega - qQ} ,$$

$$\alpha = \frac{n(n-1) + (n-3)(n+2)Q^2}{2\beta} , \qquad \beta = (n-1) + (n-3)Q^2 .$$

Appendix C

Proof of Theorem 1

In this appendix, we prove Theorem 1 given in Chapter 2, by taking $\bar{\mathscr{L}}_0\bar{\mathscr{L}}_1 S_{+1} = BS_{-1}$, as an example. To do so, we start from Eq. (2.2.29), by applying the operator $\bar{\mathscr{L}}_0\bar{\mathscr{L}}_1$ on both sides,

$$\begin{aligned}
-\lambda\bar{\mathscr{L}}_0\bar{\mathscr{L}}_1 S_{+1} &= \bar{\mathscr{L}}_0\bar{\mathscr{L}}_1(\bar{\mathscr{L}}_0{}^{\dagger}\bar{\mathscr{L}}_1 - 2a\omega\cos\theta\Xi)S_{+1} \\
&= \bar{\mathscr{L}}_0\bar{\mathscr{L}}_1\bar{\mathscr{L}}_0{}^{\dagger}\bar{\mathscr{L}}_1 S_{+1} - 2a\omega\Xi\bar{\mathscr{L}}_0(\cos\theta\bar{\mathscr{L}}_1 - \sin\theta\sqrt{\Delta_\theta})S_{+1} \\
&= \bar{\mathscr{L}}_0\bar{\mathscr{L}}_1\bar{\mathscr{L}}_0{}^{\dagger}\bar{\mathscr{L}}_1 S_{+1} - 2a\omega\Xi\cos\theta\bar{\mathscr{L}}_0\bar{\mathscr{L}}_1 S_{+1} + 4a\omega\Xi\sqrt{\Delta_\theta}\sin\theta\bar{\mathscr{L}}_1 S_{+1} \ , \quad \text{(C.0.1)}
\end{aligned}$$

where relations

$$\bar{\mathscr{L}}_n{}^{\dagger}\cos\theta = \cos\theta\bar{\mathscr{L}}_n{}^{\dagger} - \sin\theta\sqrt{\Delta_\theta} \ , \qquad \sqrt{\Delta_\theta}\sin\theta\bar{\mathscr{L}}_{n+1} = \bar{\mathscr{L}}_n\sqrt{\Delta_\theta}\sin\theta \ , \qquad \text{(C.0.2)}$$

have been used. The first term in Eq. (C.0.1) can be further simplified

$$\begin{aligned}
\bar{\mathscr{L}}_0\bar{\mathscr{L}}_1\bar{\mathscr{L}}_0{}^{\dagger}\bar{\mathscr{L}}_1 S_{+1} &= \bar{\mathscr{L}}_0\bar{\mathscr{L}}_1(\bar{\mathscr{L}}_0 + 2\sqrt{\Delta_\theta}\mathcal{Q})\bar{\mathscr{L}}_1 S_{+1} \\
&= \bar{\mathscr{L}}_0(\bar{\mathscr{L}}_1{}^{\dagger} - 2\sqrt{\Delta_\theta}\mathcal{Q})\bar{\mathscr{L}}_0\bar{\mathscr{L}}_1 S_{+1} + 2\bar{\mathscr{L}}_0\bar{\mathscr{L}}_1\sqrt{\Delta_\theta}\mathcal{Q}\bar{\mathscr{L}}_1 S_{+1} \ , \quad \text{(C.0.3)}
\end{aligned}$$

in which

$$\begin{aligned}
\bar{\mathscr{L}}_1\sqrt{\Delta_\theta}\mathcal{Q} &= \left(\bar{\mathscr{L}}_0 + \frac{1}{\sin\theta}\frac{d}{d\theta}(\sqrt{\Delta_\theta}\sin\theta)\right)\sqrt{\Delta_\theta}\mathcal{Q} \\
&= \sqrt{\Delta_\theta}\mathcal{Q}\bar{\mathscr{L}}_0 + \sqrt{\Delta_\theta}\frac{d}{d\theta}(\sqrt{\Delta_\theta}\mathcal{Q}) + \frac{\sqrt{\Delta_\theta}\mathcal{Q}}{\sin\theta}\frac{d}{d\theta}(\sqrt{\Delta_\theta}\sin\theta) \\
&= \sqrt{\Delta_\theta}\mathcal{Q}\bar{\mathscr{L}}_0 + \frac{d}{d\theta}(\Xi H) + \Xi H\cot\theta = \sqrt{\Delta_\theta}\mathcal{Q}\bar{\mathscr{L}}_0 + 2a\omega\Xi\cos\theta \ , \quad \text{(C.0.4)}
\end{aligned}$$

where $\mathcal{Q} = \frac{\Xi H}{\Delta_\theta}$, as defined in Eq. (2.2.36), and where the following relation is used

$$\frac{dH}{d\theta} + H\cot\theta = 2a\omega\cos\theta \ . \tag{C.0.5}$$

Then Eq. (C.0.1) becomes

$$\begin{aligned}
-\lambda\bar{\mathscr{L}}_0\bar{\mathscr{L}}_1 S_{+1} &= \bar{\mathscr{L}}_0(\bar{\mathscr{L}}_1^{\dagger} - 2\sqrt{\Delta_\theta}\mathcal{Q})\bar{\mathscr{L}}_0\bar{\mathscr{L}}_1 S_{+1} + 2\bar{\mathscr{L}}_0(\sqrt{\Delta_\theta}\mathcal{Q}\bar{\mathscr{L}}_0 + 2a\omega\Xi\cos\theta)\bar{\mathscr{L}}_1 S_{+1} \\
&\quad - 2a\omega\Xi\cos\theta\bar{\mathscr{L}}_0\bar{\mathscr{L}}_1 S_{+1} + 4a\omega\Xi\sqrt{\Delta_\theta}\sin\theta\bar{\mathscr{L}}_1 S_{+1} \\
&= \bar{\mathscr{L}}_0\bar{\mathscr{L}}_1^{\dagger}\bar{\mathscr{L}}_0\bar{\mathscr{L}}_1 S_{+1} + 4a\omega\Xi\bar{\mathscr{L}}_0\cos\theta\bar{\mathscr{L}}_1 S_{+1} - 2a\omega\Xi\cos\theta\bar{\mathscr{L}}_0\bar{\mathscr{L}}_1 S_{+1} \\
&\quad + 4a\omega\Xi\sqrt{\Delta_\theta}\sin\theta\bar{\mathscr{L}}_1 S_{+1} \\
&= \bar{\mathscr{L}}_0\bar{\mathscr{L}}_1^{\dagger}\bar{\mathscr{L}}_0\bar{\mathscr{L}}_1 S_{+1} + 4a\omega\Xi(\cos\theta\bar{\mathscr{L}}_0 - \sin\theta\sqrt{\Delta_\theta})\bar{\mathscr{L}}_1 S_{+1} \\
&\quad - 2a\omega\Xi\cos\theta\bar{\mathscr{L}}_0\bar{\mathscr{L}}_1 S_{+1} + 4a\omega\Xi\sqrt{\Delta_\theta}\sin\theta\bar{\mathscr{L}}_1 S_{+1} \\
&= (\bar{\mathscr{L}}_0\bar{\mathscr{L}}_1^{\dagger} + 2a\omega\Xi\cos\theta)\bar{\mathscr{L}}_0\bar{\mathscr{L}}_1 S_{+1} \ .
\end{aligned} \tag{C.0.6}$$

Comparing Eq. (C.0.6) with Eq. (2.2.31) and remembering the definition in Eq. (2.2.33), one concludes that $\bar{\mathscr{L}}_0\bar{\mathscr{L}}_1 S_{+1}$ is proportional to S_{-1}. We identify the proportionality constant as B, such that

$$\bar{\mathscr{L}}_0\bar{\mathscr{L}}_1 S_{+1} = BS_{-1} \ . \tag{C.0.7}$$

Following the same procedures as above, one can also prove that

$$\bar{\mathscr{L}}_0^{\dagger}\bar{\mathscr{L}}_1^{\dagger} S_{-1} = BS_{+1} \ , \tag{C.0.8}$$

where the same proportionality constant B is used. This property is guaranteed by the normalization conditions given in Eq. (2.2.34).

Therefore, Theorem 1 is proved.

Appendix D

Angular momentum flux

This appendix contains details on derivation of the angular momentum flux for the Maxwell field on the Kerr-AdS background. Our purpose is to show that the vanishing of the energy flux, a physical principle used in Chapter 8 to impose boundary conditions for the Maxwell field on Kerr-AdS, leads to a vanishing angular momentum flux.

From the definition of the energy-momentum tensor for the Maxwell field

$$T_{\mu\nu} = F_{\mu\sigma}F^{\sigma}{}_{\nu} + \frac{1}{4}g_{\mu\nu}F^2 \ , \tag{D.0.1}$$

we can calculate the angular momentum flux

$$\mathcal{J} = \int_{S^2} \sin\theta d\theta d\varphi \, r^2 \left(T^{r}{}_{\varphi,\, I} + T^{r}{}_{\varphi,\, II}\right) \ , \tag{D.0.2}$$

with

$$T^{r}{}_{\varphi,\, I} = -a\sin^2\theta \, T^{r}{}_{t,\, I} \ , \tag{D.0.3}$$

$$T^{r}{}_{\varphi,\, II} = -\frac{i\sin\theta\sqrt{\Delta_\theta}(r^2+a^2)}{2\Xi\rho^4}\Phi_1(\Phi_2^* + \Delta_r\Phi_0^*) + c.c \ , \tag{D.0.4}$$

where $T^{r}{}_{t,\, I}$ is given in Eq. (8.3.2), $c.c$ stands for the complex conjugate of the preceding terms, and

$$\Phi_0 = \phi_0 \ , \qquad \Phi_2 = 2\bar{\rho}^*\phi_2 \ , \qquad \bar{\rho} = r + ia\cos\theta \ . \tag{D.0.5}$$

From Eq. (D.0.3), and considering the vanishing energy flux boundary conditions, i.e.

$$\int_{S^2} \sin\theta d\theta d\varphi \, r^2 T^{r}{}_{t,\, I} \to 0 \ , \tag{D.0.6}$$

asymptotically, one concludes that there is no contributions for the angular momentum flux from the first term $T^{r}{}_{\varphi,\,I}$.

For the second term, from Eq. (D.0.4), we notice that Φ_1 is involved, which has been derived in Eq. (2.2.52). For convenience, we list this solution and related expressions below. The solution for Φ_1 is

$$\bar{\rho}^{*}\Phi_1 = g_{+1}\bar{\mathscr{L}}_1 S_{+1} - iaf_{-1}\mathscr{D}_0 P_{-1}\ , \tag{D.0.7}$$

with

$$g_{+1} = \frac{1}{B}(r\mathscr{D}_0 P_{-1} - P_{-1})\ , \tag{D.0.8}$$

$$f_{-1} = \frac{1}{B}(\cos\theta\bar{\mathscr{L}}_1 S_{+1} + \sin\theta\sqrt{\Delta_\theta}S_{+1})\ , \tag{D.0.9}$$

$$\bar{\mathscr{L}}_1 S_{+1} = \frac{(2a\omega\Xi\cos\theta - \lambda)S_{+1} - BS_{-1}}{2\mathcal{Q}\sqrt{\Delta_\theta}}\ , \tag{D.0.10}$$

where

$$\mathscr{D}_0 = \frac{\partial}{\partial r} - \frac{iK_r}{\Delta_r}\ ,\quad \mathcal{Q} = \frac{\Xi(a\omega\sin^2\theta - m)}{\sin\theta\Delta_\theta}\ ,\quad P_{-1} = BR_{-1}\ , \tag{D.0.11}$$

and the constant B is given by Eq. (2.2.37), S_{+1} and S_{-1} are spin weighted AdS spheroidal harmonics. From the properties of these spheroidal harmonic functions

$$S_{+1}(\pi-\theta) = S_{-1}(\theta)\ ,\qquad S_{-1}(\pi-\theta) = S_{+1}(\theta)\ , \tag{D.0.12}$$

which are guaranteed by the angular equations (2.2.29) and (2.2.31), then we have the following properties

$$\begin{aligned}
\int_0^\pi d\theta\sin\theta f_{odd}(\theta)S_{+1}(\theta)S^{*}_{+1}(\theta) &= -\int_0^\pi d\theta\sin\theta f_{odd}(\theta)S_{-1}(\theta)S^{*}_{-1}(\theta)\ ,\\
\int_0^\pi d\theta\sin\theta f_{even}(\theta)S_{+1}(\theta)S^{*}_{+1}(\theta) &= \int_0^\pi d\theta\sin\theta f_{even}(\theta)S_{-1}(\theta)S^{*}_{-1}(\theta)\ ,\\
\int_0^\pi d\theta\sin\theta f_{odd}(\theta)S_{-1}(\theta)S^{*}_{+1}(\theta) &= -\int_0^\pi d\theta\sin\theta f_{odd}(\theta)S_{+1}(\theta)S^{*}_{-1}(\theta)\ ,\\
\int_0^\pi d\theta\sin\theta f_{even}(\theta)S_{-1}(\theta)S^{*}_{+1}(\theta) &= \int_0^\pi d\theta\sin\theta f_{even}(\theta)S_{+1}(\theta)S^{*}_{-1}(\theta)\ ,
\end{aligned} \tag{D.0.13}$$

where

$$f_{odd}(\pi-\theta) = -f_{odd}(\theta)\ ,\qquad f_{even}(\pi-\theta) = f_{even}(\theta)\ .$$

With all of these expressions at hand, and making use of the integration properties of the spin weighted AdS spheroidal harmonics given in (D.0.13), Eq. (D.0.4) becomes

$$T^{r}{}_{\varphi,\,II} = -\frac{i\sin\theta\sqrt{\Delta_\theta}(r^2+a^2)}{2\Xi\rho^4}(\mathcal{C}_1 S_{+1}S^{*}_{-1} + \mathcal{C}_2 S_{-1}S^{*}_{-1}) + c.c\ , \tag{D.0.14}$$

where terms that vanish under the angular integration, due to the properties listed above, have been discarded. The expressions for $\mathcal{C}_1$ and $\mathcal{C}_2$ are messy in general, but they can be simplified asymptotically. The asymptotic expression for $\mathcal{C}_1$ goes as

$$\mathcal{C}_1 \sim c_0 + \mathcal{O}(1/r) \ , \tag{D.0.15}$$

where c_0 is proportional to $T^r{}_{t,\,I}$ asymptotically, so that finally $\mathcal{C}_1 \sim \mathcal{O}(1/r)$. Similar analysis can be done for $\mathcal{C}_2$ as well. The asymptotic expression for $\mathcal{C}_2$ is

$$\mathcal{C}_2 \sim \hat{c}_0 + \mathcal{O}(1/r) \ , \tag{D.0.16}$$

and, as in the former case, $\hat{c}_0$ vanishes after the vanishing energy flux boundary conditions in Eq. (8.3.9) are imposed. Then from Eq. (D.0.14), together with Eqs (D.0.15) and (D.0.16), we conclude that

$$r^2 T^r{}_{\varphi,\,II} \sim \mathcal{O}(1/r) \ , \tag{D.0.17}$$

asymptotically, which leads to the vanishing of the angular momentum flux of Eq. (D.0.2).

Appendix E

List of publications

This thesis is based on the following published papers by the author:

1. *Hawking radiation for a Proca field in D-dimensions*,
   Carlos Herdeiro, Marco O. P. Sampaio, Mengjie Wang,
   Phys. Rev. D **85** (2012) 2, 024005 (`arXiv:1110.2485`).

2. *Hawking radiation for a Proca field in D dimensions. II. charged field in a brane charged black hole*,
   Mengjie Wang, Marco O. P. Sampaio, Carlos Herdeiro,
   Phys. Rev. D **87** (2013) 4, 044011 (`arXiv:1212.2197`).

3. *Superradiant instabilities in a D-dimensional small Reissner-Nordström-anti-de Sitter black hole*,
   Mengjie Wang, Carlos Herdeiro,
   Phys. Rev. D **89** (2014) 8, 084062 (`arXiv:1403.5160`).

4. *Marginal scalar and Proca clouds around Reissner-Nordström black holes*,
   Marco O. P. Sampaio, Carlos Herdeiro, Mengjie Wang,
   Phys. Rev. D **90** (2014) 6, 064004 (`arXiv:1406.3536`).

5. *Maxwell perturbations on asymptotically anti-de Sitter spacetimes: generic boundary conditions and a new branch of quasinormal modes*,

Mengjie Wang, Carlos Herdeiro, Marco O. P. Sampaio,
Phys. Rev. D **92** (2015) 12, 124006 (`arXiv:1510.04713`).

6. *Maxwell perturbations on Kerr-anti-de Sitter: quasinormal modes, superradiant instabilities and vector clouds*,
Mengjie Wang, Carlos Herdeiro,
Accepted for publication in Phys. Rev. D (2016) (`arXiv:1512.02262`).

Bibliography

[1] A. Einstein, "The Foundation of the General Theory of Relativity," *Annalen Phys.* **49** (1916) 769–822. [Annalen Phys.14,517(2005)]. (Cited on page 25.)

[2] C. M. Will, "The Confrontation between General Relativity and Experiment," *Living Rev. Rel.* **17** (2014) 4, `arXiv:1403.7377 [gr-qc]`. (Cited on page 25.)

[3] **Virgo, LIGO Scientific** Collaboration, B. P. Abbott *et al.*, "Observation of Gravitational Waves from a Binary Black Hole Merger," *Phys. Rev. Lett.* **116** (2016) 061102, `arXiv:1602.03837 [gr-qc]`. (Cited on page 25.)

[4] J. Michell, "On the Means of Discovering the Distance, Magnitude, &c. of the Fixed Stars, in Consequence of the Diminution of the Velocity of Their Light, in Case Such a Diminution Should be Found to Take Place in any of Them, and Such Other Data Should be Procured from Observations, as Would be Farther Necessary for That Purpose.," *Phil. Trans. Roy. Soc. Lond.* **74** (1784) 35–57. (Cited on page 25.)

[5] W. Israel, "Dark stars: the evolution of an idea," in *Three Hundred Years of Gravitation*, S. W. Hawking and W. Israel, eds., pp. 199–276. Cambridge University Press, Cambridge; New York, 1987. (Cited on page 25.)

[6] J. R. Oppenheimer and G. M. Volkoff, "On massive neutron cores," *Phys. Rev.* **55** (1939) 374–381. (Cited on page 25.)

[7] J. A. Wheeler and K. Ford, *Geons, black holes, and quantum foam: A life in physics.* 1998. (Cited on page 25.)

[8] C. W. Misner, K. S. Thorne, and J. A. Wheeler, *Gravitation.* W. H. Freeman, San Francisco, 1973. (Cited on page 26.)

[9] P. Bizon, "Colored black holes," *Phys. Rev. Lett.* **64** (1990) 2844–2847. (Cited on page 26.)

[10] H. P. Kuenzle and A. K. M. Masood-ul Alam, "Spherically symmetric static SU(2) Einstein Yang-Mills fields," *J. Math. Phys.* **31** (1990) 928–935. (Cited on page 26.)

[11] M. S. Volkov and D. V. Galtsov, "Non-Abelian Einstein-Yang-Mills black holes," *JETP Lett.* **50** (1989) 346–350. [Pisma Zh. Eksp. Teor. Fiz.50,312(1989)]. (Cited on page 26.)

[12] M. S. Volkov and D. V. Galtsov, "Black holes in Einstein-Yang-Mills theory," *Soviet Journal of Nuclear Physics* **51** (1990) 747–753. (Cited on page 26.)

[13] T. P. Sotiriou and S.-Y. Zhou, "Black hole hair in generalized scalar-tensor gravity," *Phys. Rev. Lett.* **112** (2014) 251102, `arXiv:1312.3622 [gr-qc]`. (Cited on page 26.)

[14] T. P. Sotiriou and S.-Y. Zhou, "Black hole hair in generalized scalar-tensor gravity: An explicit example," *Phys. Rev.* **D90** (2014) 124063, `arXiv:1408.1698 [gr-qc]`. (Cited on page 26.)

[15] E. Babichev and C. Charmousis, "Dressing a black hole with a time-dependent Galileon," *JHEP* **08** (2014) 106, `arXiv:1312.3204 [gr-qc]`. (Cited on page 26.)

[16] C. A. R. Herdeiro and E. Radu, "Kerr black holes with scalar hair," *Phys.Rev.Lett.* **112** (2014) 221101, `arXiv:1403.2757 [gr-qc]`. (Cited on pages 26, 31, 85, 86, 107, 108, 128, 129, 150, 155, and 156.)

[17] R. Brito, V. Cardoso, and P. Pani, "Superradiance," *Lect. Notes Phys.* **906** (2015) pp.1–237, `arXiv:1501.06570 [gr-qc]`. (Cited on pages 26, 30, 111, and 131.)

[18] C. A. R. Herdeiro and E. Radu, "A new spin on black hole hair," *Int. J. Mod. Phys.* **D23** (2014) 1442014, `arXiv:1405.3696 [gr-qc]`. (Cited on pages 26, 31, 86, 107, 129, 150, and 156.)

[19] S. W. Hawking, "Black hole explosions," *Nature* **248** (1974) 30–31. (Cited on pages 26 and 27.)

[20] G. Nordstrom, "On the possibility of unifying the electromagnetic and the gravitational fields," *Phys. Z.* **15** (1914) 504–506, `arXiv:physics/0702221 [physics.gen-ph]`. (Cited on page 26.)

[21] T. Kaluza, "On the problem of unity in physics," *Sitzungsber. Preuss. Akad. Wiss. Berlin (Math. Phys.)* **1921** (1921) 966–972. (Cited on page 26.)

[22] O. Klein, "Quantum theory and five–dimensional theory of relativity. (In German and English)," *Z. Phys.* **37** (1926) 895–906. [Surveys High Energ. Phys.5,241(1986)]. (Cited on page 26.)

[23] I. Antoniadis, "A possible new dimension at a few TeV," *Phys. Lett.* **B246** (1990) 377–384. (Cited on page 26.)

[24] N. Arkani-Hamed, S. Dimopoulos, and G. R. Dvali, "The hierarchy problem and new dimensions at a millimeter," *Phys. Lett.* **B429** (1998) 263–272, `hep-ph/9803315`. (Cited on page 26.)

[25] I. Antoniadis, N. Arkani-Hamed, S. Dimopoulos, and G. R. Dvali, "New dimensions at a millimeter to a Fermi and superstrings at a TeV," *Phys. Lett.* **B436** (1998) 257–263, `hep-ph/9804398`. (Cited on page 26.)

[26] N. Arkani-Hamed, S. Dimopoulos, and G. R. Dvali, "Phenomenology, astrophysics and cosmology of theories with sub–millimeter dimensions and TeV scale quantum gravity," *Phys. Rev.* **D59** (1999) 086004, `hep-ph/9807344`. (Cited on page 26.)

[27] **CMS** Collaboration, "Search for Black Holes with Early Run 2 Data,". (Cited on page 26.)

[28] **ATLAS** Collaboration, G. Aad *et al.*, "Search for strong gravity in multijet final states produced in pp collisions at $\sqrt{s} = 13$ TeV using the ATLAS detector at the LHC," `arXiv:1512.02586 [hep-ex]`. (Cited on pages 26 and 83.)

[29] J. M. Maldacena, "The Large N limit of superconformal field theories and supergravity," *Int. J. Theor. Phys.* **38** (1999) 1113–1133, `arXiv:hep-th/9711200 [hep-th]`. [Adv. Theor. Math. Phys.2,231(1998)]. (Cited on page 27.)

[30] P. Bizon and A. Rostworowski, "On weakly turbulent instability of anti-de Sitter space," *Phys. Rev. Lett.* **107** (2011) 031102, `arXiv:1104.3702 [gr-qc]`. (Cited on page 27.)

[31] V. Cardoso, O. J. C. Dias, G. S. Hartnett, L. Lehner, and J. E. Santos, "Holographic thermalization, quasinormal modes and superradiance in Kerr–AdS," *JHEP* **04** (2014)

183, arXiv:1312.5323 [hep-th]. (Cited on pages 27, 30, 31, 127, 128, 132, 155, and 159.)

[32] N. Uchikata, S. Yoshida, and T. Futamase, "Scalar perturbations of Kerr-AdS black holes," *Phys. Rev.* **D80** (2009) 084020. (Cited on pages 27, 31, 127, 128, 130, and 155.)

[33] M. Wang and C. Herdeiro, "Maxwell perturbations on Kerr–anti–de Sitter: quasinormal modes, superradiant instabilities and vector clouds," arXiv:1512.02262 [gr-qc]. (Cited on page 27.)

[34] S. W. Hawking, "Particle creation by black holes," *Commun. Math. Phys.* **43** (1975) 199–220. (Cited on pages 27 and 30.)

[35] J. B. Hartle and S. W. Hawking, "Path integral derivation of black hole radiance," *Phys. Rev.* **D13** (1976) 2188–2203. (Cited on page 27.)

[36] T. Damour and R. Ruffini, "Black hole evaporation in the Klein–Sauter–Heisenberg–Euler formalism," *Phys. Rev.* **D14** (1976) 332–334. (Cited on page 27.)

[37] M. K. Parikh and F. Wilczek, "Hawking radiation as tunneling," *Phys. Rev. Lett.* **85** (2000) 5042–5045, arXiv:hep-th/9907001 [hep-th]. (Cited on page 27.)

[38] S. P. Robinson and F. Wilczek, "Relationship between Hawking radiation and gravitational anomalies," *Phys. Rev. Lett.* **95** (2005) 011303, arXiv:gr-qc/0502074 [gr-qc]. (Cited on page 27.)

[39] S. B. Giddings, "Hawking radiation, the Stefan–Boltzmann law, and unitarization," *Phys. Lett.* **B754** (2016) 39–42, arXiv:1511.08221 [hep-th]. (Cited on page 27.)

[40] G. 't Hooft, "Graviton Dominance in Ultrahigh–Energy Scattering," *Phys.Lett.* **B198** (1987) 61–63. (Cited on page 28.)

[41] T. Banks and W. Fischler, "A model for high energy scattering in quantum gravity," arXiv:hep-th/9906038. (Cited on page 28.)

[42] S. Dimopoulos and G. L. Landsberg, "Black holes at the LHC," *Phys. Rev. Lett.* **87** (2001) 161602, hep-ph/0106295. (Cited on page 28.)

[43] P. Kanti and E. Winstanley, "Hawking Radiation from Higher–Dimensional Black Holes," *Fundam. Theor. Phys.* **178** (2015) 229–265, arXiv:1402.3952 [hep-th]. (Cited on page 28.)

[44] S. B. Giddings and S. D. Thomas, "High energy colliders as black hole factories: The end of short distance physics," *Phys. Rev.* **D65** (2002) 056010, hep-ph/0106219. (Cited on page 28.)

[45] J. A. Frost *et al.*, "Phenomenology of Production and Decay of Spinning Extra–Dimensional Black Holes at Hadron Colliders," *JHEP* **10** (2009) 014, arXiv:0904.0979 [hep-ph]. (Cited on pages 28, 69, and 83.)

[46] M. O. P. Sampaio, *Production and evaporation of higher dimensional black holes.* PhD thesis, University of Cambridge, 2010. (Cited on pages 28, 64, and 92.)

[47] D.-C. Dai *et al.*, "BlackMax: A black–hole event generator with rotation, recoil, split branes and brane tension," *Phys. Rev.* **D77** (2008) 076007, arXiv:0711.3012 [hep-ph]. (Cited on pages 28 and 83.)

[48] R. H. Dicke, "Coherence in Spontaneous Radiation Processes," *Phys. Rev.* **93** (1954) 99–110. (Cited on page 29.)

[49] Y. Zeldovich, "Generation of Waves by a Rotating Body," *Pisma Zh.Eksp.Teor.Fiz.* **14** (1971) 270. (Cited on page 29.)

[50] Y. Zeldovich, "Amplification of cylindrical electromagnetic waves reflected by a rotating body," *Zh.Eksp.Teor.Fiz.* **62** (1972) 2076. (Cited on page 29.)

[51] R. Penrose, "Gravitational collapse: The role of general relativity," *Riv.Nuovo Cim.* **1** (1969) 252–276. (Cited on page 29.)

[52] S. A. Teukolsky and W. H. Press, "Perturbations of a rotating black hole. III – Interaction of the hole with gravitational and electromagnetic radiation," *Astrophys. J.* **193** (1974) 443–461. (Cited on page 29.)

[53] J. D. Bekenstein, "Extraction of energy and charge from a black hole," *Phys. Rev.* **D7** (1973) 949–953. (Cited on pages 29 and 86.)

[54] S. W. Hawking, "Gravitational radiation from colliding black holes," *Phys. Rev. Lett.* **26** (1971) 1344–1346. (Cited on page 29.)

[55] W. Unruh, "Separability of the Neutrino Equations in a Kerr Background," *Phys. Rev. Lett.* **31** (1973) 1265–1267. (Cited on page 29.)

[56] B. R. Iyer and A. Kumar, "Note on the Absence of Massive Fermion Superradiance from a Kerr Black Hole," *Phys. Rev.* **D18** (1978) 4799–4801. (Cited on page 29.)

[57] M. Martellini and A. Treves, "Absence of Superradiance of a Dirac Field in a Kerr Background," *Phys. Rev.* **D15** (1977) 3060–3061. (Cited on page 29.)

[58] C. H. Lee, "Massive Spin 1/2 Wave Around a Kerr-Newman Black Hole," *Phys. Lett.* **B68** (1977) 152–156. (Cited on page 29.)

[59] W. H. Press and S. A. Teukolsky, "Floating Orbits, Superradiant Scattering and the Black–hole Bomb," *Nature* **238** (1972) 211–212. (Cited on page 30.)

[60] T. Damour, N. Deruelle, and R. Ruffini, "On quantum resonances in stationary geometries," *Lett.Nuovo Cim.* **15** (1976) 257–262. (Cited on page 30.)

[61] S. L. Detweiler, "Klein-Gordon equation and rotating black holes," *Phys.Rev.* **D22** (1980) 2323–2326. (Cited on page 30.)

[62] T. Zouros and D. Eardley, "Instabilities of massive scalar perturbations of a rotating black hole," *Annals Phys.* **118** (1979) 139–155. (Cited on page 30.)

[63] S. R. Dolan, "Instability of the massive Klein–Gordon field on the Kerr spacetime," *Phys.Rev.* **D76** (2007) 084001, `arXiv:0705.2880 [gr-qc]`. (Cited on page 30.)

[64] J. Rosa, "The Extremal black hole bomb," *JHEP* **1006** (2010) 015, `arXiv:0912.1780 [hep-th]`. (Cited on pages 30, 112, and 121.)

[65] S. Hod and O. Hod, "Analytic treatment of the black–hole bomb," *Phys.Rev.* **D81** (2010) 061502, `arXiv:0910.0734 [gr-qc]`. (Cited on page 30.)

[66] H. Witek, V. Cardoso, A. Ishibashi, and U. Sperhake, "Superradiant instabilities in astrophysical systems," *Phys.Rev.* **D87** (2013) 043513, `arXiv:1212.0551 [gr-qc]`. (Cited on page 30.)

[67] J. G. Rosa, "Boosted black string bombs," *JHEP* **1302** (2013) 014, arXiv:1209.4211 [hep-th]. (Cited on page 30.)

[68] P. Pani, V. Cardoso, L. Gualtieri, E. Berti, and A. Ishibashi, "Black hole bombs and photon mass bounds," *Phys.Rev.Lett.* **109** (2012) 131102, arXiv:1209.0465 [gr-qc]. (Cited on pages 30 and 85.)

[69] S. Hod, "On the instability regime of the rotating Kerr spacetime to massive scalar perturbations," *Phys.Lett.* **B708** (2012) 320–323, arXiv:1205.1872 [gr-qc]. (Cited on page 30.)

[70] V. Cardoso and O. J. C. Dias, "Small Kerr–anti–de Sitter black holes are unstable," *Phys.Rev.* **D70** (2004) 084011, arXiv:hep-th/0405006 [hep-th]. (Cited on page 30.)

[71] V. Cardoso, O. J. C. Dias, and S. Yoshida, "Classical instability of Kerr–AdS black holes and the issue of final state," *Phys.Rev.* **D74** (2006) 044008, arXiv:hep-th/0607162 [hep-th]. (Cited on page 30.)

[72] A. N. Aliev and O. Delice, "Superradiant Instability of Five–Dimensional Rotating Charged AdS Black Holes," *Phys.Rev.* **D79** (2009) 024013, arXiv:0808.0280 [hep-th]. (Cited on pages 30, 111, and 125.)

[73] O. J. C. Dias, G. T. Horowitz, and J. E. Santos, "Black holes with only one Killing field," *JHEP* **1107** (2011) 115, arXiv:1105.4167 [hep-th]. (Cited on pages 30 and 128.)

[74] R. Li, "Superradiant instability of charged massive scalar field in Kerr–Newman–anti–de Sitter black hole," *Phys.Lett.* **B714** (2012) 337–341, arXiv:1205.3929 [gr-qc]. (Cited on page 30.)

[75] N. Uchikata and S. Yoshida, "Quasinormal modes of a massless charged scalar field on a small Reissner–Nordstrom–anti–de Sitter black hole," *Phys.Rev.* **D83** (2011) 064020, arXiv:1109.6737 [gr-qc]. (Cited on pages 30 and 114.)

[76] V. Cardoso, L. Gualtieri, C. Herdeiro, U. Sperhake, P. M. Chesler, *et al.*, "NR/HEP: roadmap for the future," *Class.Quant.Grav.* **29** (2012) 244001, arXiv:1201.5118 [hep-th]. (Cited on page 30.)

[77] H. Yoshino and H. Kodama, "Bosenova collapse of axion cloud around a rotating black hole," *Prog.Theor.Phys.* **128** (2012) 153–190, arXiv:1203.5070 [gr-qc]. (Cited on page 30.)

[78] H. Yoshino and H. Kodama, "Gravitational radiation from an axion cloud around a black hole: Superradiant phase," *PTEP* **2014** (2014) 043E02, arXiv:1312.2326 [gr-qc]. (Cited on page 30.)

[79] W. E. East, F. M. Ramazanolu, and F. Pretorius, "Black Hole Superradiance in Dynamical Spacetime," *Phys. Rev.* **D89** (2014) 061503, arXiv:1312.4529 [gr-qc]. (Cited on page 30.)

[80] H. Okawa, H. Witek, and V. Cardoso, "Black holes and fundamental fields in Numerical Relativity: initial data construction and evolution of bound states," *Phys. Rev.* **D89** (2014) 104032, arXiv:1401.1548 [gr-qc]. (Cited on page 30.)

[81] S. R. Dolan, S. Ponglertsakul, and E. Winstanley, "Stability of black holes in Einstein–charged scalar field theory in a cavity," *Phys. Rev.* **D92** (2015) 124047, arXiv:1507.02156 [gr-qc]. (Cited on pages 30, 31, and 129.)

[82] N. Sanchis-Gual, J. C. Degollado, P. J. Montero, J. A. Font, and C. Herdeiro, "Explosion and final state of the charged black hole bomb," arXiv:1512.05358 [gr-qc]. (Cited on page 30.)

[83] P. Bosch, S. R. Green, and L. Lehner, "Nonlinear evolution and final fate of (charged) superradiant instability," arXiv:1601.01384 [gr-qc]. (Cited on pages 30 and 126.)

[84] S. Hod, "No–bomb theorem for charged Reissner–Nordström black holes," *Phys.Lett.* **B718** (2013) 1489–1492, arXiv:1304.6474 [gr-qc]. (Cited on pages 30, 86, and 107.)

[85] S. Hod, "Stability of the extremal Reissner–Nordström black hole to charged scalar perturbations," *Phys.Lett.* **B713** (2012) 505–508. (Cited on pages 30, 86, and 107.)

[86] S. Hod, "Stability of highly–charged Reissner–Nordström black holes to charged scalar perturbations," *Phys. Rev.* **D91** (2015) 044047, arXiv:1504.00009 [gr-qc]. (Cited on page 30.)

[87] M. O. P. Sampaio, C. Herdeiro, and M. Wang, "Marginal scalar and Proca clouds around Reissner–Nordström black holes," *Phys. Rev.* **D90** (2014) 064004, arXiv:1406.3536 [gr-qc]. (Cited on pages 30, 31, 49, and 105.)

[88] O. J. C. Dias, P. Figueras, S. Minwalla, P. Mitra, R. Monteiro, *et al.*, "Hairy black holes and solitons in global AdS_5," *JHEP* **1208** (2012) 117, arXiv:1112.4447 [hep-th]. (Cited on pages 30 and 111.)

[89] M. Wang and C. Herdeiro, "Superradiant instabilities in a D-dimensional small Reissner-Nordström-anti-de Sitter black hole," *Phys.Rev.* **D89** (2014) 084062, arXiv:1403.5160 [gr-qc]. (Cited on page 30.)

[90] J. C. Degollado, C. A. Herdeiro, and H. F. Rúnarsson, "Rapid growth of superradiant instabilities for charged black holes in a cavity," *Phys.Rev.* **D88** (2013) 063003, arXiv:1305.5513 [gr-qc]. (Cited on pages 30, 125, and 129.)

[91] S. Hod, "Analytic treatment of the charged black–hole–mirror bomb in the highly explosive regime," *Phys. Rev.* **D88** (2013) 064055, arXiv:1310.6101 [gr-qc]. (Cited on pages 30, 125, and 129.)

[92] J. C. Degollado and C. A. R. Herdeiro, "Time evolution of superradiant instabilities for charged black holes in a cavity," *Phys.Rev.* **D89** (2014) 063005, arXiv:1312.4579 [gr-qc]. (Cited on pages 30, 125, and 129.)

[93] J. C. Degollado and C. A. R. Herdeiro, "Stationary scalar configurations around extremal charged black holes," *Gen.Rel.Grav.* **45** (2013) 2483–2492, arXiv:1303.2392 [gr-qc]. (Cited on pages 31, 86, 87, 92, 103, 105, and 108.)

[94] S. Hod, "Stationary scalar clouds around rotating black holes," *Phys.Rev.* **D86** (2012) 104026, arXiv:1211.3202 [gr-qc]. (Cited on pages 31, 85, 107, 128, and 155.)

[95] C. L. Benone, L. C. B. Crispino, C. Herdeiro, and E. Radu, "Kerr–Newman scalar clouds," *Phys. Rev.* **D90** (2014) 104024, arXiv:1409.1593 [gr-qc]. (Cited on pages 31 and 128.)

[96] C. Herdeiro, E. Radu, and H. Runarsson, "Non–linear Q–clouds around Kerr black holes," *Phys. Lett.* **B739** (2014) 302–307, arXiv:1409.2877 [gr-qc]. (Cited on pages 31 and 128.)

[97] C. A. R. Herdeiro, E. Radu, and H. Rúnarsson, "Kerr black holes with self-interacting scalar hair: hairier but not heavier," *Phys. Rev.* **D92** (2015) no. 8, 084059, arXiv:1509.02923 [gr-qc]. (Cited on page 31.)

[98] C. Herdeiro and E. Radu, "Construction and physical properties of Kerr black holes with scalar hair," *Class. Quant. Grav.* **32** (2015) 144001, arXiv:1501.04319 [gr-qc]. (Cited on pages 31 and 128.)

[99] H. Kodama, A. Ishibashi, and O. Seto, "Brane world cosmology: Gauge–invariant formalism for perturbation," *Phys. Rev.* **D62** (2000) 064022, arXiv:hep-th/0004160. (Cited on pages 33, 34, and 50.)

[100] H. Kodama and A. Ishibashi, "A Master equation for gravitational perturbations of maximally symmetric black holes in higher dimensions," *Prog. Theor. Phys.* **110** (2003) 701–722, arXiv:hep-th/0305147 [hep-th]. (Cited on page 33.)

[101] A. Ishibashi and H. Kodama, "Stability of higher dimensional Schwarzschild black holes," *Prog. Theor. Phys.* **110** (2003) 901–919, arXiv:hep-th/0305185 [hep-th]. (Cited on page 33.)

[102] H. Kodama and A. Ishibashi, "Master equations for perturbations of generalized static black holes with charge in higher dimensions," *Prog. Theor. Phys.* **111** (2004) 29–73, arXiv:hep-th/0308128 [hep-th]. (Cited on page 33.)

[103] H. Kodama, "Perturbations and Stability of Higher-Dimensional Black Holes," *Lect. Notes Phys.* **769** (2009) 427–470, arXiv:0712.2703 [hep-th]. (Cited on pages 33 and 35.)

[104] A. Ishibashi and H. Kodama, "Perturbations and Stability of Static Black Holes in Higher Dimensions," *Prog. Theor. Phys. Suppl.* **189** (2011) 165–209, arXiv:1103.6148 [hep-th]. (Cited on pages 33, 35, 36, and 63.)

[105] T. Regge and J. A. Wheeler, "Stability of a Schwarzschild singularity," *Phys. Rev.* **108** (1957) 1063–1069. (Cited on pages 33 and 127.)

[106] F. J. Zerilli, "Effective potential for even parity Regge-Wheeler gravitational perturbation equations," *Phys. Rev. Lett.* **24** (1970) 737–738. (Cited on page 33.)

[107] E. Newman and R. Penrose, "An Approach to gravitational radiation by a method of spin coefficients," *J. Math. Phys.* **3** (1962) 566–578. (Cited on page 36.)

[108] H. Stephani, D. Kramer, M. A. H. MacCallum, C. Hoenselaers, and E. Herlt, *Exact solutions of Einstein's field equations*. Cambridge University Press, 2004. (Cited on page 36.)

[109] S. Chandrasekhar, *The mathematical theory of black holes*. Oxford, UK: Clarendon (1992) 646 p. (Cited on pages 36, 37, 42, and 45.)

[110] V. P. Frolov and I. D. Novikov, *Black hole physics: Basic concepts and new developments*. Dordrecht, Netherlands: Kluwer Academic (1998) 770 p. (Cited on pages 36 and 37.)

[111] T. W. Baumgarte and S. L. Shapiro, *Numerical relativity: solving Einstein's equations on the computer*. Cambridge University Press, 2010. (Cited on page 36.)

[112] S. A. Teukolsky, "Rotating black holes–separable wave equations for gravitational and electromagnetic perturbations," *Phys.Rev.Lett.* **29** (1972) 1114–1118. (Cited on page 36.)

[113] U. Khanal, "Rotating black hole in asymptotic de Sitter space: Perturbation of the space-time with spin fields," *Phys.Rev.* **D28** (1983) 1291–1297. (Cited on pages 36 and 40.)

[114] S.-Q. Wu and M.-L. Yan, "Entropy of Kerr-de Sitter black hole due to arbitrary spin fields," *Phys.Rev.* **D69** (2004) 044019, `arXiv:gr-qc/0303076 [gr-qc]`. (Cited on page 36.)

[115] S. Yoshida, N. Uchikata, and T. Futamase, "Quasinormal modes of Kerr–de Sitter black holes," *Phys. Rev.* **D81** (2010) 044005. (Cited on page 36.)

[116] O. J. C. Dias, J. E. Santos, and M. Stein, "Kerr-AdS and its Near-horizon Geometry: Perturbations and the Kerr/CFT Correspondence," *JHEP* **1210** (2012) 182, arXiv:1208.3322 [hep-th]. (Cited on page 36.)

[117] B. Carter, "Hamilton-Jacobi and Schrodinger separable solutions of Einstein's equations," *Commun. Math. Phys.* **10** (1968) 280. (Cited on page 38.)

[118] O. J. C. Dias and J. E. Santos, "Boundary Conditions for Kerr–AdS Perturbations," *JHEP* **10** (2013) 156, arXiv:1302.1580 [hep-th]. (Cited on pages 39 and 128.)

[119] G. W. Gibbons, M. J. Perry, and C. N. Pope, "The First law of thermodynamics for Kerr-anti-de Sitter black holes," *Class. Quant. Grav.* **22** (2005) 1503–1526, arXiv:hep-th/0408217 [hep-th]. (Cited on pages 39 and 152.)

[120] M. Henneaux and C. Teitelboim, "Asymptotically anti-de Sitter Spaces," *Commun. Math. Phys.* **98** (1985) 391–424. (Cited on page 39.)

[121] E. Winstanley, "On classical superradiance in Kerr-Newman-anti-de Sitter black holes," *Phys. Rev.* **D64** (2001) 104010, arXiv:gr-qc/0106032 [gr-qc]. (Cited on page 39.)

[122] J. Goldberg, A. Macfarlane, E. T. Newman, F. Rohrlich, and E. Sudarshan, "Spin-s spherical harmonics and ð," *Journal of Mathematical Physics* **8** (1967) 2155–2161. (Cited on page 43.)

[123] B. Carter, "Global structure of the Kerr family of gravitational fields," *Phys.Rev.* **174** (1968) 1559–1571. (Cited on page 49.)

[124] **CMS** Collaboration, S. Chatrchyan *et al.*, "Observation of a new boson at a mass of 125 GeV with the CMS experiment at the LHC," *Phys. Lett.* **B716** (2012) 30–61, arXiv:1207.7235 [hep-ex]. (Cited on page 49.)

[125] **ATLAS** Collaboration, G. Aad *et al.*, "Observation of a new particle in the search for the Standard Model Higgs boson with the ATLAS detector at the LHC," *Phys. Lett.* **B716** (2012) 1–29, arXiv:1207.7214 [hep-ex]. (Cited on page 49.)

[126] A. Pawl, "The Timescale for loss of massive vector hair by a black hole and its consequences for proton decay," *Phys. Rev.* **D70** (2004) 124005, arXiv:hep-th/0411175 [hep-th]. (Cited on page 49.)

[127] R. Konoplya, "Massive vector field perturbations in the Schwarzschild background: Stability and unusual quasinormal spectrum," *Phys.Rev.* **D73** (2006) 024009, arXiv:gr-qc/0509026 [gr-qc]. (Cited on pages 49 and 53.)

[128] C. Herdeiro, M. O. P. Sampaio, and M. Wang, "Hawking radiation for a Proca field in D–dimensions," *Phys. Rev.* **D85** (2012) 024005, arXiv:1110.2485 [gr-qc]. (Cited on pages 49 and 55.)

[129] M. Wang, M. O. P. Sampaio, and C. Herdeiro, "Hawking radiation for a Proca field in D dimensions II: charged field in a brane charged black hole," *Phys.Rev.* **D87** (2013) 044011, arXiv:1212.2197 [gr-qc]. (Cited on pages 49 and 55.)

[130] J. G. Rosa and S. R. Dolan, "Massive vector fields on the Schwarzschild spacetime: quasi-normal modes and bound states," *Phys.Rev.* **D85** (2012) 044043, arXiv:1110.4494 [hep-th]. (Cited on pages 50, 85, 96, and 98.)

[131] P. Pani, V. Cardoso, L. Gualtieri, E. Berti, and A. Ishibashi, "Black-Hole Bombs and Photon-Mass Bounds," *Phys. Rev. Lett.* **109** (2012) 131102, arXiv:1209.0465 [gr-qc]. (Cited on pages 50, 72, 82, and 158.)

[132] P. Pani, V. Cardoso, L. Gualtieri, E. Berti, and A. Ishibashi, "Perturbations of slowly rotating black holes: massive vector fields in the Kerr metric," *Phys.Rev.* **D86** (2012) 104017, arXiv:1209.0773 [gr-qc]. (Cited on pages 50, 72, 82, and 158.)

[133] M. Zilhão, H. Witek, and V. Cardoso, "Nonlinear interactions between black holes and Proca fields," *Class. Quant. Grav.* **32** (2015) 234003, arXiv:1505.00797 [gr-qc]. (Cited on page 50.)

[134] D. N. Page, "Particle Emission Rates from a Black Hole: Massless Particles from an Uncharged, Nonrotating Hole," *Phys.Rev.* **D13** (1976) 198–206. (Cited on page 53.)

[135] D. Ida, K.-y. Oda, and S. C. Park, "Rotating black holes at future colliders: Greybody factors for brane fields," *Phys. Rev.* **D67** (2003) 064025, arXiv:hep-th/0212108. (Cited on page 55.)

[136] C. M. Harris and P. Kanti, "Hawking radiation from a (4+n)–dimensional black hole: Exact results for the Schwarzschild phase," *JHEP* **10** (2003) 014, hep-ph/0309054. (Cited on pages 55 and 81.)

[137] C. M. Harris and P. Kanti, "Hawking radiation from a (4+n)–dimensional rotating black hole," *Phys. Lett.* **B633** (2006) 106–110, arXiv:hep-th/0503010. (Cited on page 55.)

[138] D. Ida, K.-y. Oda, and S. C. Park, "Rotating black holes at future colliders. II: Anisotropic scalar field emission," *Phys. Rev.* **D71** (2005) 124039, arXiv:hep-th/0503052. (Cited on page 55.)

[139] G. Duffy, C. Harris, P. Kanti, and E. Winstanley, "Brane decay of a (4+n)–dimensional rotating black hole: Spin-0 particles," *JHEP* **09** (2005) 049, arXiv:hep-th/0507274. (Cited on page 55.)

[140] M. Casals, P. Kanti, and E. Winstanley, "Brane decay of a (4+n)–dimensional rotating black hole. II: Spin-1 particles," *JHEP* **02** (2006) 051, arXiv:hep-th/0511163. (Cited on page 55.)

[141] V. Cardoso, M. Cavaglia, and L. Gualtieri, "Black hole particle emission in higher–dimensional spacetimes," *Phys. Rev. Lett.* **96** (2006) 071301, arXiv:hep-th/0512002. (Cited on page 55.)

[142] V. Cardoso, M. Cavaglia, and L. Gualtieri, "Hawking emission of gravitons in higher dimensions: Non– rotating black holes," *JHEP* **02** (2006) 021, arXiv:hep-th/0512116. (Cited on page 55.)

[143] D. Ida, K.-y. Oda, and S. C. Park, "Rotating black holes at future colliders. III: Determination of black hole evolution," *Phys. Rev.* **D73** (2006) 124022, arXiv:hep-th/0602188. (Cited on page 55.)

[144] M. Casals, S. R. Dolan, P. Kanti, and E. Winstanley, "Brane decay of a (4+n)–dimensional rotating black hole. III: Spin-1/2 particles," *JHEP* **03** (2007) 019, arXiv:hep-th/0608193. (Cited on page 55.)

[145] M. Casals, S. R. Dolan, P. Kanti, and E. Winstanley, "Bulk emission of scalars by a rotating black hole," *JHEP* **06** (2008) 071, arXiv:0801.4910 [hep-th]. (Cited on page 55.)

[146] M. O. P. Sampaio, "Charge and mass effects on the evaporation of higher–dimensional rotating black holes," *JHEP* **0910** (2009) 008, arXiv:0907.5107 [hep-th]. (Cited on pages 55, 56, 68, 71, 76, 81, and 92.)

[147] M. O. P. Sampaio, "Distributions of charged massive scalars and fermions from evaporating higher–dimensional black holes," *JHEP* **1002** (2010) 042, arXiv:0911.0688 [hep-th]. (Cited on pages 55, 56, 68, 71, 76, 78, 81, 82, and 92.)

[148] F. R. Tangherlini, "Schwarzschild field in n dimensions and the dimensionality of space problem," *Nuovo Cim.* **27** (1963) 636–651. (Cited on page 55.)

[149] P. Kanti, "Black holes in theories with large extra dimensions: A Review," *Int. J. Mod. Phys.* **A19** (2004) 4899–4951, arXiv:hep-ph/0402168. (Cited on page 61.)

[150] T. Nakamura and H. Sato, "Absorption of massive scalar field by a charged black hole," *Phys. Lett.* **B61** (1976) 371–374. (Cited on page 66.)

[151] D. N. Page, "Particle emission rates from a black hole. 3. charged leptons from a nonrotating hole," *Phys. Rev.* **D16** (1977) 2402–2411. (Cited on page 66.)

[152] D. N. Page, "Particle emission rates from a black hole. 2. massless particles from a rotating hole," *Phys. Rev.* **D14** (1976) 3260–3273. (Cited on page 66.)

[153] R. Emparan, G. T. Horowitz, and R. C. Myers, "Black Holes Radiate Mainly on the Brane," *Phys. Rev. Lett.* **85** (2000) 499, arXiv:0003118 [hep-th]. (Cited on page 81.)

[154] P. Kanti and N. Pappas, "Emission of massive scalar fields by a higher–dimensional rotating black hole," *Phys. Rev.* **D82** (2010) 024039, arXiv:1003.5125 [hep-th]. (Cited on page 81.)

[155] **CMS Collaboration** Collaboration, S. Chatrchyan *et al.*, "Search for narrow resonances and quantum black holes in inclusive and b-tagged dijet mass spectra from pp collisions at $\sqrt{s} = 7$ TeV," arXiv:1210.2387 [hep-ex]. (Cited on page 83.)

[156] **The ATLAS** Collaboration, "Search for strong gravity effects in same–sign dimuon final states," *CERN report ATLAS-CONF-2011-065, April 2011* (2011) . (Cited on page 83.)

[157] **The ATLAS** Collaboration, "Search for Microscopic Black Holes in Multi–Jet Final States with the ATLAS Detector at $\sqrt{s} = 7$ TeV," *CERN report ATLAS-CONF-2011-068, May 2011* (2011) . (Cited on page 83.)

[158] D. M. Gingrich, "Experimental limits on the fundamental Planck scale in large extra dimensions," `arXiv:1210.5923 [hep-ex]`. (Cited on page 83.)

[159] S. Hod, "Stationary resonances of rapidly–rotating Kerr black holes," *Eur. Phys. J.* **C73** (2013) 2378, `arXiv:1311.5298 [gr-qc]`. (Cited on pages 85, 107, 128, and 155.)

[160] C. Herdeiro and E. Radu, "Ergosurfaces for Kerr black holes with scalar hair," *Phys. Rev.* **D89** (2014) 124018, `arXiv:1406.1225 [gr-qc]`. (Cited on pages 86 and 107.)

[161] H. Furuhashi and Y. Nambu, "Instability of massive scalar fields in Kerr–Newman spacetime," *Prog.Theor.Phys.* **112** (2004) 983–995, `arXiv:gr-qc/0402037 [gr-qc]`. (Cited on pages 86, 92, 96, and 107.)

[162] W. H. Press and S. A. Teukolsky, "Perturbations of a rotating black hole. II. Dynamical stability of the Kerr metric," *Astrophys. J.* **185** (1973) 649–674. (Cited on page 89.)

[163] H.-P. Nollert, "TOPICAL REVIEW: Quasinormal modes: the characteristic 'sound' of black holes and neutron stars," *Class.Quant.Grav.* **16** (1999) R159–R216. (Cited on page 89.)

[164] S. Majumdar, "A class of exact solutions of Einstein's field equations," *Phys.Rev.* **72** (1947) 390–398. (Cited on pages 104 and 108.)

[165] A. Papapetrou, "A static solution of the equations of the graviational field for an arbitrary charge–distribution," *Proc. R. Irish Acad.* **A51** (1945) 191. (Cited on pages 104 and 108.)

[166] S. Hod, "Kerr–Newman black holes with stationary charged scalar clouds," *Phys. Rev.* **D90** (2014) 024051, `arXiv:1406.1179 [gr-qc]`. (Cited on pages 107, 108, and 128.)

[167] S. S. Gubser and I. Mitra, "Instability of charged black holes in anti–de Sitter space," `arXiv:hep-th/0009126 [hep-th]`. (Cited on page 112.)

[168] S. S. Gubser and I. Mitra, "The Evolution of unstable black holes in anti–de Sitter space," *JHEP* **0108** (2001) 018, `arXiv:hep-th/0011127 [hep-th]`. (Cited on page 112.)

[169] R. Konoplya and A. Zhidenko, "Stability of higher dimensional Reissner–Nordstrom–anti–de Sitter black holes," *Phys.Rev.* **D78** (2008) 104017, `arXiv:0809.2048 [hep-th]`. (Cited on page 112.)

[170] S. A. Hartnoll, C. P. Herzog, and G. T. Horowitz, "Holographic Superconductors," *JHEP* **0812** (2008) 015, `arXiv:0810.1563 [hep-th]`. (Cited on page 112.)

[171] P. Breitenlohner and D. Z. Freedman, "Positive energy in anti–de Sitter backgrounds and gauged extended supergravity," *Phys.Lett.* **B115** (1982) 197. (Cited on page 112.)

[172] P. Breitenlohner and D. Z. Freedman, "Stability in gauged extended supergravity," *Annals Phys.* **144** (1982) 249. (Cited on page 112.)

[173] G. T. Horowitz, "Introduction to Holographic Superconductors," *Lect.Notes Phys.* **828** (2011) 313–347, `arXiv:1002.1722 [hep-th]`. (Cited on page 114.)

[174] M. Abramowitz and I. A. Stegun, *Handbook of Mathematical Functions with Formulas, Graphs, and Mathematical Tables.* Dover, New York, ninth dover printing, tenth gpo printing ed., 1964. (Cited on pages 117, 118, 121, and 135.)

[175] R. Konoplya, "On quasinormal modes of small Schwarzschild–anti–de Sitter black hole," *Phys.Rev.* **D66** (2002) 044009, `arXiv:hep-th/0205142 [hep-th]`. (Cited on pages 122 and 141.)

[176] A. N. Aliev, "Superradiance and instability of small rotating charged AdS black holes in all dimensions," *Eur. Phys. J.* **C76** (2016) no. 2, 58, `arXiv:1503.08607 [hep-th]`. (Cited on page 124.)

[177] O. Delice and T. Durğut, "Superradiance instability of small rotating AdS black holes in arbitrary dimensions," *Phys. Rev.* **D92** (2015) 024053, `arXiv:1503.05818 [gr-qc]`. (Cited on page 124.)

[178] R. Emparan, R. Suzuki, and K. Tanabe, "The large D limit of General Relativity," *JHEP* **1306** (2013) 009, arXiv:1302.6382 [hep-th]. (Cited on pages 126 and 158.)

[179] V. Cardoso and J. P. S. Lemos, "Quasinormal modes of Schwarzschild anti–de Sitter black holes: Electromagnetic and gravitational perturbations," *Phys. Rev.* **D64** (2001) 084017, arXiv:gr-qc/0105103 [gr-qc]. (Cited on pages 127 and 141.)

[180] V. Cardoso, R. Konoplya, and J. P. S. Lemos, "Quasinormal frequencies of Schwarzschild black holes in anti–de Sitter spacetimes: A complete study on the asymptotic behavior," *Phys. Rev.* **D68** (2003) 044024, arXiv:gr-qc/0305037 [gr-qc]. (Cited on pages 127, 130, 140, and 141.)

[181] Y. Shlapentokh-Rothman, "Exponentially growing finite energy solutions for the Klein–Gordon equation on sub–extremal Kerr spacetimes," *Commun. Math. Phys.* **329** (2014) 859–891, arXiv:1302.3448 [gr-qc]. (Cited on page 128.)

[182] S. Hod, "Rotating black holes can have short bristles," *Phys. Lett.* **B739** (2014) 196–200, arXiv:1411.2609 [gr-qc]. (Cited on page 128.)

[183] S. Hod, "Onset of superradiant instabilities in the composed Kerr–black–hole–mirror bomb," *Phys. Lett.* **B736** (2014) 398–402, arXiv:1412.6108 [gr-qc]. (Cited on page 128.)

[184] C. L. Benone, L. C. B. Crispino, C. Herdeiro, and E. Radu, "Acoustic clouds: standing sound waves around a black hole analogue," *Phys. Rev.* **D91** (2015) 104038, arXiv:1412.7278 [gr-qc]. (Cited on page 128.)

[185] S. Hod, "The large–mass limit of cloudy black holes," *Class. Quant. Grav.* **32** (2015) 134002. (Cited on page 128.)

[186] J. Wilson-Gerow and A. Ritz, "Black hole energy extraction via a stationary scalar analog of the Blandford–Znajek mechanism," *Phys. Rev.* **D93** (2016) 044043, arXiv:1509.06681 [hep-th]. (Cited on page 128.)

[187] S. Hod, "Extremal Kerr–Newman black holes with extremely short charged scalar hair," *Phys. Lett.* **B751** (2015) 177–183. (Cited on page 128.)

[188] O. J. C. Dias, J. E. Santos, and B. Way, "Black holes with a single Killing vector field: black resonators," *JHEP* **12** (2015) 171, arXiv:1505.04793 [hep-th]. (Cited on page 128.)

[189] O. Chodosh and Y. Shlapentokh-Rothman, "Time–Periodic Einstein–Klein–Gordon Bifurcations of Kerr," arXiv:1510.08025 [gr-qc]. (Cited on page 129.)

[190] S. A. Teukolsky, "Perturbations of a rotating black hole. I. Fundamental equations for gravitational, electromagnetic and neutrino field perturbations," *Astrophys. J.* **185** (1973) 635–647. (Cited on page 131.)

[191] E. Berti and K. D. Kokkotas, "Quasinormal modes of Reissner–Nordstrom–anti–de Sitter black holes: Scalar, electromagnetic and gravitational perturbations," *Phys. Rev.* **D67** (2003) 064020, arXiv:gr-qc/0301052 [gr-qc]. (Cited on pages 140 and 141.)

[192] G. T. Horowitz and V. E. Hubeny, "Quasinormal modes of AdS black holes and the approach to thermal equilibrium," *Phys. Rev.* **D62** (2000) 024027, arXiv:hep-th/9909056 [hep-th]. (Cited on page 141.)

[193] E. Berti, V. Cardoso, and P. Pani, "Breit–Wigner resonances and the quasinormal modes of anti–de Sitter black holes," *Phys. Rev.* **D79** (2009) 101501, arXiv:0903.5311 [gr-qc]. (Cited on page 141.)

[194] M. Wang, C. Herdeiro, and M. O. P. Sampaio, "Maxwell perturbations on asymptotically anti–de Sitter spacetimes: Generic boundary conditions and a new branch of quasinormal modes," *Phys. Rev.* **D92** (2015) 124006, arXiv:1510.04713 [gr-qc]. (Cited on page 143.)

[195] Y. Brihaye, C. Herdeiro, and E. Radu, "Myers–Perry black holes with scalar hair and a mass gap," *Phys. Lett.* **B739** (2014) 1–7, arXiv:1408.5581 [gr-qc]. (Cited on page 150.)

[196] C. Herdeiro, J. Kunz, E. Radu, and B. Subagyo, "Myers–Perry black holes with scalar hair and a mass gap: Unequal spins," *Phys. Lett.* **B748** (2015) 30–36, arXiv:1505.02407 [gr-qc]. (Cited on page 150.)